Experimental characterization of a bio-liquid fuel to be used as an additive for improving biodiesel combustion in cold weather conditions

By

Abu Mahmud Iqbal Chowdhury

A Thesis submitted to the Faculty of Graduate Studies of

The University of Manitoba

in partial fulfillment of the requirements of the degree of

Master of Science

Department of Mechanical and Manufacturing Engineering

University of Manitoba

Winnipeg

ACKNOWLEDGEMENTS

I would like to thank my supervisor Dr. Madjid Birouk for giving me the opportunity and also providing guidance throughout the course of this thesis. To my colleagues in the lab, I would like to thank them for their technical assistance and helpful insights. I extend special thanks to Stephen L. Toth for providing consultation as well as technical assistance. From the technical staff, I would like to thank Sviatoslaw Karnaoukh for providing technical assistance and expertise whenever I sought their help. I would like to acknowledge the financial support provided through research assistantships by BioFuelNet Canada. I would also like to thank the Department of Mechanical and Manufacturing Engineering of the University of Manitoba for providing me with financial support through a number of teaching assistantships. Last but not the least; I would like to thank my parents and my wife for providing encouragement as well as support in all facets of life during this program.

Table of Contents

LIST OF FIGURES

LIST OF TABLES

ABSTRACT

Improvement of biodiesel's cold flow properties still remains one of the major challenges for using it as an alternative fuel in diesel engines. Therefore, the main objective of the present research was to use newly developed liquid biofuels, 3-hydroxyl fatty acid esters and ethers, as an additive for improving biodiesel cold weather properties. Test results revealed that blending with 10% 3-hydroxyl fatty acid esters (C4, C6, C8 and C12) improved biodiesel volatility, cloud point, flash point and kinematic viscosity without a significant loss in LHV. However, blending biodiesel with 3-hydroxyl fatty acid esters negatively affected the oxidation stability which was then found to improve by blending with 3-hydroxyl fatty acid ethers (1,3-DMO and 1,3-DMD). The latter novel fuel substance (1,3-DMO and 1,3-DMD) exhibited much higher evaporation rate compared to biodiesel and only slightly lower than that of decane, gasoline or ethanol. Moreover, the LHV of 1,3-DMO and 1,3-DMD was found to be almost equal to that of canola biodiesel, and higher than that of methanol and ethanol. These findings suggest that 1,3-DMO and 1,3-DMD have the potential to be used as additive to improve biodiesel cold weather combustion performance or as standalone fuels.

Keywords: Biodiesel, Cold flow properties, Volatility, Combustion, LHV, Additives.

NOMENCLATURE

d	Droplet diameter [mm]
d_0	Initial droplet diameter [mm]
t	Time [s]
(t/d_o^2)	Droplet lifetime
k	Evaporation/vaporization rate [mm^2/sec]
$(d/d_o)^2$	Droplet normalized diameter
N	Fans rotational speed [rpm]
LHV	Lower heating value [kJ/kg]
1,3-DMO	1,3-dimethoxyoctane
1,3-DMD	1,3-dimethoxydecane

Chapter 1. INTRODUCTION

The world is faced with a huge increase in the demand of petroleum-based fuels due to rapid industrialization, growth in transportation, electricity generation, agricultural sector and other basic human needs, all of which contribute to environmental degradation [1], [2]. In addition, environmental pollution as well as ecosystem unbalance and global climate change have become major issues around the world in recent years [3] [4]. According to International Energy Agency (IEA) report, the world′s primary energy demand is expected to increase by 55% at an average annual rate of 1.8% per year between 2005 and 2030 [5]. If this trend continues, the world will encounter a huge energy crisis. In addition, the reserves of Petroleum-based fuels are concentrated in certain geopolitically sensitive regions of the world. All these factors, which contribute to a shortage of conventional fossil fuels and also to an increase in emissions of combustion-generated pollutants, are among the driving causes for a global effort to develop renewable energy sources [6], [7]. It was reported that, to date, about 15% of global energy consumption comes from renewable resources (e.g., [8], [9], [10]). The slow progress in the development and implementation of renewable energy sources is mainly attributed to several factors such as economic limitations, lack of supply, and technical know-how of users (e.g., [11]). Renewable energy sources can be categorized into two groups; the first consists of clean energy technologies such as, solar, wind, hydroelectric, wave and rain energy; while the second one consists of biofuel technologies derived from renewable biomass (e.g., [12]). Renewable biofuels, such as bioethanol and biodiesel, can be used to ease the consumption of petroleum-derived diesel and gasoline in transportation and offer the potential for growth in the direction of sustainable mobility with the involvement of the energy, agricultural, automotive, and aerospace transportation sectors.

Biodiesel, which is one of the most widely used biofuel, is mainly composed of mono-alkyl esters of long chain fatty acids produced from biomass such as agricultural oil seed crops, animal fats, algae and other non-edible oil sources [13], [14], [3], [15]. A number of studies have shown that biodiesel obtained from numerous vegetable oils hold promise as alternative fuels for compression ignition engines [16], [17], [18], [19]. Biodiesel has various advantages over diesel which include higher flash point and cetane number; lower toxicity; lower emissions of particulates, CO, CO_2, SO_x, NO_x and hydrocarbons; better lubricity and safety [20], [21], [22], [23]. For instance, biodiesel can offer other benefits, including reduction of greenhouse gases by emitting fewer pollutants over the whole range of air–fuel ratio when compared to diesel (e.g., [24]). The density, power output and lower heating values of biodiesel are also close to those of diesel fuel [25]. In spite of the above advantages, some drawbacks such as reduced cold flow properties (higher cloud point and pour point) [26], [27], [28], lower oxidation stability, storage and thermal instability and higher crystallization temperatures [21],[29] have restricted the adoption of biodiesel as a stand-alone fuel for diesel engines. Moreover, certain physical and chemical characteristics (high viscosity, high surface tension, lower volatility [30], lower energy content) of vegetable oils causes some ignition problems such as coking of the combustion chamber [31], [32], [33], reduction of engine speed and power [34], polymerization and thermal decomposition under certain conditions of temperature [35]. For instance, biodiesel derived from fats or oils with significant amounts of saturated fatty compounds have undesirable fuel properties that limit their applications in cold weather conditions [36].

Considerable research has been carried out to develop biodiesel derivatives that resemble the properties and characteristics of the hydrocarbon-based fossil fuels. The properties of biodiesel depend greatly on the different raw materials used for biodiesel production [37], [38], [39] and

[40]. Moreover, the evaporation and combustion process of different fuels are affected by their physical properties. Several methods have been suggested to reduce the viscosity, engine emission and formation of deposits when using vegetable oils as fuel. These methods include formulation of biodiesel [41], [42], [43], [44]; pyrolysis [45], [46], [47]; preheating [48], [49], [50]; blending, [51], [52]. For example, biodiesel is blended with conventional diesel fuel to deal with the issues arising from the relatively high cloud and pour points, high freezing point and high viscosity of biodiesel fuels. The main objective of the present research was to evaluate the possibility of using a newly developed renewable liquid biofuel (from fatty acid methyl or ethyl esters, and/or fatty acid methyl or ethyl ethers) as an additive for improving biodiesel properties for cold flow conditions operations. It was also the aim of this research to evaluate the possibility of using this novel biofuel as a standalone fuel.

The thesis consists of 6 chapters and 4 appendices. The literature review is presented in Chapter 2. The experimental test rigs and test conditions are reported in Chapter 3. The results and discussion for droplet evaporation and fuel properties are presented in Chapter 4. Conclusions and recommendations for future work are summarized in Chapter 5.

Chapter 2. LITERATURE REVIEW

In this chapter, published literature concerning the cold flow properties improvement, evaporation and combustion process as well as emission of biodiesel and their blends is reviewed.

2.1. Improvement of Cold Flow Properties

A considerable number of research studies have focused on developing biodiesel derivatives with properties approaching those of hydrocarbon-based fossil fuels. Improvement of the cold flow properties of biodiesel still remains one of the major challenges of biodiesel combustion. For instance, biodiesel shows higher cloud and pour points while derived from fats or oils which contain significant amounts of saturated fatty compounds , thus limits their applications in cold weather conditions [36]. Different laboratory tests, such as cloud point (CP), cold filter plugging point (CFPP), pour point (PP), iodine value (IV), lubricity, kinematic viscosity (KV), acid value (AV), induction period (IP), oil stability index (OSI), and low-temperature flow tests (LTFT) are used to quantify the low temperature performance of biodiesels [53], [54]. Several methods have been suggested to improve the biodiesel characteristics at lower temperatures, such as blending with petroleum fuel or vegetable oils ([55], [28], [56], [53], [57]) using additives ([58],[59]) winterization ([60], [61] ,[62]) modification of biodiesel feedstock via the addition of branched alcohols and other treatments ([63][64][65][66][67][68]). These approaches are aimed at diluting a fraction of the saturated long-chain methyl esters, and lowering both CP and LTFT ([69][70][71] [72]).

2.1.1. Blending with fossil fuels and vegetable oils

Blending biodiesel with petroleum-derived diesel fuel (DF) and vegetable oil methyl esters are the most widely used methods for improving cold flow properties ([28], [26], [53], [54]). However, these methods limit the biodiesel blend content to 20% or less ([73]). In some cases, the cold flow properties were not significantly improved by blending with 10% methyl esters [74] or 20% methyl esters [55], or by the removal of minor components from biodiesel samples [54]. Blending of biodiesel with more saturated fatty acids improved the IV and decreased the CFPP with the addition of cold flow improvers such as ethylene–vinyl acetate copolymer and octadecene-1-maleic anhydride copolymer [75]. On the other hand, a decrease in saturated fatty acid methyl esters (FAMEs) was observed to affect the ignition quality of the fuel, while an increase in un-saturated FAMEs was shown to decrease the oxidation stability [20]. Different antioxidants (e.g.; *tert*-butylhydroquinone, butylated hydroxytoluene, propyl gallate, pyrogallol, *a*-tocopherol and butylated hydroxyanisole) have been tested for the improvement of oxidation stability ([26], [75]).

Xu [76] reported that the CFPP of different biodiesel fuels synthesized from different sources of vegetable oils, such as rapeseed, cotton and soybean dropped, while the viscosity and density increased when blending the FAMEs with diesel fuel. Kim et al. [77] studied different volume ratios (B5, B10, and B20) of six different types of biodiesel blends and reported that the presence of unsaturated structures and the length of hydrocarbon chains affected significantly the low temperature properties of biodiesel. Wu et al. [78] also reported acceptable low-temperature properties and diesel engine performance when monoalkyl FAMEs derived from tallow and recycled grease were blended with petroleum diesel fuel. Lown et al. [79] investigated the

effectiveness of decreasing CP by applying different functional groups of ethers, esters, alkanes, ketones, and diesters, where diesel and jet fuels were mixed with compounds of low molecular weight. Zuleta et al. [80] examined blends of biodiesel from palm–castor, palm–sacha inchi and castor–jatropha, with different quantities. They reported that the lowest CFPP (12°C) was observed for FAMEs derived from a blend made of 75% jatropha and 25% castor oils, but the viscosity was higher than that of international standards.

2.1.2. Blending with chemical additives

The use of additives appears to be the most effective technique because it is more convenient and economical than the other methods ([81], [82], [83], [84]). Most of the research focusing on the improvement of biodiesel cold properties involved the use of suitable additives, such as polymeric cold flow improvers, poly-methyl acrylate (PMA), olefin-ester copolymers (OECP) ([85], [86]), surfactants like polyglycerol esters [82], and cold flow improvers like kerosene and ethanol [87]. It was found that the use of additives with biodiesel not only yielded improvement of the cold flow properties, but also improved emissions [87], oxidative stability [72], and viscosity via modifying and inhibiting the formation of crystals of biodiesel at lower temperatures ([85], [86]). Cold flow improvers (CFIs) including petroleum diesel pour point depressants (PPDs) ([28], [88], [87], [89], [90], [81] [83]), surfactants ([88], [89], [82]), and diluents ([81], [91], [84], [92], [93], [94]) act mainly as PP depressants rather than CP depressants.

The addition of cold flow improvers (CFIs) such as kerosene, ethanol and commercial additives can cause a significant reduction in the pour point and combustion emissions of biodiesel ([83] [87] [95]). For example, Shi et al. [96] reported that ethanol–diesel–biodiesel fuel blends

exhibited similar or better fuel properties than petroleum diesel fuel and were stable at lower subzero temperature. Similarly, Kwanchareon and Luengnaruemitchai [97] reported that diesel–biodiesel–ethanol blends have similar fuel properties and heating value to diesel when using an ethanol content of less than 10%. On the other hand, blending with 20% ethanol and kerosene improved the CP and PP, as well as the combustion properties of FAMEs derived from mahua oil [83]. Zhu et al. [95] reported that, with an increase of alcohol in the biodiesel blends (5 to 15%), NO and particulates emissions reduced, while HC and CO emissions increased.

It has been reported that commercially available CFIs for commercial diesel fuel can improve the low temperature performance of biodiesel ([98], [99]). For example, Chen et al. [86] reported a reduction in PP and CP of soybean biodiesel when using CFIs such as OECP, EACP, and PMA. Polymeric CFIs, such as poly-methyl acrylate (PMA) and olefin-ester copolymers (OECP) yielded improved lower temperature properties (PP, CFPP) and retarded viscosity increase via modifying both the shape of FAME crystals and preventing the development of larger FAME crystals at lower temperatures ([85], [86]). Wang et al. [85] reported that polymethyl acrylate (PMA), among four polymeric additives (EVAC, poly-α-olefin, PMA, and polymaleic anhydride) showed the best results for improving the low temperature properties of biodiesel derived from waste cooking oil. Similarly, PP, CFPP and the oxidative stability of biodiesel were improved using a bio-based diluent (ethyl acetoacetate) as an additive [72]. Ming et al. [100] reported reduced CP and PP for palm oil biodiesel when using different commercially available additives, including palm-based polyol (P-P), dihydroxy fatty acid (DHFA), DHFA+ ethyl hexanol, DHFA+ P-P, and castor oil ricinoleate. A reduction (from −10 °C to −16 °C) of the CFPP was achieved by the addition of 0.02 wt% of polyglycerol ester [82], and a reduction of 4–

5 °C in CP, 3–4 °C in PP, and 3 °C in CFPP was achieved by adding 20 vol% of the bio-based CFI, ethyl levulinate [93].

2.1.3. Winterization

The use of "winterization" was found to improve the low temperature properties of biodiesel by lowering the concentration of saturated compounds ([62], [81], [101]). This method was found to eliminate the high-temperature freezing constituents via partial crystallization [102]. Winterization should be done carefully without eliminating all saturated FAME's from biodiesel because of its negative effect on the yield and as they can improved caloric value and ignition quality [103], [17], [61]. In addition, these FAMEs can improve the fuel caloric value and fuel ignition quality ([103], [17], [61]). This method can be applied to both biodiesel and pure oils ([61][104]). For example, it was reported that the application of winterization to waste cooking oil FAMEs was suitable in finding the process conditions needed to improve the low temperature fuel performance [24]. Similarly, Kerschbaum et al. [62] used winterization to reduce LTFT of biodiesel derived from waste cooking oil without using additives. Dogan and Temur [101] removed the saturated FAMEs in beef tallow biodiesel by using fractional crystallization process to improve the low temperature properties.

2.1.4. Application of branched alcohols

The addition of branched alcohols was reported to improve cold flow properties of biodiesel ([56], [74]). It was found that branched alcohols significantly reduce the crystallization temperatures (lower CP) by weakening the intramolecular associations between linear, long-chain methyl esters ([63][64] [65]). However, this technique would involve additional costs

because of the greater molecular weight and higher prices of branched alcohols. Bouaid et al. [63] reported that the biodiesel formed by adding biobutanol as an additive improved low temperature properties such as PP, CP and CFPP compared to European standard biodiesel. Some other alcohols were also implemented to develop the biodiesel cold flow characteristics. For example, Lee et al. [64] reduced the crystallization temperature of soybean biodiesel by using isopropyl or 2-butyl alcohols. The crystal temperatures of soybean biodiesel containing isopropyl and 2-butyl alcohols were significantly lower (7–11 °C and 12–14 °C, respectively) compared to soybean oil FAMEs alone. Giraldo et al. [84] reported that 2-butyl alcohol was the best among the three CFIs (glycerol acetates, glycerol ketals, and branched alcohol-derived fatty esters) for increasing the low-temperature performance (6 °C reduction in CP and PP) of palm oil biodiesel. Similarly, Wang et al. [65] reported improved cold flow performance (15 °C reduction in PP) of canola oil biodiesel by using branched-chain head-groups of 3-methyl-1-butanol and 1-methoxy-2-propanol. Wen-Hsin Wu [78] reported that isopropyl tallowate showed better physical and low-temperature properties than ethyl tallowate.

2.1.5. Other methods

Some other methods, such as thermal cracking [105], urea complexation [106], epoxidation and alkoxylation [73] have also been used to improve the low temperature properties and stability of biodiesel. The presence of alkoxy groups, epoxy groups, and hydroxyl groups in the fatty acid chain can improve the biodiesel lubricity and cold flow properties [107]. For example, Wadumesthrige et al. [66] reported that the modification of the chemical structure of biodiesel chains by introducing an epoxide group (“epoxidation”) resulted in acceptable improvement of cold flow properties among the three different methods (catalytic hydrogenation, epoxidation,

and hydroxylation). Similarly, Kongyai et al. [67] used epoxidation of waste oil derived biodiesel to investigate the improvement of different characteristics. Smith et al. [22] reported that the cloud point of 2-ethylhexoxy butyl biodiesel was improved by using alkoxylation process. Mushtaq et al. [68] used both epoxidation and alkoxylation methods with biodiesel containing high concentrations of oleic acid methyl esters and reported that the methoxy biodiesel had the lowest KV, while the N-decoxy biodiesel had the lowest cloud point and pour point. Reaume and Ellis [108] reported improvement of CP and overall cold flow properties of eight different animal fats and vegetable oils by using isomerization process. In some cases, ozonated vegetable oils were used to improve the PP and FP, while the CP remained unaffected ([109], [110]). For instance, Soriano et al. [109] observed a significant improvement in PP or CP of different biodiesels by adding ozonated oils (1–1.5-wt%).

2.2. Evaporation of biodiesel and its blends

Study of the vaporization properties of a single droplet is important to characterize spray vaporization and combustion. Many experimental and numerical investigations on the evaporation characteristics of biodiesel have been done in different environments to emphasize the influence of different related parameters [111] [112] [113] [114] [115] [116] [117] [118] [119] [120] [121] [122] [123] [124] [125]. For example, effect of temperature at standard pressure has been studied by [111] [112] [114] [116] [117] [118] [120] [121] [122] [123] [124] [125]. The effect of both ambient temperature and pressure have been evaluated by [113], [115]; [119]; [120]. In addition, only a few literatures studied the effect of ambient pressure and temperature in turbulent environment [113] and the effect of droplet size [123]. Different methods have been used for the experimental investigations, such as fiber-suspended droplet

technique [112] [114], cross flow technique [124] [125]. Biodiesels derived from different feedstock such as soybean, palm, canola, rapeseed and sunflower oils were investigated by different researchers to evaluate the evaporation characteristics.

There are several published experimental investigations concerning droplet evaporation characteristics at high temperatures. For instance, Hashimoto et al. [111] evaluated the droplet vaporization characteristics of biodiesel derived from palm methyl ester (PME) at high ambient temperatures (400–900 K) and atmospheric pressure. They reported that the initial heating period and droplet lifetime decreases while the average evaporation rate increases with the increase of ambient temperature for all fuels. The evaporation rate of PME was found to be almost similar to that of diesel with PME showed longer droplet lifetime due to the higher boiling points [111]. Manjunath et al. [112] used suspended droplet technique to evaluate the evaporation characteristics of biodiesel fuels derived from sources such as jatropha, karanja, palm and coconut, and their blends with diesel at high ambient temperatures (423K-523K) and atmospheric pressure. They reported that the heat transport and mass transport parameters significantly influence the vaporization characteristics of these different fuels. Similarly, Morin et al. [114] used fiber-suspended droplet technique to evaluate droplet evaporation of rapeseed and sunflower oil methyl ester at elevated ambient temperature (473 K and 1020 K) and standard atmospheric pressure. They found that the average evaporation rate for both biodiesels was lower than that of n-heptane droplet. Moreover, both biodiesel droplets showed significantly long heating period while following the d^2-law after the elapse of the heating period. Promvongsa et al. [118] studied the evaporation of palm oil biodiesel and its blends with diesel at a relatively low ambient temperature of 473 K and atmospheric pressure. They reported that blending of diesel with 5% biodiesel reduced the evaporation constant by 20%.

Several numerical studies of biodiesel droplet evaporation at high temperature were also reported in the literature. For example, Daho et al. [116] used a quasi-steady model to predict the vaporization process of cottonseed oil biodiesel at ambient temperature ranging between 684 K and 917 K and atmospheric pressure. They reported that the consideration of convection and heating period of the droplet is important for accurate prediction of the vaporization rate at high ambient temperature. Hallet et al. [121] used continuous mixture theory model to evaluate the droplet vaporization of soybean biodiesel at atmospheric pressure and ambient temperature ranging from 693 K to 993 K. They found that the results from the model agreed with the experimental results of single suspended droplets and the measurements are within 3% of d^2 law. Similarly, Zhang and Kong [119] numerically investigated the droplet vaporization of soybean biodiesel and its blends with diesel at elevated ambient temperature (748 K-1019 K) and standard atmospheric pressure using a hybrid vaporization model. They reported that the droplet lifetime increases with the biodiesel proportion in the blend, while in general the droplet lifetime decreases rapidly with ambient temperature after exhibiting a significantly long heating period. In a numerical study, Dirbude et al. [122] investigated the droplet vaporization of biodiesel derived from rapeseed and sunflower methyl esters at ambient temperature ranging between 550K-1050K and atmospheric pressure (0.1 MPa). They reported that the prediction of their model, which was developed by using an effective Reynolds number, was better than the data of Morin et al. [114]. They also reported that the oxidation of rapeseed and sunflower oil methyl esters is similar to n-decane.

A few studies have done concerning the coupled effect of both ambient pressure and temperature on the evaporation characteristics of biodiesel droplet. For example, Morin et al. [115] evaluated the evaporation of rapeseed oil biodiesel by varying ambient temperature (between 373 K and

973 K) and ambient pressure (between 0.1 MPa and 5 MPa). They reported that the evaporation rate increased with ambient pressure for pressures greater than the critical pressure at ambient temperatures up to 873 K. In a numerical study, Zhang and Kong, [120] used a high-pressure droplet vaporization model to investigate the droplet evaporation of biodiesel by varying the pressure from 0.1 MPa to 5 MPa at an ambient temperature of 900 K. They found that the droplet lifetime of biodiesel increased with increasing pressure; whereas it decreased rapidly with ambient temperature. On the other hand, droplet lifetime increased as the proportion of biodiesel in the fuel blend increases. They also reported that the effect of ambient pressure is greatly dependent upon the ambient temperature for the biodiesel droplet evaporation.

The effect of ambient pressure and temperature on biodiesel droplet evaporation in turbulent environment have been evaluated by Birouk and Toth [113]. In their experimental study, they investigated the droplet evaporation characteristics of biodiesel derived from soybean oil in a turbulent environment for the ambient pressure ranging between 1-16 bar at 473K. They found that the biodiesel droplet evaporates by following d^2-law and it is dependent on both ambient pressure and turbulence while the increases of ambient pressure greatly influence the effect of turbulence.

Moreover, some other techniques were also used by different authors to evaluate the evaporation characteristics of biodiesel. For instance, Saha et al. [123] investigated the effect of droplet size on the vaporization process of rapeseed methyl esters (RME) and their blends with diesel by using a hot air jet (up to 800 K) at atmospheric pressure. They found that for homogenous mixture, the smaller droplets vaporize quicker compared to larger droplets. Barata [124] and Gu et al. [125] numerically evaluated the evaporation characteristics of biodiesel by using convective (cross) flow at atmospheric pressure. Barata [124] used an Eulerian/Lagragian

approach to account for turbulent transport, dispersion, and evaporation for biofuel (RME) droplets evaporating in a cross-flow. Similarly, Gu et al. [125] evaluated the evaporation process of Rapeseed Methyl Esters (RME) in a turbulent crossflow pre-mixer with temperature of around 800 K and air velocity of 10 m/s. They reported that droplet surface temperature was strongly influenced by the fuel properties. Founti et al. [126] investigated the evaporation characteristics of FAME and its blend with diesel by using IR-Thermography for temperature range 353K to 367K at atmospheric pressure. They reported that droplet lifetime decreases with the increase of droplet surface temperatures.

2.3. Combustion of biodiesel and it`s blends

2.3.1. Engine combustion of biodiesel and its blends

The experimental investigation of different combustion properties (such as ignition temperature, ignition delay, ignition pressure, rate of heat release, and combustion efficiency) of different biodiesel fuels has been reviewed in in the subsequent paragraphs. Different biodiesels derived from methyl and ethyl esters (vegetable oils like rapeseed, jojoba , Jatropha , karanji , sunflower , tallowate , soybean , palm , neem , pine , hazelnut kernel) [127] [128] [129] [130] [131] [132] [133] [134] [135] [136] [137] [138] [139] [140] [141] [142] [143], and waste cooking oil [144] [145] [146] [147] [148] [149] are used by different research groups to investigate these combustion properties.

Ignition Delay (ID) is a vital factor in the combustion phenomenon. Biodiesel and its blends have higher cetane number which makes autoignition easy and gives a shorter ID compared to diesel [138]. The ignition delay is influenced by a large number of parameters such as fuel type, fuel

ignition quality, engine speed, air–fuel ratio, compression ratio, intake air temperature and pressure, quality of fuel atomization [150]. According to most of the literature, it is common trend that biodiesel gives shorter ignition delay compared to diesel [127], [128], [129], [145], [148], [149], [140], [151], [152], [141], [138]. For example, Zhang and Van Gerpen [127] found that the blends of methyl esters of soybean oil and diesel showed shorter ignition delay and similar combustion characteristics as diesel. Similarly, McDonald et al. [128] reported a similar overall combustion characteristics and shorter ignition delay as diesel for soybean oil methyl ester. Radwan et al. [129] found that jojoba methyl ester showed lower ignition delay period and higher ignition pressure and ignition temperature. Yu et al. [145] reported that the premixed combustion phase of waste cooking oil (WCO) was less intense than that of diesel because of the shorter ignition delay. Rao et al. [148] observed a lower ignition delay periods for used cooking oil methyl ester (UCOME)-diesel blends than that of diesel, which decreases with the increase in the proportion of UCOME. They also reported that, UCOME-diesel blends exhibit a general trend of decrease in ignition delay with increase in load [148]. Buyukkaya [140] reported that ignition delay of neat rapeseed oil and its blends with diesel was smaller compared to that of standard diesel. Tsolakis et al. [151] found a reduced ignition delay for biodiesel (rapeseed methyl ester, RME) and different diesel/biodiesel blends. Yoon and Lee [152] found shorter ignition delay for biogas-biodiesel blend. Özener et al. [141] found a shorter ignition delay for the addition of biodiesel (soybean oil) to conventional diesel fuel. Gumus [138] reported a decrease in ignition delay with the increase of biodiesel content in the biodiesel-diesel blends. Kannan et al. [149] also found shorter ignition delay for waste cooking palm oil based biodiesel by adding fuel borne catalyst (FBC) (ferric chloride ($FeCl_3$)).

On the other hand, several authors reported an increase in ignition delay of biodiesel [130], [139], [137]. For instance, Kumar et al. [130] found a higher ignition delay for Jatropha oil methyl ester as compared to diesel on a constant speed diesel engine. In another study, Kumar et al. [139] found that Ignition delay increased with the blends of Jatropha oil with methanol and orange oil and reduced with the methyl ester of Jatropha oil. Anand et al. [137] reported that (karanji oil)-methanol blend showed higher ignition delay and higher maximum rate of pressure rise as compared to neat biodiesel. Combustion and heat release (HR) are other important parameters in combustion phenomenon of biodiesel which must be known in order to decrease fuel consumption and engine emissions while keeping other engine performance factors at a satisfactory level [138]. Moreover, different physical properties, combustion and HR characteristics of biodiesel increase the brake specific fuel consumption slightly relative to diesel fuel for biodiesel and its blends [153], [127], [128], [145], [150], [130], [154], [135], [134] and [155]. The combustion and HR characteristics are affected by the differences in physical properties between diesel and biodiesel fuels [17], [156], [157], [158] and [159]. Different investigations related to HR characteristics and combustion of biodiesel have been reported in the literatures [136], [160], [132], [161], [148], [144], [147]. Test parameters of these studies include the percentage of biodiesel in the blend, energy input, engine load (EL) and injection pressure (IP). For example, Tashtoush et al. [136] examined the combustion characteristics of ethyl ester of used palm oil and found that biodiesel burned more efficiently with higher combustion efficiency (66%) at a lower energy input compared to 56% for the diesel fuel. On the other hand, biodiesel combustion performance deteriorated at higher energy input, because of its high viscosity, density and low volatility [136]. Lif and Holmberg [160] reported an improvement in combustion efficiency while using emulsified water with diesel. Dorado et al.

[132] reported that combustion efficiency remained almost constant by using either waste olive oil methyl ester or diesel fuel. Sinha and Agarwal [161] examined the combustion properties of rice bran oil and found a higher peak pressure and rate of pressure rise for B20 fuel (blend of 80% diesel and 20% rice bran biodiesel by volume) at low engine loads (up to 10% load) which becomes lower with the increase of engine load. Rao et al. [148] also observed a slightly higher peak pressure for UCOME-diesel blends than that of diesel. On the other hand, they reported a lower rate of pressure rise for UCOME and its blends as compared to diesel, which decreases with the increase of UCOME in the blend [148]. Sudhir et al. [144] reported that waste cooking oil (WCO) derived from palm oil showed lower combustion temperature and pressure as compared to esters of fresh palm oil and diesel fuel. Selim et al. [135] reported a delayed combustion and a lower pressure rise rate for jojoba oil methyl ester (JME) when compared to that of gas oil.

Regarding the peak pressure, Ozkan et al. [147] reported that used cooking oil biodiesel and its blend with with glycerine and petroleum-based diesel showed similar effective presure. Similarly, Qi et al. [162] reported that the peak pressure, peak heat release rate and peak pressure rise rate of BE-1 (5% diethyl ether, 25% biodiesel and 70% diesel in vol.) are almost similar to those of B30 (30% soybean biodiesel,70% diesel),and higher than those of BE-2 (5% ethanol, 25% biodiesel and 70% diesel in vol.) at lower engine loads. On the other hand, BE-1 showed the highest and B30 (soybean) showed the lowest peak pressure, peak heat release rate and peak pressure rise rate at higher engine loads [162]. Yoon and Lee [152] reported that the peak pressure and heat release for biogas–biodiesel were slightly lower at low load and higher at 60% load compared to biogas–diesel.

Several other experiments have been done to test the rate of heat release (ROHR) of biodiesel. According to most of these studies heat release rate increased for biodiesel and its blends [163], [149], [151], [143], [164]. For example, Chen et al. [163] found that the addition of ethanol to diesel-biodiesel blend decreased the combustion duration while increased the ignition time, peak pressure and maximum heat release ratio . Kannan et al. [149] reported a higher heat release rate by using a fuel borne catalyst (FBC) such as ferric chloride (FeCl3)for waste cooking palm oil based biodiesel. Tsolakis et al. [151] also reported an increase in heat release for biodiesel (rapeseed methyl ester, RME) and different diesel/biodiesel blends. Vallinayagam et al. [143] reported 27% increase in maximum heat release rate for pine oil when compared to diesel. Lu et al. [164] reported an increase in maximum heat release rate (HRR) for biodiesel-fueled engines with premixed ethanol.

However, some literatures showed there was no significant difference [146], [142] or sometimes even a decrease in the rate of heat release (ROHR) [133], [137], [148]. For instance, Yusuf et al. [133] reported a lower peak rate of heat release for the blend of diesel and methyl tallowate esters compared to diesel. Anand et al. [137] reported a decrease in peak cylinder pressure and peak energy release rate for biodiesel-methanol blend than that of neat biodiesel fuel. Rao et al. [148] reported an early occurrence of maximum heat release rate which decreases with an increase in proportion of UCOME in the blend. On the other hand, Lapuerta et al. [146] reported similar premixed peak of the rate of heat release of waste cooking oil methyl and ethyl ester, and their blends with diesel fuels . Dhar at al. [142] reported a similar rate of heat release for the blends of neem oil biodiesel with mineral diesel.

Some other combustion properties are also determined in different studies; for instance, Senatore et al. [134] found an earlier injection and heat release, and a higher average cylinder gas temperature for rapeseed oil methyl ester than that of diesel. Dagaut et al. [165] studied the kinetics of oxidation of rapeseed oil methyl ester (RME) in a jet-stirred reactor. Saikishan et al. [166] determined the cetane number by investigating the influence of the various fuel properties namely viscosity, density, flash and fire points of biodiesel and its various blends using simulation techniques. James et al. [167] found that fuel injection and ignition processes can be changed by the presence of biodiesel in both neat and blend form.

2.3.2. Droplet combustion of biodiesel and its blends

Droplet combustion of biodiesel and its blends have been studied both numerically and experimentally [168], [169], [170], [171], [172], [173], [174], [175], [176], [177], [178], [113]. These studies on the combustion characteristics of biodiesel have been done in different test conditions. For example, the effect of temperature at standard atmospheric pressure has been studied by [168] [169]. On the other hand, some studies evaluated the effect of forced convection at atmospheric pressure [172], [173], [174], [175]. Whereas, only a few studies investigated the effect of both ambient temperature and pressure in turbulent environment [113]. Different methods have been used for the experimental investigations, such as fiber-suspended droplet technique [169], freely-falling droplet technique [172], and porous sphere technique [173], [174], [175].

Combustion characteristics, such as ignition delay and burning rate were studied in particular. For example, Marchese et al. [168] investigated the combustion characteristics of fatty acid methyl ester (FAME) in both normal gravity and microgravity (10^{-4} m/s^2) conditions at ambient

temperature above the fuel critical value ranging from 1000 K and 1300 K and atmospheric pressure. They reported that both methyl decanoate and methyl dodecanoate showed shorter ignition delay at higher temperature as compared to commercial biodiesel. On the other hand, at lower temperature, methyl decanoate showed similar ignition delays, while methyl dodecanoate showed much longer ignition delays than biodiesel. In addition, methyl oleate displayed similar ignition delays for the entire temperature range as compared to biodiesel. Pan and Chiu [170] investigated the droplet combustion of biodiesel in a reduced gravity environment. They reported that the presence of a heating period can be reduced and the burning rate can be increased by the addition of alcohol prior to combustion of diesel–biodiesel blends where the droplet follows the d^2-law in microgravity conditions. Furthermore, the introduction of microexplosion with higher volatile alcohol led to substantial disintegration and faster combustion of fuel droplets. Raslavicius and Bazaras [176] reported that the ignition delay of B30 decreased with ambient temperature which ranged from 930 K to 1010 K at atmospheric pressure and normal gravity. In another study, Raslavicius and Bazaras [177] reported a decrease in ignition delay at ambient temperature ranging from 770 K to 870 K and atmospheric pressure in normal gravity conditions. They also reported that the significance of droplet size became important at lower ambient temperatures. Similarly, Zhu et al. [169] investigated the combustion characteristics of biodiesel at elevated ambient temperatures ranging between 923K to 1073K by using a suspended fiber technique. They reported that the burning rate and ignition delay period of biodiesel droplet were higher than those of the diesel droplets. Pan et al. [178] evaluated the burning rate of biodiesel-diesel blends in normal and microgravity conditions and reported that the burning rate decreased with diesel content in microgravity conditions.

Several techniques have been used by different authors to examine the effect of forced convection on droplet combustion characteristics of biodiesel and its blends. For example, Botero et al. [172] investigated the freely-falling droplets of biodiesel derived from castor oil and their mixtures with ethanol and diesel in a high-temperature combustion chamber. They reported that the addition of ethanol to diesel and biodiesel caused microexplosion and reduced the burning rate. Raghavan et al. [173] investigated the combustion characteristics of karanja biodiesel and its blends with diesel using the porous sphere technique. They reported an increase in the burning rate for blends of B60, B70, B80 and B90 when varying a free stream velocity (from 0.4 m/s to 1 m/s) in normal gravity at room temperature. Similarly, Rajesh et al. [174] used the porous sphere technique to evaluate the combustion properties of Jatropha biodiesel in a mixed convective air environment. They reported that the burning rate of biodiesel was reduced by 11% compared to diesel for the same air velocity and sphere size. Prakash et al. [175] used the porous sphere technique by varying the relative velocity between the oxidizer and droplet, and found that the biodiesel blends didn't follow the d^2-law under room conditions where the free stream velocity was constant at 42 m/s. Birouk and Toth [113] evaluated the droplet combustion characteristics of biodiesel derived from soybean oil in a turbulent environment for ambient pressure ranging between 1-16 bar at 473K by using the fiber suspended technique. They reported that the burning rate of biodiesel droplet increased with turbulence only at elevated ambient pressure. Moreover, they reported that the droplet flame extinction was caused by the heat loss from the flame at high levels of turbulence.

2.4. Emission of biodiesel and its blends

2.4.1. NO_X emission

NO_X is considered as the most unpleasant emission from Compression ignition engine. The key reason behind increased NO_X emissions of biodiesel involved better combustion and higher combustion temperature [179]. Numerous publications reported an increase of NOx emissions with the increase of biodiesel content [180], [181], [182], [183], [184], [185], [186], [187], [188], [189], [190], [191], [192], [193], [151], [194], [195], [196] and [197]. For example, Lin et al. [198] reported an increase of NOx emissions from 5.58% to 25.97% by using vegetable oil methyl ester fuels in the diesel engine. Ozsezen et al. [150] found that the NOx emissions increased by 22.13% and 6.48% for waste palm oil methyl ester (WPOME) and canola oil methyl ester (COME), respectively. Similarly, a maximum of 15% increase in NOx emissions observed for karanja (Pongamia Pinnata) oil [199]. Devan and Mahalakshmi [200] found a 2.7% increase in NOx emission for the 50-50 blend of methyl ester of paradise oil and eucalyptus oil. Tsolakis et al. [151] reported that NOx emission increased for diesel/RME (rapeseed methyl ester) blends. Luján et al. [190] found an increase in NOx emissions for B30, B50 and B100 as 20.6%, 25.9% and 44.8%, respectively. Canakci [159] showed that NOx emission for biodiesel (soybean oil) blends with petroleum diesel fuels (No. 1 and No. 2) increased by 1.2% and 11.2%, respectively. Additionally, Gumus and Kasifoglu [186] and Godiganur et al. [188] found an increase in NOx emissions with the increase of biodiesel proportion in the blends. Lertsathapornsuka et al. [197] reported that the blends of waste palm oil biodiesel (B50 and B100) showed 1.84% and12.62% higher NOx emissions respectively compared to diesel. Zheng et al. [201] reported a comparable NOx emission for high-cetane number (CN) biodiesel while

the biodiesel with a CN similar to the diesel fuel produced relatively higher NOx. Karra et al. [202] found that biodiesel blends generally produced higher NOx emissions compared to regular diesel fuel. They also reported that the NOx emissions of 20% biodiesel blend was almost similar to that of regular diesel fuel, while 100% biodiesel still produced relatively higher NOx emissions. Vallinayagam et al. [143] reported that NOx emission is higher for pine oil-diesel blends (25%, 50%, and 75%) compared to diesel fuel. Similarly, Nabi et al. [203] found higher emission for diesel–biodiesel (neem oil) blends. Özener et al. [141] tested soybean oil and its blends with diesel fuel (B10, B20, B50 where B refers to biodiesel and 10, 20 and 50 being the percentage of biodiesel in the blend) and found an increase by 6.95–17.62% of NOx emission.

Some published literature reported the reduction of NOx emissions when using biodiesel [204], [205], [156], [206], [207], [208], [209], [210], [211], [132], [42], [212], [213], [214], [215], [139], [216]. Yoon and Lee [152] found NOx emission is significantly lower for biogas-biodiesel dual fuel. Puhan et al. [213] reported an average reduction of NOx emission was around 12% for MOEE as compared to diesel fuel. Dorado et al. [132] found 20% decrease in NOx emissions for the case of waste olive oil biodiesel. Banapurmatha et al. [216] found a decrease in NOx emission for three biodiesels SOME, JOME and HOME than that of diesel fuel. Similarly, Aydin and Bayindir [204] observed that the NOx emission reduced with the increasing content of CSOME biodiesel in the blends (B20, B50 and B75). Kalligeros et al. [214] reported similar trend for olive oil and sunflower oil methyl esters and their 10%, 20%, and 50% blends. In addition, in the literatures [206], [156], [211], [42] and [215], close to 5% decrease in NOx emission was reported for biodiesel.

Other studies reported small difference between biodiesel and diesel NOx emission [146], [217], [218] [203]. It has been reported that the NOx emission of biodiesel and diesel is almost similar [146] [203]. Wang et al. [217] reported that NOx emission is similar for 35% biodiesel blend of soybean oil and diesel. Durbin and Norbeck [218] found very small difference in NOx emissions for pure biodiesel and their 20% blends with diesel. Some others literature showed that the increase of NOx emission did not follow any particular trend with the increased proportion of pure biodiesel. For example, Sahoo et al. [191] reported that the NOx emission increased for karanja and polanga oil and their blends with the increased content of biodiesel while jatropha oil followed a variation. Additionally, Sahoo et al. [42] reported that B100 NOx emission decreased by about 4%, while it increased by about 2% for B20 with respect to diesel.

Different additives, such as metal-based additives [219], [220], [221] and [222]; alcohol (methanol and ethanol) [96], [182], [209], [223], [95], [224], [164], [225], [162], [97], [226], [227], [228] [87]; cetane number improver [184], [229]; and emulsifiers [230]; were used to improve NOx emissions for biodiesel. For example, Keskin et al. [219] reported lower NOx emissions by adding Mg and Mo additives with B60 biodiesel blends. In another work, Keskin et al. [231] reported that NOx emission can be lowered by adding Mn and Ni based additives with tall oil biodiesel. Shi et al. [232] reported that NOx emission can be reduced by the combination of EB-diesel and a SCR catalyst (selective catalytic reduction). Kalam and Masjuki [221] reported that using 1% 4-NPAA additive can improve NOx emission for B20. Labeckas and Slavinskas [233] used multi-functional fuel additives Marisol FT (Sweden) and SO-2E (Estonia) with shale oil treated and found that the total NOx emission reduced by 29.1% (SO-2E) and 23.0% (Marisol FT), respectively. Kass et al. [234] found significantly lower NOx emission by using biodiesel-water emulsions. Similarly, Balaji and Cheralathan [235] reported 9.31%

reduction in NOx emission by the addition of antioxidant additives (L-ascorbic) with cottonseed methyl ester as compared to biodiesel without additives. Sajith et al. [236] found the addition of cerium oxide nano additive with biodiesel reduced the NOx emission due to its effect of oxidation catalyst. Venkatesan and Kadiresh [237] reported that the addition of cerium oxide additive with jatropha biodiesel reduced NO_X emission by 23.5% compared to diesel fuel.

On the other hand, Guru et al. [220] reported 5% increase of NOx emissions for a blend of 10% biodiesel with regard to diesel by adding synthetic Mg additive with chicken fat biodiesel. Szybist et al. [229] used a conventional soy-derived biodiesel fuel with methyl oleate or with cetane improver and found NOx emission increase 3–5% for B20 blend relative to petroleum diesel. Shia et al. [96] found 2-14% increase of NO_X emission by using biodiesel-ethanol blend.

Regarding the addition of alcohols, Zhu et al. [95] reported a reduction of NOx with the increase of ethanol or methanol from 5-15% in the biodiesel blend. They also reported that the blends of biodiesel–methanol were more effective than the blends of biodiesel–ethanol. In another work, Zhu et al. [228] reported that the ethanol–biodiesel blend (BE) could lead to a reduction of NOx emission of diesel engine, while the effectiveness of NOx reduction increases with increasing ethanol in the blend. Hansen et al. [182] reported that the increase of NOx emission (2.6%) reduced by the addition of 5% ethanol to biodiesel compared to B100 (12% increase). Bhale et al. [87] found low NOx emission for MME (mahua methyl ester) biodiesel blended with ethanol; which was the lowest for MME E20 blend. Rahimi et al. [224] found that NOx concentration decreased by increasing the biofuel composition of diesterol (a mixture of diesel (D) sun flower oil methyl ester (B) and bioethanol produced from potato waste (E)). Lu et al. [164] observed a decrease in NOx emission by about 35–85% compared to neat biodiesel when they added ethanol

by port injection. Qi et al. [225] reported that NOx emission is slightly lower for ethanol–biodiesel–water micro-emulsions. Additionally, Kumar et al. [226] reported a decrease in NOx emission by using methanol with jatropha oil. Cheung et al. [209] observed that NOx emission can be decreased by increasing the proportion of methanol from 5-15% in the biodiesel blends. Cheng et al. [227] found that the NOx emission of biodiesel could be improved by using 10% methanol in either the blended mode or the fumigation mode.

On the other hand, Qi et al. [162] found a slightly higher NOx emission for BE-2 (5% ethanol, 25% biodiesel and 70% diesel in vol.) compared to B30 (30% biodiesel and 70% diesel in vol.) and BE-1 (5% diethyl ether, 25% biodiesel and 70% diesel in vol.). Panga et al. [223] reported a slight increase in NOx emission as compared with fossil diesel for biodiesel–ethanol–diesel blends. Shia et al. [96] reported a 2–14% increase of NOx emissions while using ethanol–biodiesel–diesel fuel blend (EB-diesel). Kwanchareon et al. [97] found an increase in NOx emission compared to diesel for the diesel–biodiesel–ethanol blends for different purities of ethanol at different temperatures.

2.4.2. CO_2 emission

It has been reported that biodiesel and its blends emit lower CO_2 than diesel during complete combustion due to the smaller ratio of carbon to hydrogen [150], [206], [219], [238], [42]. For instance, Fangsuwannarak et al. [239] reported a lower CO_2 emission than pure diesel fuel but higher than that of biodiesel fuel by using natural organic based additive with diesel fuel and palm biodiesel. Cheng et al. [240] reported a reduction of CO_2 emission for waste cooking oil biodiesel with ethanol compared to diesel fuel. Lin and Lin [238] reported a lower CO_2 emission

for three kinds of soybean oil biodiesels compared to ASTM No. 2D diesel by using CO_2 emission index.

On the other hand, some of the studies reported that CO_2 emission rises [241], [242], [192], [195], [243], [213] or remains unchanged [183], [131]. The presence of oxygen and relatively lower amount of carbon in biodiesel is the reasons behind higher CO_2 emission [244]. For example, Ulusoy et al. [241] reported that CO_2 emission increased by about 2.62% for used frying oil. Ramadhas et al. [242] reported an increase of CO_2 emission for rubber seed oil with the increases in load. Usta et al. [131] found that the CO_2 emissios of hazelnut soapstock/waste sunflower oil was very close to that of Diesel No. 2 at partial loads. In another study, Carraretto et al. [245] and Lapuerta et al. [146] evaluated the effect of greenhouse gas emission of biodiesel through the CO_2 emission life cycle. They reported that a 50–80% reduction in CO_2 emission can be caused by biodiesel compared to petroleum diesel.

2.4.3. CO emission

According to most published studies reported that CO emission reduces using biodiesel [159], [246], [206], [211], [150], [205], [247]. For example, Canakci [159] reported that CO emission reduced significantly for biodiesel compared with No. 2 diesel fuel. Wu et al. [246] found that CO emission reduced by 4–16% on average for palm oil methyl ester (PME), soybean methyl ester (SME), rapeseed methyl ester (RME), cottonseed methyl ester (CME) and waste cooking oil methyl ester (WME). Utlu and Koçak [206] reported a decrease of average 17.13% for waste frying oil (WFO) compared to diesel fuel. Puhan et al. [211] claimed a reduction of around 30% compared to diesel. However, some literature reported much higher reduction [150], [205], [247]. For example, Ozsezen [150] reported a decrease of 86.89% and 72.68% in CO emission

for WPOME and COME, respectively. Raheman and Phadatare [205] observed that CO emission was reduced by 73–94% for the karanja methyl ester (B100) and its blends (B20, B40, B60 and B80) than that of diesel. Krahl et al. [247] reported that CO emissions reduced 50% for biodiesel derived from rapeseed oil as compared to diesel fuel.

Numerous studies reported a reduction of CO emission using the biodiesel-diesel fuel blend [200], [248], [41], [141], [143], [203], [140], [50]. For example, Devan and Mahalakshmi [200] found that CO emission reduced by 37% for the 50-50 blend of paradise oil–eucalyptus oil compared to diesel. Ng and Gan [248] tested palm oil methyl ester (POME) and its blends with No. 2 diesel and found that exhaust CO improved with increasing POME proportion in the fuel blends. Rakopoulos [41] reported a reduction in CO emission with the use of bio-diesel blends of various origins with respect to that of Diesel fuel. Ozener et al. [141] found that CO emission reduced by 28%, 31%, 38% and 46% an average for, respectively, B10, B20, B50 and B100 blends of soybean oil and diesel. Vallinayagam et al. [143] reported that CO emission decreased with the increase of pine oil percentage (25%-75%) in the blends with diesel. Nabi et al. [203] investigated the exhaust emission of neem oil-diesel blends and found a lower CO emission compared with conventional diesel fuel. Buyukkaya [140] reported that the CO emission of B5 and B100 (rapeseed oil and diesel fuel blends) was 9% and 32%, respectively, lower than that of the diesel fuel. Agarwal and Agarwal [50] reported an increase in CO emission with the increasing proportion of Jatropha oil in the blends compared to diesel.

However, some studies reported no change [183], [26], [29]; while others reported significant increase in CO emission for pure biodiesel compared to diesel fuel [190], [191], [192], [216]. For example, Song and Zhang [183] found that, at partial loads, CO emission did not show any

significant difference for the increase of biodiesel content in the blends, but it varied at full load. On the other hand, Luján et al. [190] observed that the higher the biodiesel content, the greater the CO emission. Sahoo et al. [191] found an increase in CO emission for jatropha oil, while a decrease for karanja and polanga biodiesel. Fontaras et al. [192] found that the use of B50 and B100 increased the CO emission by 54% and 95%, respectively. Banapurmatha et al. [216] reported an increase in CO emission for JOME, SOME and HOME compared to diesel fuel at 80% load.

It was reported that the use of different metal based additives also led to a decrease in the CO emission of biodiesel [221], [249], [219], [231], [220] [149], [250], [233], [232]. Kalam and Masjuki [221] reported that the CO emission is lowest for B20X (added 1% 4-NPAA additive into B20) fuel as compared to B20 and B0 blends of palm oil and diesel. Mofijur et al. [249] reported 18% and 10% lower CO emission for B35 fuel with 1% NPAA additives as compared to diesel fuel and biodiesel without additives, respectively. Keskin et al. [219] found a reduction of CO emission for biodiesel fuel with added Mg and Mo based additives. In another work, Keskin et al. [231] tested Biodiesel derived from tall oil synthesized with Mn and Ni based additives and found a decrease in CO up to 64.28%. Similarly, Guru et al. [220] found that CO emission decreased by 13% when using Mg additive with chicken fat based biodiesel. Kannan et al. [149] added ferric chloride (FeCl3) as a fuel borne catalyst (FBC) with biodiesel derived from waste cooking palm oil and found that CO emission of FBC added biodiesel decreased by 52.6% compared to biodiesel without FBC. Swaminathan and Sarangan [250] reported 91% reduction in in CO emission by adding diethyl ether as an additive with fish oil biodiesel compared to diesel fuel. On the other hand, Labeckas and Slavinskas [233] reported that tCO emission increased by 16.3% and 48.0% for, SO-2E and Marisol FT, respectively. In a different study, Shi

et al. [232] found a significant increase in CO emission of biodiesel–ethanol–diesel fuel blend by using ethanol-selective catalytic reduction (SCR) .

As additives, alcohol (methanol and ethanol) were also added to biodiesel with the aim to reduce the CO emission. For example, Cheung et al. [209] reported a 6% reduction of CO emission for biodiesel and its blend with 5% methanol. Zhu et al. [95] and [228] reported that 5% blend of biodiesel with alcohol (ethanol or methanol) reduced the CO emission while high proportion of alcohol in the blends increased the CO emission. They also reported that using diesel oxidation catalyst (DOC), CO emission can be further reduced. Bhale et al. [87] also reported a decrease in CO emission for the blend of Mahua biodiesel with ethanol. Rahimi et al. [224] reported that the concentration of CO in the smoke reduced by increasing the biofuel composition of diesterol (a mixture of fossil fuel diesel (D) sun flower oil methyl ester called biodiesel (B) and bioethanol produced from potato waste (E)) . Kwanchareon et al. [97] reported that the CO emission was lowest for the blend of 80% diesel, 15% biodiesel and 5% ethanol at full engine load. Similarly, Kumar et al. [226] applied methanol in jatropha oil to a diesel engine and found that CO emission increased at low loads but decreased at high loads. Labecka and Slavinskas [251] found that the CO emission emitted from engine fuelled with three agent blends of rapeseed oil (RO) and its blends with petrol (PRO) (EPRO) increased by 39.5–18.8% and 27.5–16.1% for 5% and 7.5% blends, respectively, comparing with RO case. Qi et al. [162] tested the emission characteristics of three different fuels, B30 (30% biodiesel and 70% diesel in vol.), BE-1 (5% diethyl ether, 25% biodiesel and 70% diesel in vol.) and BE-2 (5% ethanol, 25% biodiesel and 70% diesel in vol.) and found that CO emission was slightly lower for BE-1 and BE-2 compared with B30. In another work, Qi et al. [225] reported that CO emission was slightly higher for the ethanol–biodiesel–water micro-emulsions compared with that for biodiesel.

2.4.4. HC emission

Numerous investigators reported a decrease in hydrocarbon (HC) emission when pure biodiesel was used instead of diesel [191], [198], [159], [213], [246]. For example, Canakci [159] reported that B100 (soybean oil) produced significant reduction in HC emission compared with No. 2 diesel fuel; while No. 1 diesel fuel produced lower HC emission compared with No. 2 diesel fuel. Lin et al. [198] found that a reduction in HC emission by about 22.47–33.15% for 8 kinds of VOMEs. Sahoo et al. [191] reported that HC emission for jatropha, karanja and polanga biodiesels reduced by 20.73%, 20.64% and 6.75%, respectively, compared to diesel. However, some studies reported a higher decrease in HC emission. Wu et al. [246] reported that HC emission for 5 different biodiesels reduced by 45–67% on average as compared to diesel fuel. Puhan et al. [213] reported 63% decrease in HC emission for biodiesel compared with diesel.

Numerous studies reported that HC emission decreased for biodiesel and its blends [183], [188], [191], [200], [143], [141], [252], [142]. Devan and Mahalakshmi [200] reported that HC emission reduced by 34.5% for the 50-50 blend of paradise oil and eucalyptus oil. Dhar et al. [142] found that HC emission for biodiesel fuelled engine were lower than mineral diesel for neem oil and diesel blends. Vallinayagam et al. [143] tested pine oil biofuel and their blends of 25%, 50%, and 75% with diesel in a diesel engine and reported a reduction of 30% in HC of 100% pine oil at full load engine conditions. Ozener et al. [141] tested biodiesel produced from soybean oil and its blends (B10, B20, B50) in a diesel engine and found that biodiesel significantly reduced unburned total hydrocarbons (THCs) emission. Sahoo et al. [191] found a reduction on the order of 32.28%, 18.19% and 20.73% for JB20, JB50, JB100,I respectively.

Several other studies reported that the emission of HC increased for biodiesel as compared to diesel [190], [192], [139], [216], [41]. Kumar et al. [139] reported that HC emission increased by 10% for jatropha oil methyl ester as compared to diesel fuel. Fontaras et al. [192] observed 58% increase in HC emission for pure biodiesel compared with diesel. Banapurmatha et al. [216] reported higher HC emission for JOME, SOME and HOME biodiesels as compared to the standard diesel fuel. Similarly, Luján et al. [190] found an increase of 22.9%, 17.7% and 16.4% in HC emission for B30, B50 and B100, respectively, compared with diesel. Rakopoulos et al. [41] observed an increase in HC emission for the blends among vegetable oils and a decrease in HC emission for the bio-diesel blends compared to the neat Diesel fuel.

Some investigators added metal based additives to improve biodiesel HC emission [149], [253], [254]. Fattah et al. [253] found that the addition of BHT and BHA reduced the HC emission by, respectively, 23.81% and 21.21% compared to biodiesel without additives. Kannan et al. [149] used ferric chloride ($FeCl_3$) as a fuel borne catalyst (FBC) for biodiesel derived from waste cooking palm oil and found a reduction of 26.6% and 50% of HC emission for FBC added biodiesel compared to biodiesel without FBC and diesel fuel, respectively. Shi et al. [254] used two diesel oxidation catalyst assemblies after Ag/Al2O3 converter to remove HC from biodiesel–ethanol–diesel fuel blend.

Methanol and ethanol were also used as an additives to biodiesel with aim to examine their effect on HC emission [87], [209], [95], [224], [184], [225], [162], [97], [226], [228]. Bhale et al. [87] reported that areduction in HC emission for 10% and 20% blend of ethanol-biodiesel was lower than 5.25% and 9.15%, respectively. Kwanchareon et al. [97] reported that a higher percentage of biodiesel led to lower HC emission while it increased with a higher percentage of ethanol.

Rahimi et al. [224] found that the concentration of HC in the smoke was reduced by increasing the biofuel amount in diesterol. However, Kim and Choi [184] found that the blend of 15% biodiesel, 5% bioethanol and 80% diesel produced a lower HC emission than the blend of 20% biodiesel and 80% diesel. Kumar et al. [226] HC emission increased at low loads but decreased at high loads when methanol is added with jatropha oil in a diesel engine. Additionally, Cheung et al. [209] found that the HC emission of 5% and 10% blend of methanol-biodiesel were lower than that of biodiesel and higher for 15% methanol-biodiesel blend. Zhu et al. [95] tested pure biodiesel and biodiesel blended with 5%, 10% and 15% of ethanol or methanol and found that with high percentage of alcohol in the blends, the HC emission could increase but the use of 5% blends could reduce the HC emission. They also reported that the diesel oxidation catalyst (DOC) can reduce HC emission furthermore. Similarly, in another work, Zhu et al. [228] reported that with high percentage of ethanol in the BE blends, the HC emission could increase while the use of BE5 could reduce the HC emission. Qi et al. [162] reported a slightly higher HC emission for BE-1 (5% diethyl ether, 25% biodiesel and 70% diesel in vol.) and BE-2 (5% ethanol, 25% biodiesel and 70% diesel in vol.) compared with B30 (30% biodiesel and 70% diesel in vol.). In another work, Qi et al. [225] used ethanol–biodiesel–water micro-emulsions in a diesel engine and found a slightly higher HC emission for the micro-emulsions than that for biodiesel at low and medium engine loads.

2.4.5. PM and smoke emissions

It has been reported that use of biodiesel instead of diesel causes a reduction in PM emission [198], [246]. For example, Lin et al. [198] reported a significant reduction (ranging from 50% to 72.73%) in the smoke emission for 8 kinds of vegetable oil methyl esters. Wu et al. [246] found

a reduction in PM emission ranging from 53%–69% for five pure biodiesels compared with the diesel fuel. Generally, PM emission decreases significantly with increasing biodiesel proportion in blends. For example, Sahoo et al. [191] reported that the use karanja blends caused a maximum reduction in smoke by 68.83% with respect to diesel. Similarly, maximum decrease in smoke of 64.28 and 69.48% for jatropha blends and polanga blends, respectively. Buyukkaya [140] found a reduction of a maximum of 60% for the smoke opacity of pure rapeseed oil and its blends of 5%, 20% and 70% with standard diesel fuel. Luján et al. [190] reported a reduction in PM emission of 32.3%, 42.9% and 53% for B30, B50 and B100, respectively. Additionally, Haas et al. [255] reported a decrease of 20% and 50% in PM emission for B20 and B100 blends of biodiesel, respectively. Canakci [195] showed that 20% blend of soybean oil methyl ester (SME) and diesel produced less smoke than No. 2 and No. 1 diesel fuel, while SME100 produced the least smoke. Devan and Mahalakshmi [200] found a reeducation of smoke emission by 49% for a 50-50 blend of methyl ester of paradise oil and eucalyptus oil. Tsolakis et al. [151] found a reduction of smoke for both advanced combustion and exhaust gas recirculation (EGR) for different diesel/RME blends. Vallinayagam et al. [143] reported a reduction of smoke for Pine oil biofuel and their blends (25%, 50%, and 75%) with diesel where a maximum in smoke emission of 70% was reported for 100% Pine oil. Nabi et al. [203] reported a reduction of smoke emission for diesel-NOME blends associated with the oxygen content in the fuel. Lapuerta et al. [256] reported 25% reduction in PM emission for the B25 blends compared to B50, B70 and B100 biodiesel blends.

Some investigators reported a slight increase in PM emission [214], [192], [204], [151], [50]. For example, Kalligeros et al. [214] reported that the PM emission for the 10% blend of sunflower and olive oil was maximum, while 50% blend produced the minimum PM emission. Aydin and

Bayindir [204] reported that the PM emission increased with the higher content of biodiesel in the blend with diesel. Similarly, Tsolakis et al. [151] found a small increase of smoke for pure RME and 50/50 (by volume) blend with diesel. In addition, Smoke opacity was found to increase with increasing the proportion of Jatropha oil in the blends compared to diesel [50].

Some literatures reported the effect of metal based additives, alcohols such as ethanol or methanol, and bio-solution additive on PM and smoke emission [96], [146],[219], [220], [222], [209], [163], [223], [257], [95], [224], [184], [251], [164], [137], [225], [162], [231], [234], [149], [258], [233]. For instance, Subbaiah et al. [259] found that the smoke opacity is 2.55% higher for the blend of 5% ethanol-10% biodiesel-diesel compared to diesel fuel. Keskin et al. [260] found a decrease in smoke emission by 29.4% using cobalt (Co) based additive with tall oil biodiesel compared to diesel. Qi et al. [225] reported a drastic reduction in smoke by using ethanol–biodiesel–water micro-emulsions in a diesel engine. In another work, Qi et al. [162] used diethyl ether and ethanol as additives to biodiesel/diesel blends in a diesel engine and found drastic reduction in smoke with both BE-1 (5% diethyl ether, 25% biodiesel and 70% diesel in vol.) and BE-2 (5% ethanol, 25% biodiesel and 70% diesel in vol.) blends. Chen et al. [257] found that a mixture of 16 vol% bio-solution + 20 vol% palm-biodiesel + 64 vol% premium diesel fuel with an additional of 1 vol% surfactant reduced emission of PM by 90.1%. Keskin et al. [219] reported that the addition of metal based additives such as Mg and Mo with biodiesel blends showed better effect on PM and smoke (decreased by 30.43%) due to catalyst effect. In another work, Keskin et al. [231] found a decrease in smoke opacity of up to 30.91% by using biodiesel derived from tall oil synthesized with Mn and Ni based additives. Similarly, Gürü et al. [220] reported a 9% decrease in smoke emission using synthetic Mg additive with chicken fat based biodiesel. However, Ryu [222] found a difference in exhaust emission by using

antioxidants compared to biodiesel without antioxidants. Kass et al. [234] used biodiesel-water emulsions and found that the total PM mass was lowered dramatically for 27% EGR conditions. Kannan et al. [149] investigated the use of ferric chloride (FeCl3) as a fuel borne catalyst (FBC) for waste cooking palm oil based biodiesel and found a decrease by 6.9% in smoke emission of FBC added biodiesel compared to biodiesel without FBC. Oxygenates, such as methanol and ethanol were added to biodiesel to improve the PM emissions [146], [209], [95], [184], [164], [137]. On the other hand, some studies reported a blend of biodiesel–ethanol–diesel caused a significant reduction in PM emission [163], [223], [224], [96], [251]. Chen et al. [163], found that both smoke and PM can be reduced with the increase of ethanol in the ester–ethanol–diesel blended fuel. Rahimi et al. [224] reported that the smoke reduced by increasing the biofuel composition of diesterol. Kim and Choi [184] found 50% reduction of smoke emission with the use of the bioethanol–diesel blend in a diesel engine. Labecka and Slavinskas [251] found that, for three agent blends Ethanol-petrol-Rapeseed Oil (EPRO5–7.5), the smoke opacity were lower by 3.3–9.0% and 24.1–17.6% for 5 vol%, 7.5 vol% of Rapeseed oil, respectively, compared with RO case. Lu et al. [164] found a simultaneous reduction of about 35–85% in smoke by using premixed ethanol on a biodiesel-fueled engine compared to that of a biodiesel-fueled engine. Anand et al. [137] reported a significant reduction in smoke emission with the karanji biodiesel-methanol blend in a diesel engine. However, some literature reported an increase in PM emission. For example, Shi et al. [258] observed that PM emission increased by 14% by using EB-diesel while the addition of SCR catalyst with EB-diesel could provide the assistances for PM emissions control. Labeckas and Slavinskas [233] found an increase of 35% and 70% in smoke opacity for shale oil blended with Marisol FT (Sweden) and SO-2E (Estonia) fuel additives, respectively.

2.5. Summary of the literature

It is clear from the above reviewed literature that a considerable amount of research has been carried out on improving the cold flow properties, evaporation and combustion characteristics as well as emission of biodiesel and their blends for potential use in engines as an additive or alternative to conventional fuels. From the literature reviewed above, it is evident that the cold flow characteristics of biodiesel can be improved by blending with petroleum fuel or vegetable oils, using additives, winterization, modification of biodiesel feedstock via the addition of branched alcohols and some other treatments such as thermal cracking, urea complexation, epoxidation and alkoxylation. All of these proposed methods, which could improve the cold flow properties of biodiesel to a certain level, pose other challenges. For example, winterization, which is found to improve biodiesel properties for cold weather conditions, is less acceptable because of its negative effect on yields. The use of some additives seems to be restricted because of their slight influence on cloud point as it is more important for improving low temperature flow characteristics compared to pour point. Moreover, the use of different additives is quite costly which increases the cost of biodiesel. Blending biodiesel with vegetable oil is restricted because it is mainly applicable to biodiesel derived from certain feedstocks only. Blending with petroleum fuel is restricted to lower biodiesel blends (up to 30 vol%) with cloud point nearing up to around 10 ^{0}C [60] because mixing with fossil fuel do not change the chemical nature of the blends. On the other hand, very limited investigations are available regarding the use thermal cracking, urea complexation, epoxidation and alkoxylation for improving the low temperature properties of biodiesel. Although significant progress has been made on low-temperature flow problem of biodiesel, it is still an unresolved issue.

In addition, there are several studies, which dealt with the improvement of emission and combustion characteristics of biodiesel, did not reach clear results due to the dependency on biodiesel types, engine types, operating and maintenance conditions, testing methods, injection system, etc. In regard to the emission of biodiesel in diesel engine, it has been found that the use of biodiesel or its blends can reduce HC, CO and PM emissions, but increases the NOx emissions due to higher oxygen content and shorter ignition delay of biodiesel in comparison with the base line petroleum diesel fuel. Although the increase in NO_x emission can be controlled by adding appropriate additives such as ethanol, it is very difficult to reduce NOx and PM emission at the same time due to the nature of diffusion combustion [261]. Several studies have been performed to investigate the combustion characteristics either via the vaporization and combustion of a single droplet or in piston-cylinder engine. Most of these studies reported that biodiesel has shorter ignition delay (ID), lower heat release rate (HRR) and lower calorific value compared to diesel. The difference in the combustion behavior between biodiesel and diesel is due mainly to the variance in viscosity, volatility and compressibility. Moreover, studies on the evaporation and combustion behaviour of biodiesel blends under different engine conditions are still lacking.

Therefore, the main objective of the present research, which builds upon the aforementioned reviewed literature, is to further develop potential cost effective additives from different feedstock (fatty acid methyl or ethyl esters, and/or fatty acid methyl or ethyl ethers), and evaluate their effects on biodiesel properties when blended with canola-derived biodiesel. The ultimate aim of the research presented in this thesis is to determine the properties and some combustion characteristics of biodiesel fuel and its blends.

Chapter 3. EXPERIMENTAL TEST RIGS AND TEST CONDITIONS

The experimental apparatus to determine the fuel vaporization rate will be discussed in this section; however, certain aspects will only be mentioned in brevity as the majority of the details were reported in [262], [263]. The test rig for determining the fuel heat of combustion (that is, the lower heat value (LHV)) is also described below.

3.1. Test Rig for Fuel Vaporization

3.1.1. Spherical Chamber

The experimental setup used for testing the fuel evaporation consisted of a spherical combustion chamber/vessel (see Figure 3.1). The chamber has a capacity of about 29 liters with an outer and an inner diameter of 405 mm and 380 mm, respectively. Stainless steel was selected as the chamber material to protect the inside of the chamber from corrosion potential of combustion products. The vessel wall thickness was selected to withstand elevated pressure conditions [262], [263].

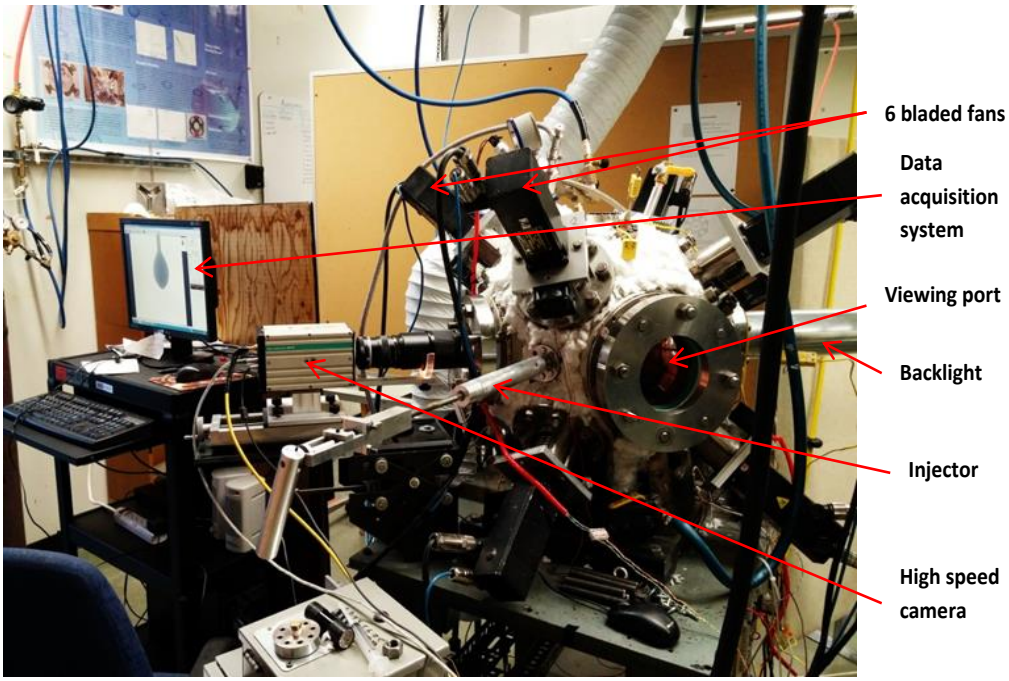

Figure 3.1: A real image of the combustion chamber (spherical chamber)

The chamber has two pairs of viewing ports, four pairs of flanges for mounting fan blade assemblies and ten additional ports to mount sensors and probes (see Figure 3.2). All these ports were welded to the outside surface of the spherical vessel. The two pairs of viewing ports are positioned 90-degree apart from each other; two of them have five-inch inner diameter while the other two have four-inch inner diameter. The 4-inch viewing ports are covered with quartz windows [262], [263] which are designed to enable high quality optical visualization and imaging at elevated temperature and pressure conditions. The 5-inch viewing ports can be used either to mount the heating system plates (described below) or to provide additional viewing using quartz windows in order to conduct flow field measurements using Particle Image Velocimetry (PIV) and Laser Doppler Velocimetry (2D-LDV). The optical quartz glass has a thickness of 40 mm which is capable of withstanding high pressure conditions [262].

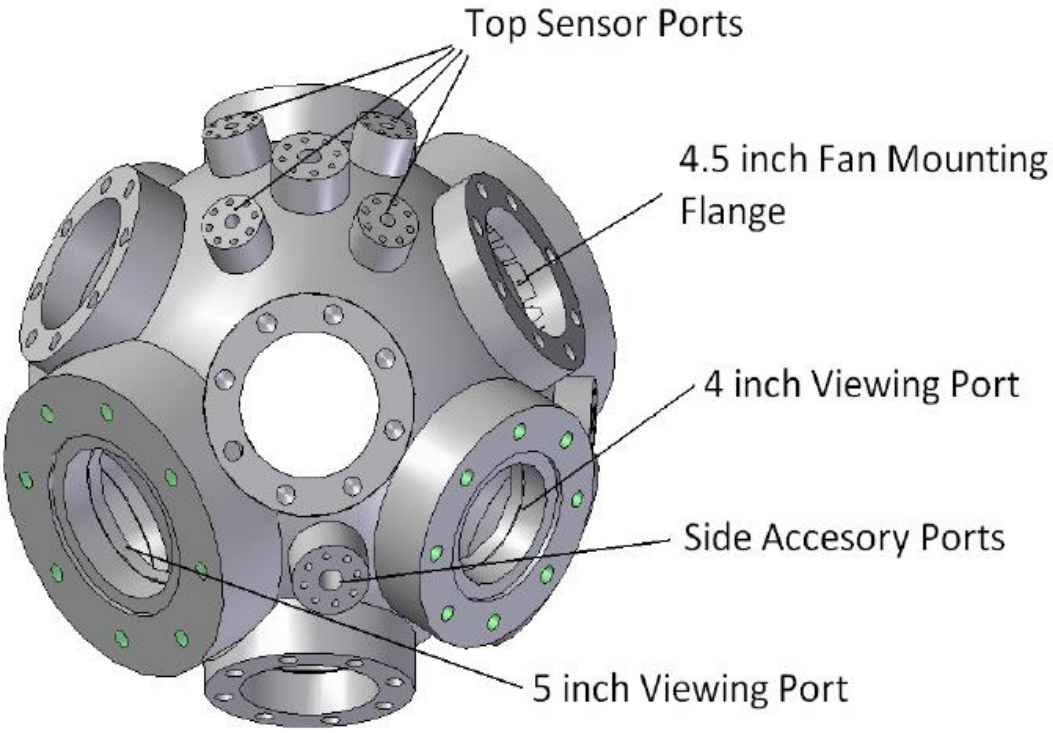

Figure 3.2: Schematic diagram of the spherical chamber with flanges arrangement [262]**,** [263]**.**

The smallest ports (see in Figure 3.2) can be grouped as top sensor ports, side accessory ports and one bottom accessory port. The top center port was used to mount a quartz fibre hold for droplet experiments (described below). The other four adjacent top ports can be used to mount pressure gauge, pressure transducer, mechanical pressure release valve and the remaining port is a spare one which is sealed with a plumbing plug (see Appendix A for details). The mechanical pressure release valve is used for safe operational purpose which only actuates if the pressure inside of the chamber exceeds the set pressure. There are 4 side accessory ports, where one port was used to mount a supply line for compressed air or nitrogen, another port was used for the droplet injector/ignition system (described below) and the final two ports were each used to mount a thermocouple (see Appendix A for details) for each respective heating system plate. The

bottom accessory port was used as scavenging/exhaust port, which facilitates the drainage of any fluids that may build up after the testing.

3.1.2. Sealing Surfaces

The spherical chamber must be properly sealed to maintain the set ambient pressure and hence prevent gases leakage. There are 3 types of seals named as gasket seals. O-ring seals (both static and dynamic) and shaft seals; which are used to seal most of the flanges of the spherical chamber. Extreme-Temperature Silicone Rubber Gasket seals were used to seal the quartz windows which were originally sealed using NA60 gaskets (see Appendix B). Silicone Rubber Gasket (see Figure 3.3) has a thickness of either 3/32 or 3/16 inches with the thinner used at low pressure and the thicker for elevated pressure test conditions.

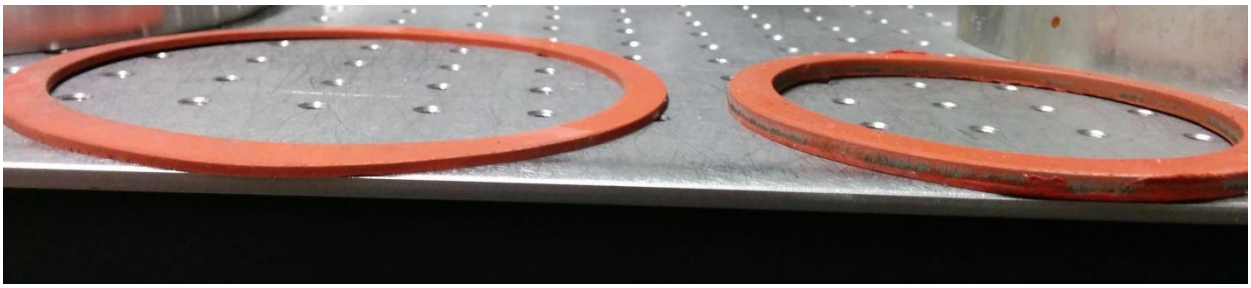

Figure 3.3: Silicon rubber seal

The rest of flanges were sealed using o-rings. The majority of the o-ring seals were static seals, with one exception being the droplet injector/ignition system which used a dynamic seal [262], [263]. All of the o-ring seals with the exception of the heating system plates were made of Viton Fluoroelastomer (see Appendix B), while silicon materials was used for the heating system plates [2]. The o-rings chosen for the heating system plates were made of silicon because of the proximity to the heating elements which then requires an o-ring with a higher temperature rating

(see Appendix B) [264]. The seals, which were used for the fan shafts to prevent leakage from the chamber, were made of poly-amide filled Teflon (see material specs/properties and manufacturer's contact info – see Appendix B) [262]. These seals were designed and manufactured in house [262].

3.1.3. Turbulence Generation and Control System

The chamber was designed to generate isotropic and homogeneous turbulence under elevated pressure and temperature conditions [262]. The turbulent flow-field is generated by four pairs of axial opposed fans located at a distance of 200 mm across from one another inside the spherical chamber [262]. Each six bladed fan is capable of spinning up to 6000 RPM, which can be driven by a servomotor connected via a fan transmission assembly [262]. The 4.5-inch fan mounting flanges are used to mount each of the 8 fans with their motors [262]. Each servomotor is synchronized by manual adjustment of the servomotor drive's amplifier. The synchronization of all the eight fans is within ±5 revolutions per minute (RPM) which can be measured using a Stroboscope from Shimpo Instruments (see Appendix A) [262].

3.1.4. Pressure and Heating Control System

The vessel can be pressurized using nitrogen supplied from a compressed cylinder. Test pressure can be varied from atmospheric pressure up to 16 bar, where 16 bar was the highest ambient pressure used due to limitations of the gasket material that seals the quartz windows. The set pressure inside the vessel was controlled using a Cecomp Electronics pressure gauge having an accuracy of ±0.25% of full scale (see Appendix A) [262].

The experimental setup was also designed to operate at elevated temperature of the gas inside of the spherical chamber in order to create test conditions that are realistic to many combustion systems [264]. The nitrogen inside the vessel was heated using a 2-kW bank of Etirex heating elements (seen in Figure 3.4) and the set temperature was controlled using an Omega K-type thermocouple (see Appendix A) with an accuracy of ± 0.75% of full scale [264]. The maximum ambient temperature achieved was 200^{o} C due to the seal materials used on the experimental setup.

Figure 3.4: Heating plate [264]**.**

The chamber inner walls are insulated by alumina-silica fibers with a thickness of 0.125 inches to reduce the heat loss. The insulation was placed along the inside wall of the chamber using a high temperature silicone adhesive (see in Figure 3.5) [264]. Insulation was also placed onto the inside face (between the heating elements and the steel plate) of the heating plates to further aid

in minimizing heat loss. No insulation behind the fans was used as it is susceptible to rip apart at high rotational speeds (high levels of turbulence) under elevated ambient pressure.

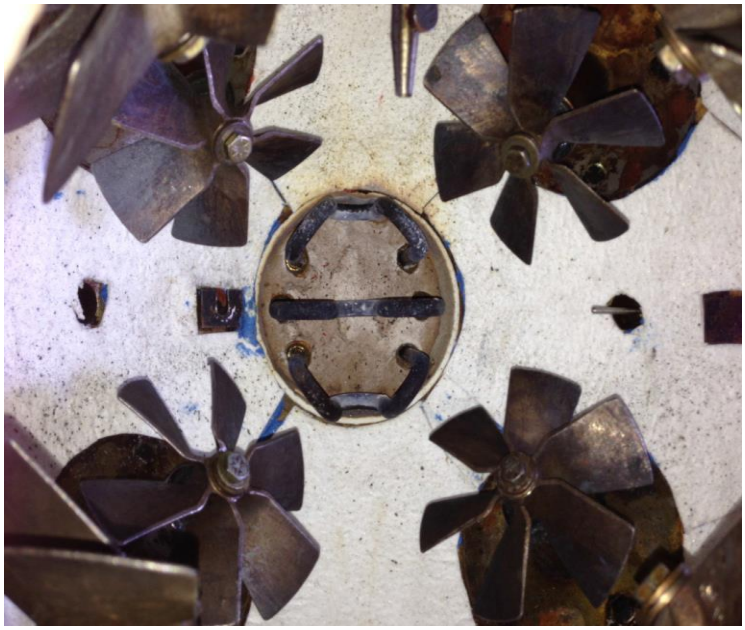

Figure 3.5: Insulation of inner chamber wall.

Insulation of the outside surface/walls of the chamber was performed using a blanket made from alumina-silica fibers with an approximately of 1 inch thickness. The external insulation was cut into rectangular shapes that fit in between the various flanges of the chamber as well as on top of the accessory ports with two layers of the insulation were installed over all accessible areas to further reduce heat loss (see Figure 3.6). Additionally, the flange faces for each of the viewing ports had a layer of the 0.125 inch thick insulation attached to the surface using a high temperature silicone.

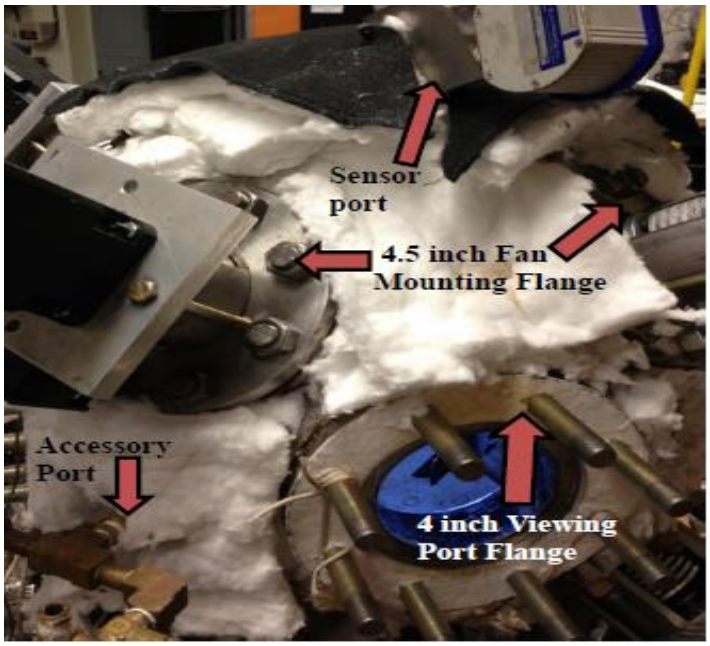

Figure 3.6: Outside view of chamber with external insulation.

3.1.5. Droplet Formation and Suspension System

A single droplet was formed in the centre point of the chamber using an in-house designed retractable injection system (see in Figure 3.7) capable of operating at elevated pressure conditions [262]. The system is composed of a syringe pump mounted on the end of an actuating tube and cylinder assembly [262]. Approximately 10 ml of liquid fuel can be stored in the injector which is fed through a small diameter tube that runs through the centre of the large support tube. At the end of the tube there is an injection head which supports a small 0.254 mm diameter needle used for forming the droplets [262]. The droplet was formed by pumping/discharging liquid through the needle.

Figure 3.7: Retractable Injector [262]**.**

The droplet is deposited onto the tip of quartz filament (see in Figure 3.8) and suspended in the center of the combustion chamber/vessel [262]. The droplet initial diameter ranges between approximately 1 mm and 1.50 mm. The quartz filaments employed ranged between 150 to 290 μm at the stem with an approximately 400 to 500 μm diameter spherical nodule/sphere at the tip to support the droplet. Several advantages are associated with the use a quartz fibre. For example, it provides a rigid support even though it has a very small diameter. It will not be affected by or take part in combustion because of chemical unitability. Moreover it has a low thermal conduction coefficient [262], [263].

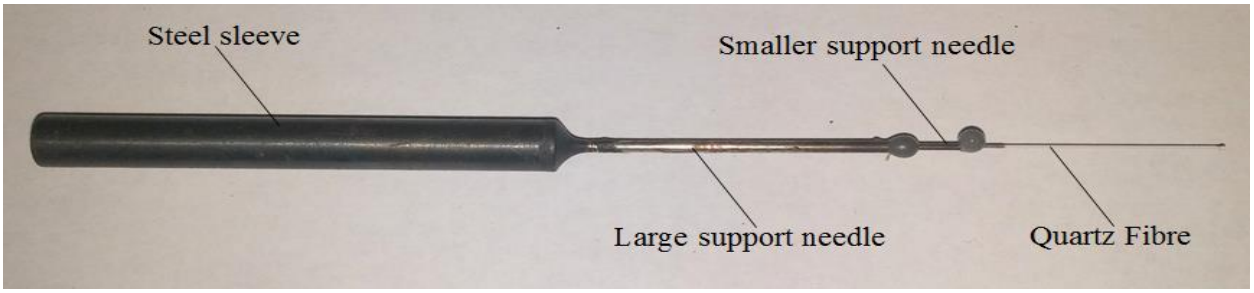

Figure 3.8: Quartz Fiber [262]

A reinforced holder was required in order to hold the fibre rigidly (see Figure 3.9). The holder is comprised of a lock down thumb screw and a fibre assembly to chamber extension [262].

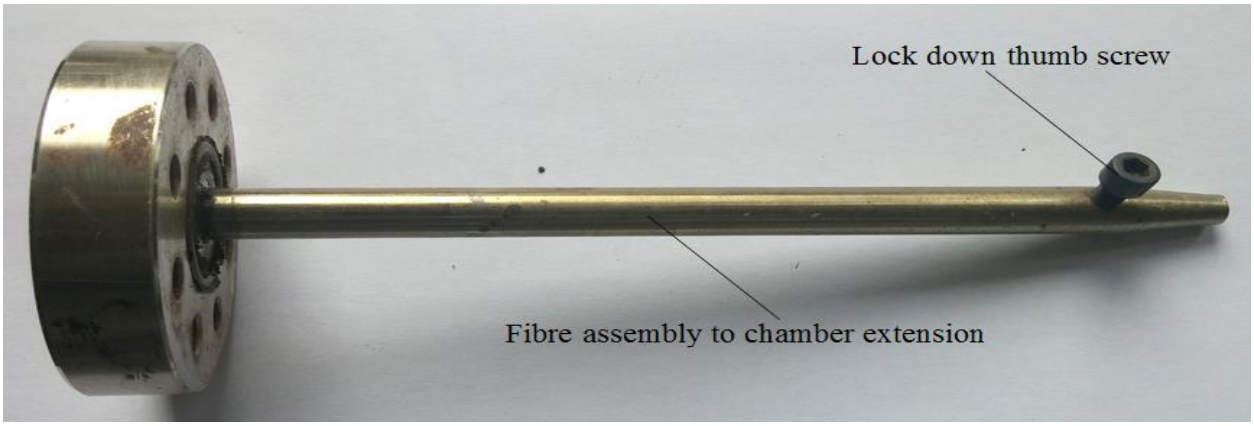

Figure 3.9: Fiber holder [262]

3.1.6. Experiment Control Panel System

LabView software is used to control and monitor the spherical combustion chamber (see Figure 3.10) [262]. Each of the sensors can be monitored as well as the fan speed can be controlled by using the main panel of LabView on the computer screen. It is possible to get high speed synchronization between systems as the control panel is configurable and automation capable.

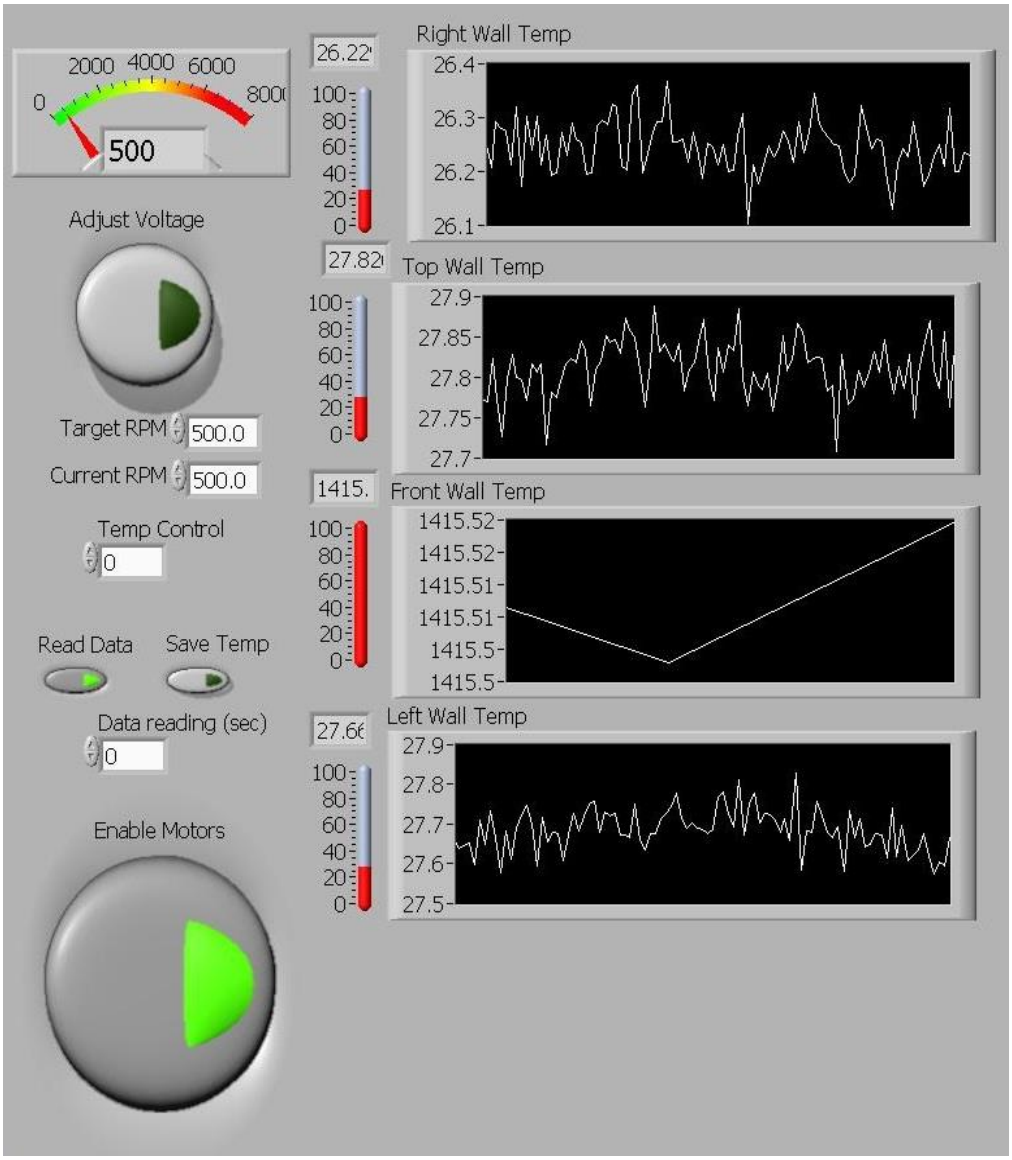

Figure 3.10: LabView™ Control Panel [262]

The camera timing control panel provides the control of Nanosence MKIII high speed CCD camera (see Figure 3.11). This control panel helps to adjust the frame speed of the camera for different experimental conditions. Camera control is needed in order to adjust the number of frames per second for each specific droplet vaporization event, as some are slow and others are fast.

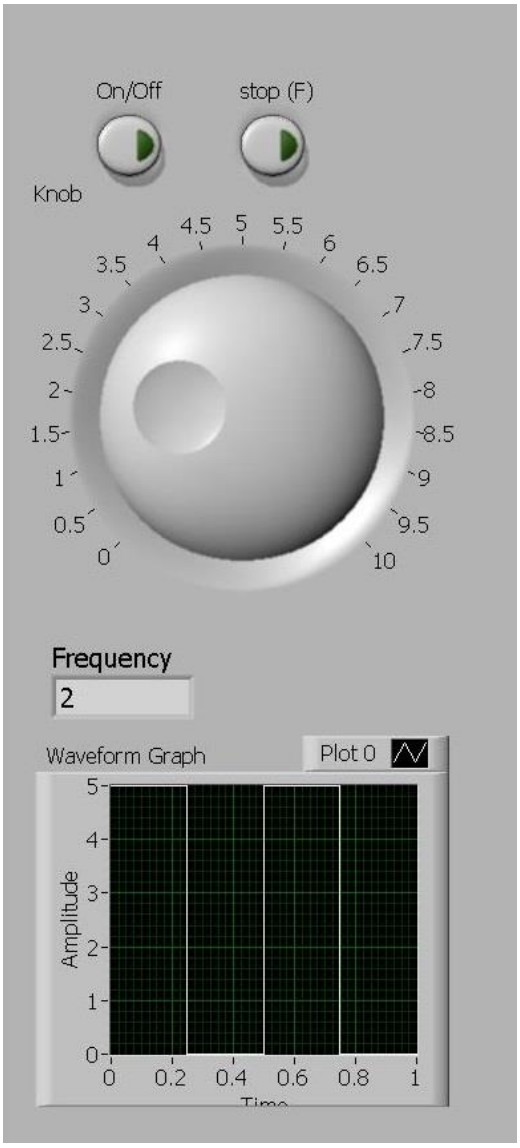

Figure 3.11: High Speed Camera Timing Control Panel

3.2. Image Capture Setup and image processing

A schematic of the droplet formation system and image capturing setup is shown in Figure 3.12. In order to image the droplet evaporation process (that is, the regression of the droplet image captured by the camera), a halogen lamp was used to backlit the droplet surface so to enhance the image contrast. Moreover, the halogen lamp can provide a more intense light background, which

in turn helps to optimize the contrast of the droplet with respect to the rest of the image background. A Nanosence MKIII high speed CCD camera is used to capture the temporal regression of the projected droplet surface area. The camera has a maximum of 1000 frames per second at full resolution of 1280 x 1024 pixels. Three experiments were carried at each test condition, and the results were repeatable to less than ±7%. An uncertainty error analysis is provided in appendix D.

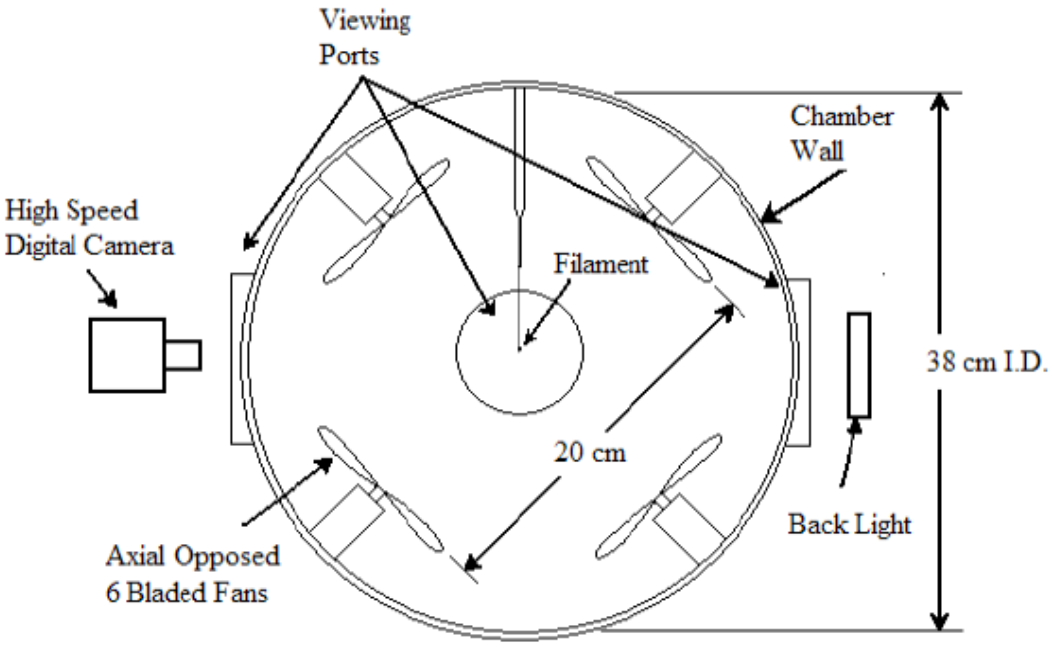

Figure 3.12: Schematic diagram of image capture setup in the high pressure Spherical vessel/chamber [262]**,** [263]

An in-house developed Matlab code was used to determine the droplet size by analyzing the image contrast and defining the droplet surface area [262] [264]. The method uses a calibration image of a ruler in place of where the droplet is suspended onto the fiber, that is in the centre of the chamber, which is subsequently printed and measured on a paper using a ruler (see Figure 3.13). This uses edge detection in combination with closure conditions for the upper and lower

edges of the droplet. The droplet projected surface area, which was not circular in shape (droplet departs from sphericity due to gravity forces), was then calculated in pixels and converted into volume from which the droplet instantaneous diameter was deduced. At least three experiments were carried at each test condition, and the results were found repeatable to less than ±5%. An uncertainty error analysis is provided in appendix D.

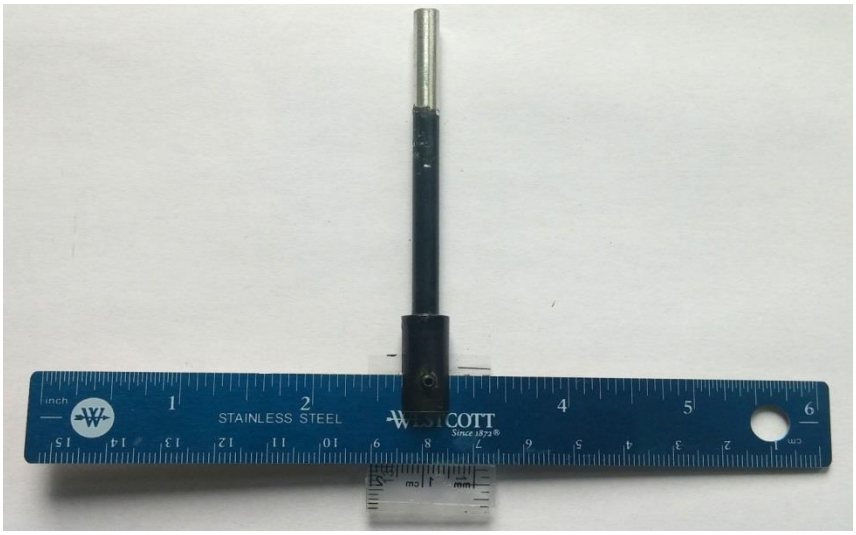

Figure 3.13: Calibration ruler

3.3. Bomb Calorimeter

The experimental setup, which was used for determining the fuel heat of combustion (called also lower heating value (LHV)), consisted of an "IKA Isoperibol bomb calorimeter" where the combustion occurs at high pressure (Figure 3.14). It is a sealed container designed to measure the heating value of liquid fuels. A carefully weighed sample (1.00 g) of a substance (i.e., liquid fuel) is placed inside the bomb in contact with an igniter. The bomb is then filled up with oxygen to a pressure of 30 bar, sealed, and placed into a known amount of water. Burning takes place by igniting the substance with an electric current which is passed through a wire. The heat released raises the temperature of the calorimeter and its surrounding water as the combustion takes place.

The temperature difference of the water is measured by a thermocouple from start to finish. In order to make this determination the effective heat capacity of the bomb calorimeter must first be calibrated by measuring burning a standard material of known heat of combustion. Benzoic acid of high purity is usually employed for calibration. The temperature rise due to the sample is noted, and the number of joules of heat released in the combustion is calculated. These two values enable one to calculate the heat capacity of the calorimeter system. This is then used to calculate the heat of combustion of any liquid material/fuel. Additionally, corrections for the combustion of the fuse wire, formation of nitric acid, exchange of heat between the calorimeter and its surroundings, and mechanical energy added to the system by the stirrer must be applied if an accurate measurement of the heat of combustion is to be made. Three experiments were carried out for each sample, and the results were repeatable to less than ± 2%. An uncertainty error analysis is provided in appendix D.

Figure 3.14: Schematic diagram of the high-pressure bomb calorimeter and Combustible crucible

3.4. Test Conditions

Fuel vaporization test conditions explored in the present study can be divided into three types. The first one was performed in quiescent atmospheric pressure by varying the ambient

temperature from room temperature up to 448 K, and the second one was conducted by varying the ambient pressure from 1 bar up to 16 bar in a hot atmospheric quiescent environment (i.e., 373 K). The third one consisted of varying the turbulent flow intensity by increasing the fan blades rotational speed from zero up to 2000 rpm in a hot atmospheric environment (i.e., 1 atm, 373 K) and 1 bar. The experimental tests were performed using different blends of canola biodiesel which consisted of 5%, 10%, 15% and 20% (by volume) of the novel fuel in canola biodiesel. Two types of novel liquid fuels were used for the blending. 3-hydroxyl fatty acid methyl and ethyl esters (named 3-OH FAME C4, C6, C8, C10 and C12), and 3-hydroxyl fatty acid methyl and ethyl ethers (1,3-dimethoxyoctane and 1,3-dimethoxydecane referred hereafter 1,3-DMO and 1,3-DMD, respectively). All the novel fuels were prepared in collaboration with the Dr. Sorensen's lab in the Department of Chemistry and Dr. Levin's lab in the Biosystems Engineering, at the University of Manitoba. The test conditions are provided in Tables 3.1 and 3.2 for each fuel sample, where q is the turbulent kinetic energy [262] and [264].

Droplet diameter d_0 (mm)	**$\sqrt{q}$ (m/s)**	**P_∞ (bar)**	**T_∞ [K]**
1.00−1.50	0	1	423-448

Table 3:1: 3-hydroxyl fatty acid methyl and ethyl esters droplet and flow test conditions

Droplet diameter d_0 (mm)	**$\sqrt{q}$ (m/s)**	**P_∞ (bar)**	**T_∞ [K]**
1.00−1.50	0−1.86	1−16	295−423

Table 3:2: 1,3-DMO and 1,3-DMD droplet and flow test conditions

Chapter 4. RESULTS AND DISCUSSION

4.1. Introduction

This chapter presents the results of the vaporization process of the novel biofuel substances/fuels reported in chapter 3 and recalled below, as well as their blends with biodiesel. These results include also the heat of combustion of these pure fuels and blends. Some other lab fuel properties were also obtained externally and will also be presented. Two types of biofuels are used, named as 3-hydroxyl fatty acid methyl and ethyl esters (3-OH FAME C4, C6, C8, C10 and C12) and 3-hydroxyl fatty acid methyl and ethyl ethers (1,3-dimethoxyoctane, 1,3-dimethoxydecane). Different evaporation characteristics such as droplet time histories and evaporation rate are presented. Moreover, the droplet evaporation rate and the fuel properties of 3-hydroxyl fatty acid methyl and ethyl ethers are compared with some conventional fuel such as ethanol, biodiesel and decane.

4.2. Droplet evaporation

(a)

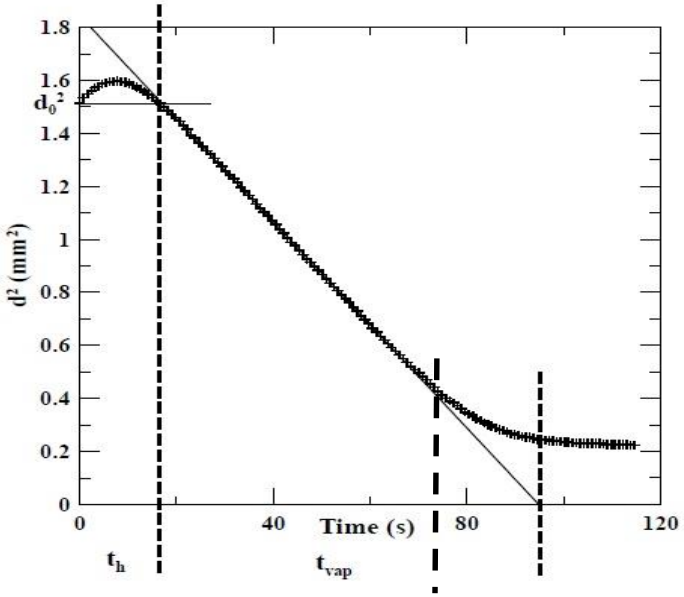

(b)

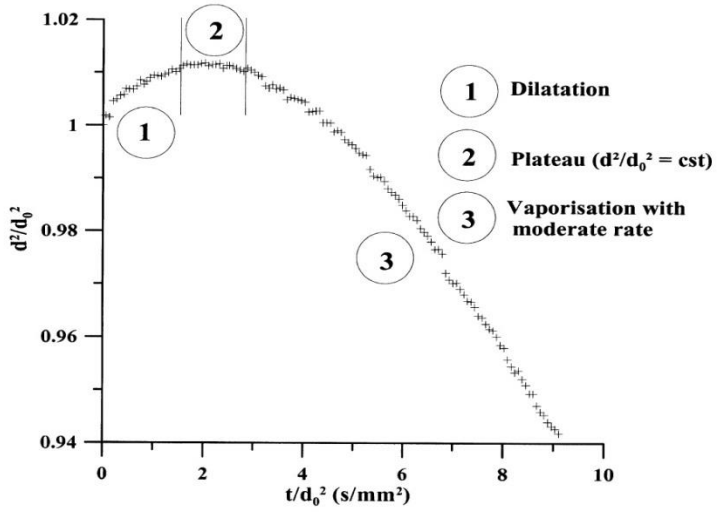

Figure 4.1: Typical time histories of liquid fuel droplet heating and vaporization at high temperature and pressure by (a) Nomura et al. [265]**, (b) Morin et al.** [115]**.**

Fig. 4.1 shows typical time histories of the vaporization of a liquid fuel droplet at high pressure and temperature; it is expressed in terms of droplet squared diameter versus droplet evaporation time. Since it is difficult to generate a fuel droplet with exactly the same diameter in all experiments, the droplet diameter was normalized by the initial droplet diameter as well as the evaporation time. This is because the droplet lifetime is strongly affected by the droplet initial diameter. In general, upon the injection/formation of droplet inside the combustion chamber, the droplet heats up (Figure 4.1), and starts evaporating as soon as its surface reaches equilibrium (Wet-Bulb) temperature. The time histories are composed of three stages. The first consists of heating period, which can be divided into droplet dilatation (maximum increase in initial diameter with a positive slope), a plateau ($d^2=d^2_0$ = constant) with a zero slope, and evaporation with a moderate rate. The second phase occurs after the heating period and it is characterized by the time period during which the droplet squared diameter drops continuously with increasing

time. In general (with the exception, e.g., at high pressure or temperature conditions (e.g. [118]), after the heating period, the droplet squared diameter follows a linear variation with time, that is steady-state, where the negative value of the slope is defined as the vaporization rate following the d^2-law (e.g., [266] [267] [263]. The d^2-law model can be termed as "Quasi-Steady model" demonstrated that, during the gasification process, the droplet surface area represented by the droplet-squared diameter varies linearly during its lifetime [267]. The last stage is the portion of the time history represents the vaporization of the heaviest components of the liquid droplets, and thus does not follow the d^2-law (see Fig. 4.1a). It is also possible that some liquid fuels do not exhibit a linear variation of d^2 with time, such as diesel and biodiesel especially at relatively warm temperatures, and blends [264]. Therefore, in this study, the evaporation rate is estimated by using a linear fit of the linear curve following the classical d^2-law to describe the evaporation process. However, for blends, where the continuous variations of the droplet interior and surface properties prohibits the establishment of the d^2-law, and thus the droplet lifetime is used instead to determine the evaporation rate for the blended fuels.

4.2.1. 3-hydroxyl fatty acid methyl and ethyl esters

4.2.1.1. Droplet evaporation of pure fuels

Figure 4.2 shows the time histories of the normalized d^2 for C4-OET, C4-OME, C8-OET and C8-OME. For all the cases C4-OME shows the maximum evaporation rate compared to the other fuels. These tests were conducted at different ambient temperatures (ranging from 423 K to 448 K) and standard atmospheric pressure. The droplet diameter followed a linear decrease which indicates that the time histories follow the d^2-law. This scenario is similar at different ambient

temperatures. Moreover, no significant heating period is observed when varying the ambient temperature except for C8-OME at 448 K.

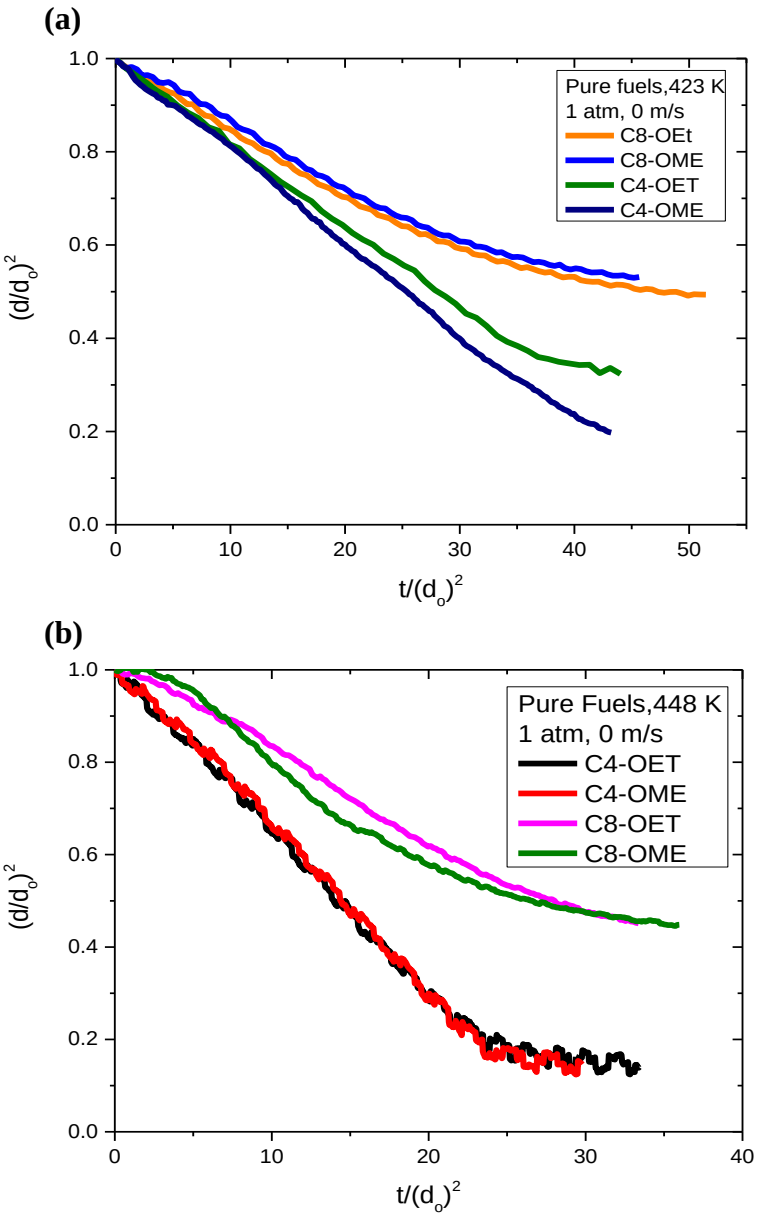

Figure 4.2: Time histories of the vaporization of pure biofuels for standard pressure in quiescent atmosphere at (a) 423 K and (b) 448 K temperatures.

However, the d^2-law does not hold when the droplet is nearing its depletion where the evolution of d^2 departs from a linear variation. This is caused by the accumulation of the heaviest components of the fuel. More importantly, Figure 4.2 shows a rapid reduction in the lifetime of

the droplet with increasing ambient temperature indicating a strong dependence of the droplet vaporization upon the surrounding gas temperature. In addition, for all the ambient temperatures, C4-OME resulted in a slightly higher gasification rate when compared with C4-OET, C8-OET and C8-OME. A summary of droplet evaporation rate at different temperatures is given in Table 4.1.

vaporization rate, k [mm^2/sec]	At 423 K	At 448 K
C4-OET	0.01939	0.035328
C4-OME	0.02070	0.035212
C8-OET	0.00978	0.019811
C8-OME	0.01413	0.023656

Table 4:1: Average droplet vaporization rate of C4-OET, C4-OME, C8-OET and C8-OME at 1 atm

4.2.1.2. Droplet evaporation of 10% blends with biodiesel (canola)

(a)

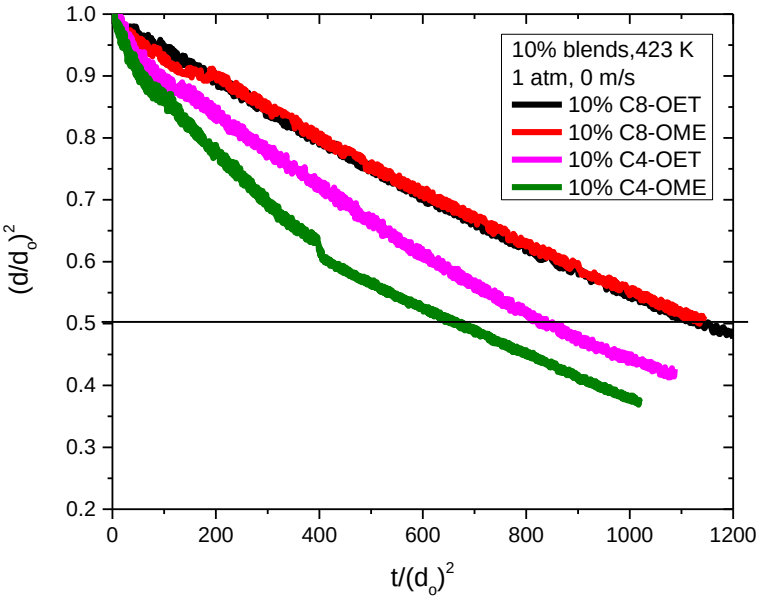

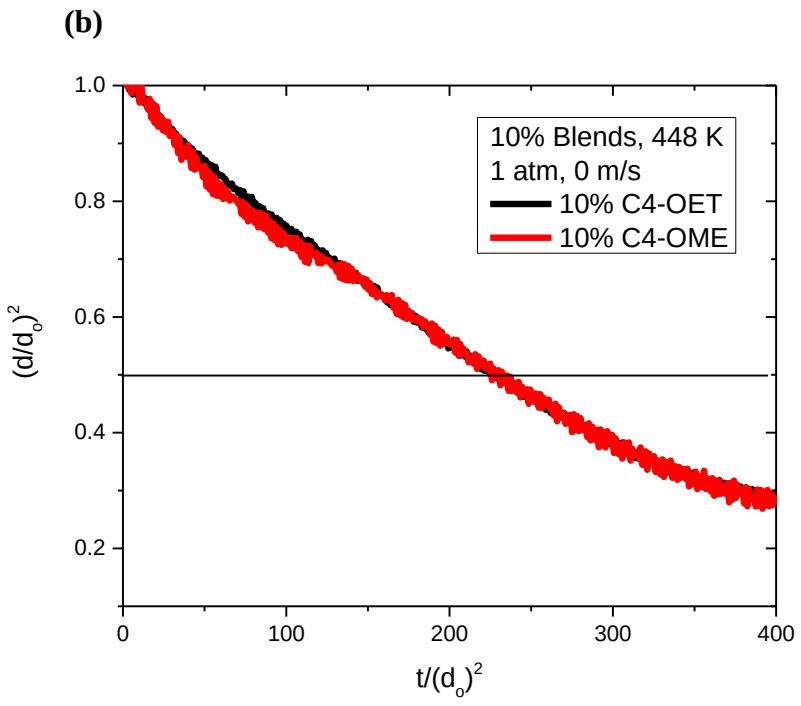

Figure 4.3: Time histories of the vaporization of 10% biofuel Blends for standard pressure in quiescent atmosphere at (a) 423 K and (b) at 448 K temperature.

Figure 4.3 shows the time histories of the normalized d^2 of canola biodiesel blended with 10% of 3-hydroxy fatty acid methyl and ethyl esters of different carbon chain lengths (C4-OET, C4-OME, C8-OET and C8-OME). These tests were conducted at two different temperatures (423 K and 448 K) and standard atmospheric pressure. Droplet gasification experiments of canola biodiesel blended with 3-hydroxy fatty acid methyl and ethyl ester have shown to accelerate the vaporization rate of biodiesel. Initial observations show the influence of both parent fuels on each respective fuel blend, where the beginning of droplet evaporation shows a steeper linear decrease in the projected droplet surface area. This steeper linear behaviour is representative of 3-hydroxy fatty acid methyl and ethyl esters droplet evaporation under these ambient conditions. The steeper slope at the onset of vaporization of all the blends is also an indication of increased fuel vaporization. On the other hand, the steeper linear behaviour becomes a less significant

portion of the droplet lifetime with the increase of ambient temperature for the fuel blends. In addition, Figure 4.3 shows a rapid reduction in the lifetime of 10% blends with increasing ambient temperature indicating a strong dependence of the droplet vaporization upon the surrounding gas temperature. However, biodiesel blended with 10% C4-OME resulted in a slightly higher gasification rate when compared with biodiesel blended with 10% of C4-OET, C8-OET and C8-OME for both the ambient temperatures. Due to the no-linearity of the time histories, the evaporation rate were analyzed in terms of droplet lifetime when $(d/d_o)^2=0.5$ which is the smallest common point among all tested blends. For example, the droplet lifetime (t/d_0^2) of 10% C4-OME for $(d/d_o)^2=0.5$ is 674 [sec/mm^2] at 423 K which is shorter than that of C4-OET, C8-OET and C8-OME. Further increases in ambient temperature lead to shorter droplet lifetimes. However, the differences of droplet lifetimes become less in comparison to the 423K with the 448 K transition. A summary of droplet lifetime can be found in Table 4.2.

Lifetime (t/d_0^2) [sec/mm^2] for $(d/d_o)^2=0.5$	**At 423 K**		**At 448 K**	
10% of C4-OET	840	1046.97	230.65	200.84
10% of C4-OME	672	676.73	203.09	224
10% of C8-OET	1127.58	1114.68		
10% of C8-OME	1150	1164		

Table 4:2: Droplet lifetime of Canola biodiesel blended with 10% of C4-OET, C4-OME, C8-OET and C8-OME at 1 atm

4.2.2. 1,3-dimethoxyoctane (1,3-DMO) and 1,3-dimethoxydecane (1,3-DMD)

4.2.2.1. Effect of temperature on droplet evaporation

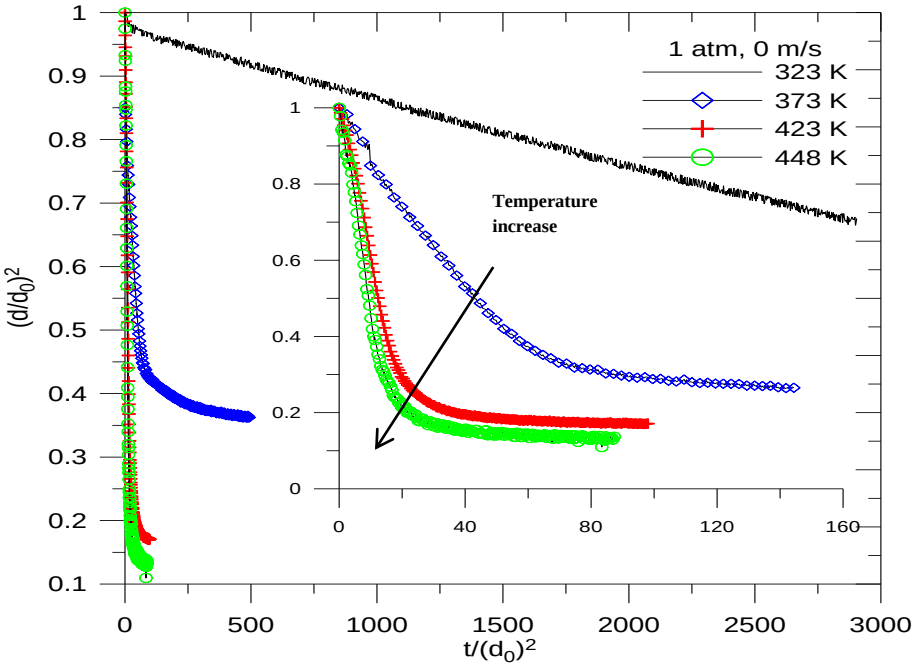

Figure 4.4: Time histories of the vaporization of 1,3-DMO droplet for different ambient temperatures at standard pressure in quiescent atmosphere

Figure 4.4 shows the temporal variation of the normalized squared diameter of 1,3-DMO droplet at different ambient temperatures and standard atmospheric pressure. The initial increase in the droplet diameter was clearly observed for the ambient temperature up to 373 K. Instantly after the droplet is formed inside the chamber, the droplet starts to evaporate. Nevertheless, the droplet diameter initially increases because of the thermal expansion effect due to the increase in droplet temperature. The droplet squared diameter followed a linear decrease with time indicating the applicability of the d^2-law. The period between the time when a droplet is inserted in the chamber and the time when the droplet diameter becomes equal to the initial diameter was defined as the initial heating period, as shown in Figure. 4.1. This scenario is similar at different

ambient temperatures. However, the d^2-law does not hold when the droplet is nearing its depletion where the evolution of d^2 departs from a linear variation. This is caused by the accumulation of the heaviest components of the fuel. More importantly, Figure 4.4 shows a rapid reduction in the lifetime of the droplet with increasing ambient temperature indicating a strong dependence of the 1,3-DMO droplet vaporization upon the surrounding gas temperature.

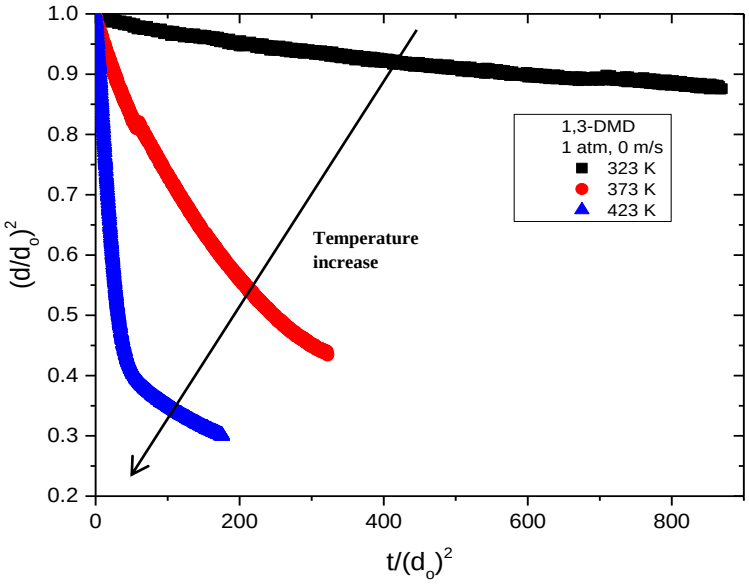

Figure 4.5: Time histories of the vaporization of 1,3-DMD droplet for different ambient temperatures at standard pressure in quiescent atmosphere

Figure 4.5 shows the temporal variation of the normalized squared diameter of 1,3-DMD droplet at different ambient temperatures (ranging between 323K to 423K) and standard atmospheric pressure. In this figure, d_0 and d are the droplet initial and instantaneous diameter, respectively. This figure also shows a rapid reduction in the lifetime of the droplet with increasing ambient temperature, which indicates a strong dependence of the droplet vaporization upon the surrounding gas temperature similar to 1,3-DMO. On the other hand, no significant heating

period is observed when varying the ambient temperature as the $(d/d_0)^2$ varies linearly with time indicating the applicability of the classical d^2-law.

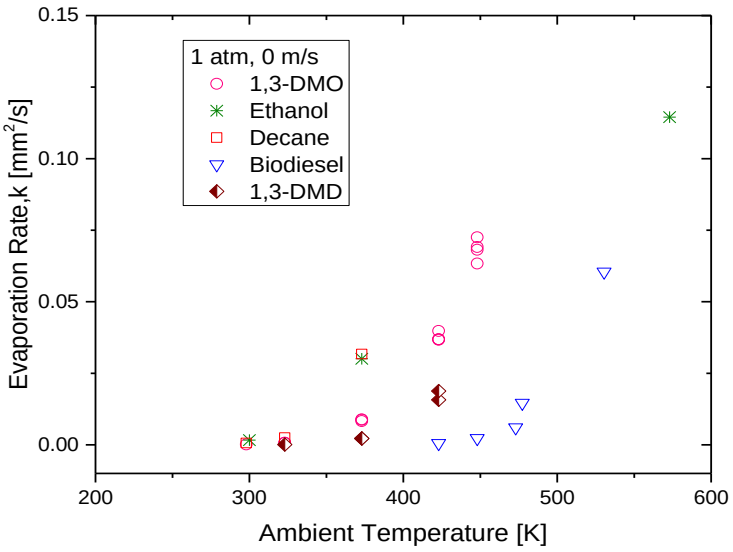

Figure 4.6: Evaporation rate of 1,3-DMO, 1,3-DMD, ethanol, decane and biodiesel droplet as a function of ambient temperature in quiescent atmosphere

Figure 4.6 shows the vaporization rate of 1,3-DMO and 1,3-DMD droplet as a function of ambient temperature in quiescent atmosphere. The average vaporization rate, K, was calculated as the slope of the linear portion the temporal variation of $(d/d_0)^2$ in Figures 4.4 and 4.5. In this figure, the data of at least three tests at each fixed ambient temperature are plotted. Published experimental data of decane, biodiesel and ethanol droplet are also included in this figure, which were obtained at ambient temperatures ranging between room and 573 K [268], [269], [270]. Figure 4.6 shows that the evaporation rate of both 1,3-DMO and 1,3-DMD biofuel droplet increases with the ambient temperature in quiescent atmosphere. In addition, 1,3-DMO, 1,3-DMD along with decane and biodiesel droplets exhibit similar trends within the ambient temperature in the range up to 373 K; whereas ethanol shows a linear trend with the temperature rise (see Figure 4.6). Nevertheless, both 1,3-DMO and 1,3-DMD droplet exhibit a lower

vaporization rate than ethanol and decane, but a higher than that of 1,3-DMD and biodiesel. For instance, the vaporization rate of 1,3-DMO, at 373 K, is only about 3 times less than that of ethanol and decane (and also gasoline; not shown here). On the other hand, the vaporization rate of the 1,3-DMO droplet is approximately 60 and 35 times higher than that of biodiesel at 423 K and 448 K temperature, respectively (Table 4.3). However, 1,3-DMD droplet shows only 25 times higher evaporation rate than that of biodiesel at 423 K.

	At 423 K	**At 448 K**
1,3-DMO	0.03757	0.06829
1,3-DMD	0.01574	N/A
Biodiesel	0.000597	0.00194

Table 4:3: Droplet vaporization rate of 1,3-DMO, 1,3-DMD and biodiesel at 1 atm

4.2.2.2. Effect of pressure on droplet evaporation

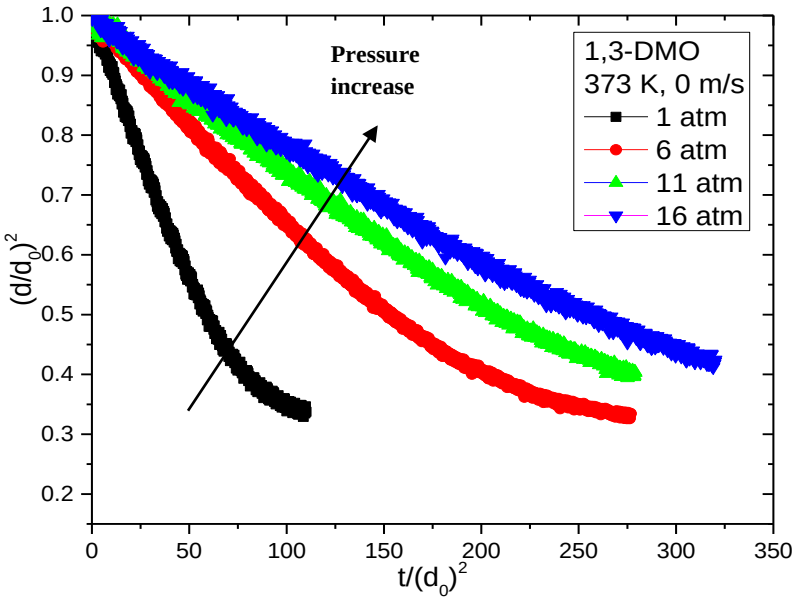

Figure 4.7: Time histories of the vaporization of 1,3-DMO droplet for different ambient pressure at 373 K

Figure 4.7 depicts the time histories of the 1,3-DMO droplet for different ambient pressure at a constant ambient temperature of 373 K in quiescent atmosphere (no flow: 0 m/s). Unlike with ambient temperature, no significant heating period is observed when varying the ambient pressure as the $(d/d_0)^2$ varies linearly with time indicating the applicability of the classical d^2-law. The same figure reveals also that the droplet lifetime increases significantly as pressure increases.

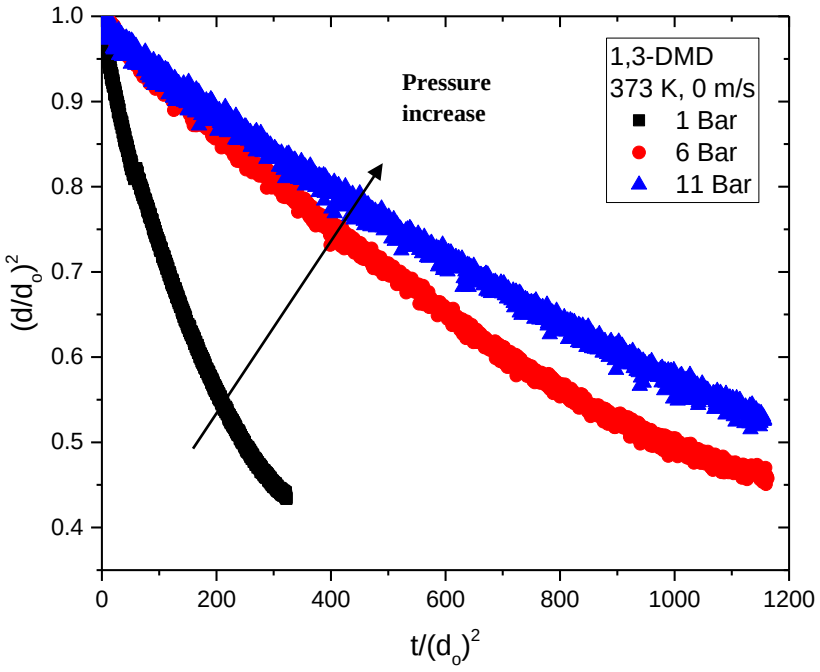

Figure 4.8: Time histories of the vaporization of 1,3-DMD droplet for different ambient pressure at 373 K

Figure 4.8 depicts the time histories of the 1,3-DMD droplet for different ambient pressure at a constant ambient temperature of 373 K in quiescent atmosphere (no flow: 0 m/s). This figure clearly shows that the squared normalized diameter of the 1,3-DMD droplet follows the d^2-law at any ambient pressure. The same figure shows a significant increase in the droplet lifetime as pressure increases similar to 1,3-DMO droplet. Moreover, no significant heating period is

observed for 1,3-DMD droplet when varying the ambient pressure at 373 K in quiescent atmosphere.

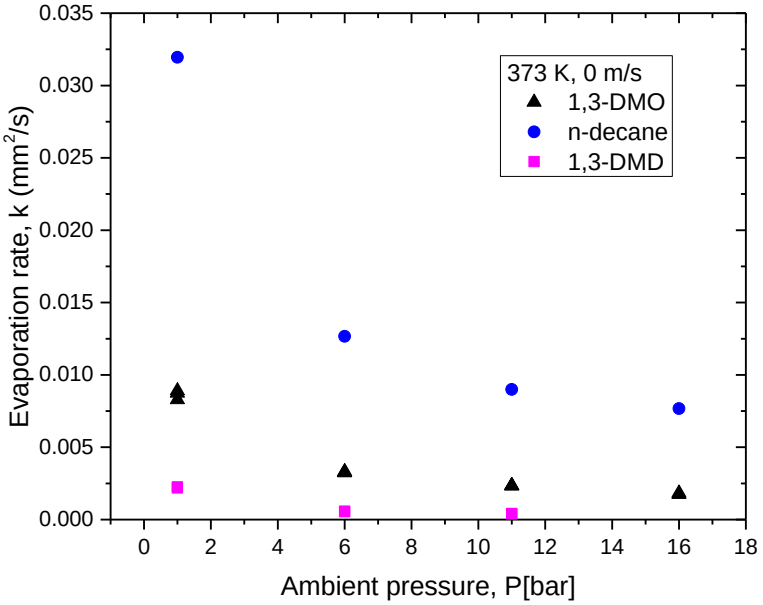

Figure 4.9: Variation of the vaporization rate of 1,3-DMO, 1,3-DMD and n-decane droplet with ambient pressure at 373 K

Figure 4.9 shows the vaporization rate of 1,3-DMO and 1,3-DMD droplet as a function of ambient pressure at a constant ambient temperature of 373 K in quiescent atmosphere. Figure 4.9 reveals that, similar to decane, the averaged vaporization rate of 1,3-DMO and 1,3-DMD droplet decreases with ambient pressure at 373 K. In this figure, the data of at least three tests at each fixed ambient pressure are plotted for 1,3-DMO and 1,3-DMD droplet along with published experimental data of decane [268]. This figure also reveals that both 1,3-DMO and 1,3-DMD droplet average evaporation rates are smaller than that of decane droplet at any given ambient pressure. However, the difference in evaporation rate of 1,3-DMO and decane remains almost the same (about 4 times) for ambient pressure from 1 bar up to 16 bar. However, the difference become higher for 1,3-DMD droplet. In comparison with biodiesel, the droplet evaporation rates

of 1,3-DMO and 1,3-DMD are higher for any ambient temperature at atmospheric pressure (Table 4.3). Moreover, the evaporation rate of 1,3-DMO and 1,3-DMD showed similar trend of biodiesel with the increase of pressure at different temperatures.

4.2.2.3. Effect of turbulence intensity on droplet evaporation

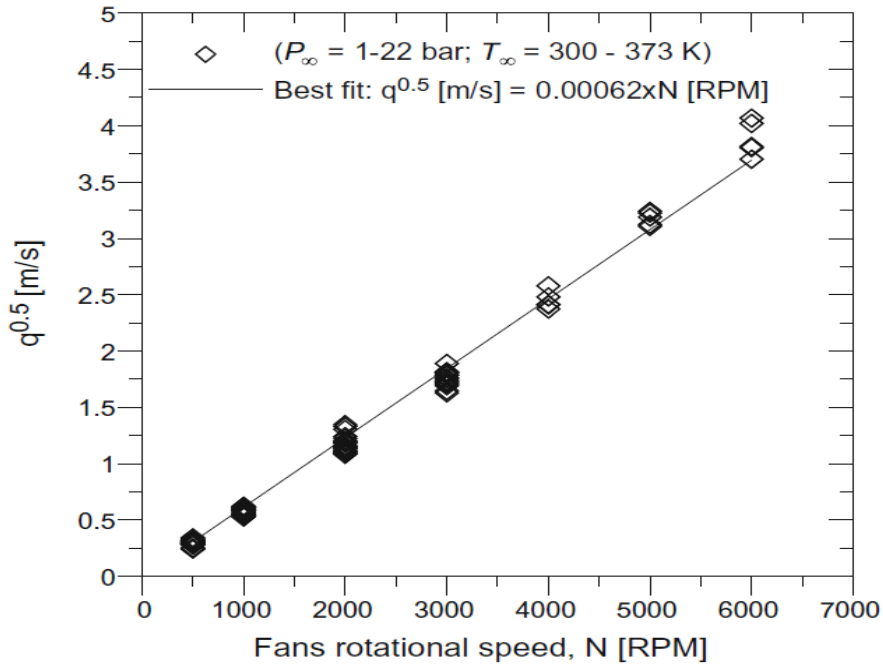

Figure 4.10: Turbulence intensity variation with rotational speed of fans (T∞ = 293 K - 373 K and P∞ = 1 bar - 22 bar) [262],[271]

Characterization of the turbulent flow field (such as homogeneity and isotropy of the turbulent field) inside the vessel was accomplished using laser Doppler velocimetry (LDV) measurements and reported in [262],[271]. Detailed characterization at room temperature and elevated ambient pressure was reported in [271]. Additional measurements were performed at ambient temperature up to 373 K and reported in [271]. Therefore only Figure 4.10 is presented here. This figure shows the variation of turbulence intensity as a function of the fans rotational speed in the central volume of the spherical chamber which has an approximate diameter of 40 mm. It is found that

the relationship between the turbulence intensity $q^{0.5}$ and the fans rotational speed reported previously reported in [271] at ambient pressure up to 22 bar remains approximately linear and unaffected by the variation in the ambient temperature. This relationship was found to be $\sqrt{q} = 0.00062 \times N$ where $q^{0.5}$ is expressed in m/s and N is the rotational speed of the axial fans expressed in RPM [271]. This relationship is valid for variations in ambient temperature and pressure up to 373 K and 21 bar, respectively as well as fan speeds up to 6000 RPM.

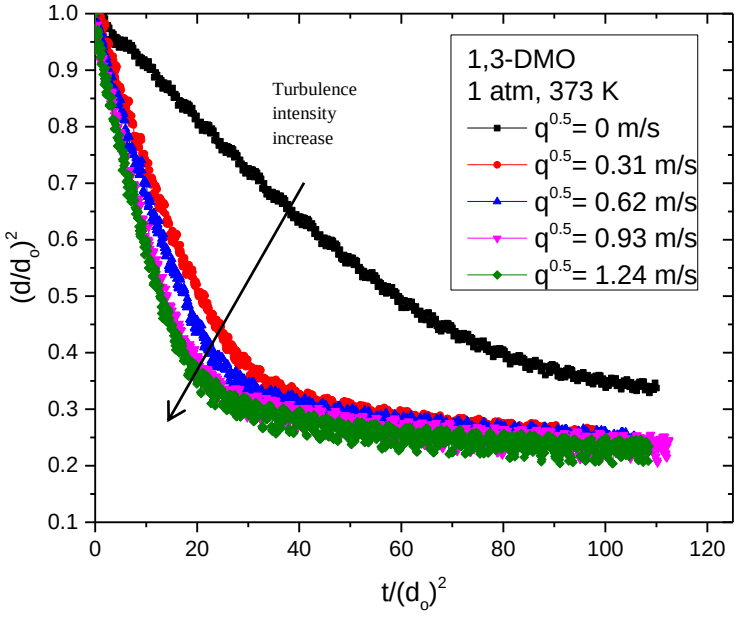

Figure 4.11: Time histories of the vaporization of 1,3-DMO droplet for different turbulence intensities at atmospheric ambient pressure and hot environment (373 K).

Figure 4.11 presents a typical temporal variation of the normalized squared diameter, $(d/d_0)^2$, of the 1,3-DMO droplet for different ambient turbulence levels (i.e., fans rotational speed) at a constant ambient temperature, 373 K, and atmospheric pressure. The droplet 1,3-DMO droplet normalized diameter follows the d^2-law at any turbulence intensity as no significant heating period is observed. The same figure shows that the droplet lifetime shortens significantly as turbulence intensity increases.

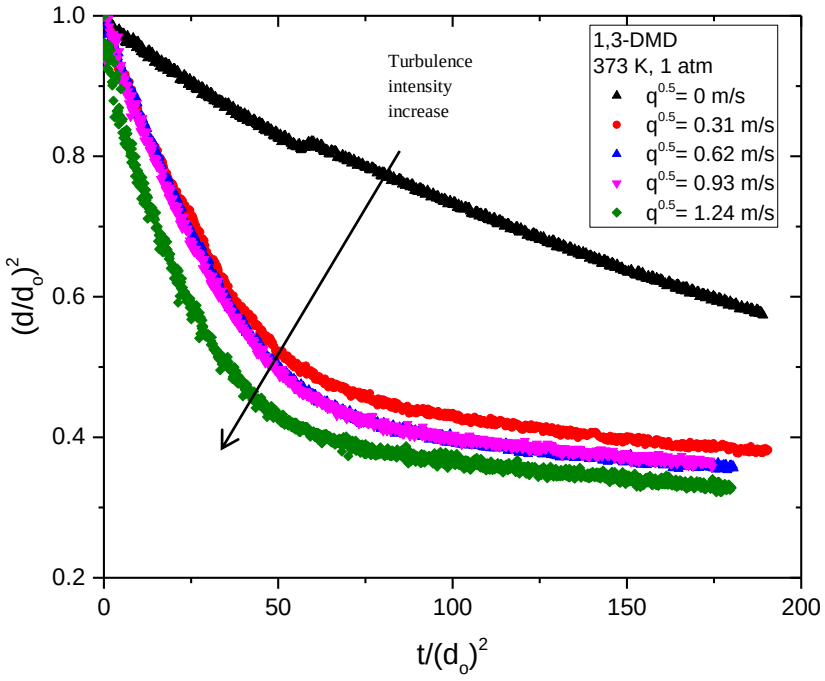

Figure 4.12: Time histories of the vaporization of 1,3-DMD droplet for different turbulence intensities at atmospheric ambient pressure and hot environment (373 K).

Figure 4.12 depicts the time histories of the 1,3-DMD droplet for different ambient turbulence levels at a constant ambient temperature, 373 K, and atmospheric pressure. No significant heating period is observed in the presence of a turbulent flow field as the $(d/d_0)^2$ varies linearly with time indicating the applicability of the classical d^2-law similar to 1,3-DMO. Moreover, the same figure shows a significant decrease in the droplet lifetime as turbulence intensity increases similar to 1,3-DMO droplet.

Figure 4.13 presents the droplet vaporization rate as a function of turbulence intensity at a constant ambient temperature of 373 K and standard atmosphere pressure. The data of at least three tests at each fixed turbulence levels for 1,3-DMO and 1,3-DMD are plotted. Published experimental data of decane [268] is also included in this figure, which were obtained at turbulence intensities ranging between 0 and 1.24 m/s (fan speed 0 to 2000 rpm).

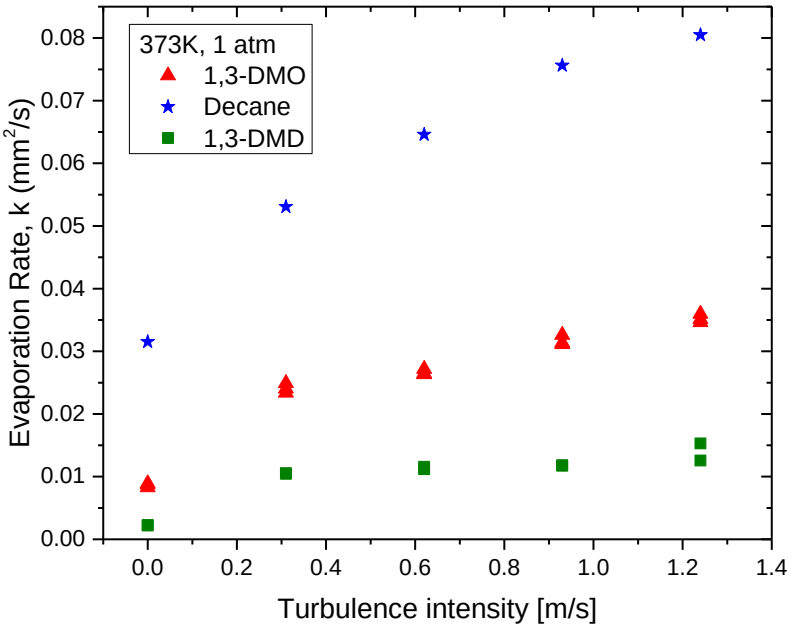

Figure 4.13: Variation of evaporation rate of 1,3-DMO, 1,3-DMD and n-decane droplet [268] as a function of fan speed at 1 atm and 373 K.

This figure shows that the droplet evaporation rate of decane, 1,3-DMO and 1,3-DMD increases with turbulence intensity where the increase is more higher for the transition from free convection (0 rpm) to forced convection (500 rpm). Further increases in fan speed beyond 500 RPM exhibits less increase in the droplet evaporation rate. The difference in evaporation rate of 1,3-DMO and decane decreases for fan speed from zero up to 2000 rpm (0 and 1.24 m/s), which is least at 2000 rpm (2.3 times). Similarly, 1,3-DMD also followed the same trend. For example, the evaporation rate of 1,3-DMD is about 6.4 and 2.8 times lower than decane and 1,3-DMO, respectively, at 1.24 m/s. However, the increase in the evaporation rate with the increase in turbulence intensity is in agreement with the previous findings on the effect of turbulence on the vaporization of hydrocarbon [268] and biodiesel [272] droplets where the effect turbulence was shown to exert a greater influence at low turbulence levels indicating that the dominant role of turbulence is to diffuse the vapor away from the droplet surface.

4.3. Thermo-Physical Properties and Heat of Combustion

The heat of combustion was measured for the pure fuels and 10% blends of 3-hydroxyl fatty acid methyl and ethyl esters as well as improved version of 3-hydroxyl fatty acid methyl and ethyl esters (i. e., 1,3-DMO, 1,3-DMD). The tests conducted in our lab revealed that these blends led to only a slight reduction in the blended fuel heat of combustion ranging between 0.46% and 4.69% for the 10% blends with canola biodiesel. For instance, the maximum and minimum decrease in LHV occurs for 10% blends of C4-OME and 1,3-DMD, respectively, as shown in Table 4.4.

Name	LHV (kJ/kg) for pure fuel	LHV (kJ/kg) for 10% blend	% Decrease in LHV
C4-OET	25591±95	38147±161	4.10
C4-OME	22956±93	37912±168	4.69
C6-OET	26853±124	38794±409	2.47
C6-OME	25908±104	38820±196	2.41
C8-OET	29503±163	38587±56	2.99
C8-OME	29573±15	38582±317	3.00
C10-OET	32154±69	39139±45	1.60
C10-OME	32150±101	38973±133	2.02
C12-OET	33137±245	38844±99	2.35
C12-OME	33330±218	39091±113	1.72

1,3-DMO	37745±110	39541±67	0.59
1,3-DMD	39594±296	39530±52	0.46
Canola Biodiesel	39777±130		

Table 4:4: Heat of combustion of the pure and blends

The properties of 1,3-DMO and 1,3-DMD are measured and compared with diesel, biodiesel, ethanol and methanol, decane, heptane (see Table 4.5). The density of 1,3-DMO is higher than that of methanol, ethanol, heptane and decane, and almost equal to that of diesel and only slight less than the density of biodiesel and 1,3-DMD. On the other hand, the density of 1,3-DMD is almost similar to biodiesel and higher than that of methanol, ethanol, heptane, decane, diesel and 1,3-DMO. The heat of combustion (LHV) was measured for 1,3-DMO and 1,3-DMD fuels by using the calorimeter set-up described above. Three tests were conducted to ensure the accuracy and repeatability of the measurements. The tests results summarized in Table 4.5 revealed that contrary to other alcohol type fuels such as ethanol and methanol, 1,3-DMO and 1,3-DMD have higher calorific value, which makes them as one of the appropriate biofuels to be used in diesel engine. For example, the heat of combustion of 1,3-DMO is 37.745±0.11 MJ/kg, which is 47.87% and 28.99% higher than that of methanol and ethanol, respectively. Similarly, 1,3-DMD shows 50% and 33% higher lower heating value than methanol and ethanol, respectively. However, the heat of combustion of the 1,3-DMO fuel is comparable to that of biodiesel; for example, it is only about 5% less than that of Canola biodiesel, and about 15% less than that of decane fuel, and only 11% less than that of petroleum diesel. On the other hand, the heat of combustion of 1,3-DMD is similar to that of biodiesel, and about 7% and 11% lower than that of diesel and decane, respectively.

Property	Chemical formula	LHV (MJ/kg)	Density [g/ml]	Molecular weight [g/mol]
Methanol	CH_3OH	19.67 [273]	0.79 [273]	32.04
Ethanol	C_2H_5OH	26.80 [274]	0.788 [274]	46.07
1,3-DMO	$C_{10}H_{22}O_2$	37.75	0.826	174.28
1,3-DMD	$C_{12}H_{28}O_2$	39.59	0.855	204.34
Canola Biodiesel	$C_{18.8}H_{34.5}O_2$	39.78	0.87 [274]	292.24
Diesel	$C_{12}H_{23}$	42.50 [273]	0.84 [273]	170
Decane	$C_{10}H_{22}$	44.60 [275]	0.73 [276]	142.29
Heptane	C_7H_{16}	44.97 [275]	0.68 [276]	100.16

Table 4:5: Main properties of 3-hydroxyl fatty acid methyl and ethyl ethers (1,3-DMO, 1,3-DMD) and other conventional fuels

4.4. Improvement of fuel properties

Fuel properties of 10% blends were measured by an independent laboratory (The Olds College Centre for Innovation, Biofuel Quality Laboratory, Alberta). The laboratory test results, which are summarized in Table 4.6, confirm our findings concerning the volatility of the biodiesel blends. That is, the flash point, which is shown to decrease significantly when blending biodiesel with 10% of the 3-hydroxyl fatty acid methyl and ethyl esters as well as improved version of 3-hydroxyl fatty acid methyl and ethyl esters (e.g., 1,3-DMO, 1,3-DMD). For instance, the flash point of 10% blends drops by about 74°C for the C4-OME and 70°C for the C4-OET. The

maximum drop in flash point occurs with the 10% blend of 1,3-DMD which is 132 °C. This is an evidence of the improvement of biodiesel volatility, and hence its cold flow properties, when using the 1,3-DMO or 1,3-DMD as blends/additives with biodiesel.

Test	Cloud Point (°C)	Total Acid Number (mg KOH/g)	Oxidation Stability (Hours)	Flash Point (°C)	Kinematic Viscosity cSt at 40^0C (mm^2/sec)
C4-OME	-4	29.11	0.14	101.9	4.349
C4-OET	-4	22.93	0.69	105.9	4.365
C6-OME	-4	3.315	0.99	103.9	4.269
C6-OET	-4	3.337	1.05	117.8	4.249
C12-OME	-4	0.238	2.8	65.4	4.56
C12-OET	-4	0.332	1.34	131.3	4.622
1,3- DMO	-5	0.157	5.51	94.4	3.991
1,3-DMD	-5	0.127	3.73	43.2	4.078
Biodiesel	**-3**	**0.19**	**3.51**	**175.8**	**4.435**

Table 4:6: Fuel properties of 10% blends with biodiesel

The tests done externally showed also improvement of some of the blended biodiesel properties. For example, it revealed a decrease in the kinematic viscosity when blending biodiesel with up to 10% of C4-esters and C6-esters; whereas it increases for the C12-esters. The test data showed also that the blends cloud point (CP) improved by 1-degree for C4, C6, C12 esters and 2-degree for 1,3-DMO and 1,3-DMD, which means an improvement of the biofuel cold flow properties.

The only fuel property that was negatively affected when bleeding biodiesel with up to 10% of 3-hydroxyl fatty acid methyl and ethyl esters was the oxidation stability. However, blending biodiesel with improved version of 3-hydroxyl fatty acid methyl and ethyl esters (i,e., 1,3-DMO, 1,3-DMD) resulted in a better oxidative stability. One major issue with oxidation of liquid fuels is the formation of precipitates (e.g., high molecular weight sediment and gum) as a result of polymerization of oxidation products (e.g., hydroperoxides) [277]. These precipitates impact modern internal combustion engines by clogging fuel filters and creating small deposits on fuel system components. In addition, oxidation also increases the fuel acid value or total acid number which is primarily a long term issue which affects the service life of engine components [277] [278]. Moreover, oxidation of biodiesel has been reported to increase fuel kinematic viscosity [278] while decreasing the heating value [277].

Chapter 5. CONCLUSIONS AND RECOMMENDATIONS

5.1. Conclusions

In the present study, some of the fuel and combustion properties of novel liquid biofuels and their blends with biodiesel were determined. These characteristics include the droplet average vaporization rate, heat of combustion and some other fuel properties. Two types of biofuels were tested which are named 3-hydroxyl fatty acid methyl and ethyl esters (3-OH FAME C4, C6, C8, C10 and C12) and 3-hydroxyl fatty acid methyl and ethyl ethers (1,3-dimethoxyoctane, 1,3-dimethoxydecane). The main findings of the study are summarized as follows:

- Droplet gasification experiments of canola biodiesel blended with 10% of the aforementioned biofuels have shown to accelerate the vaporization rate of biodiesel. All the time histories of the vaporization of canola biodiesel blended with novel biofuels shows a steeper slope at the onset of vaporization process which is an indication of increased fuel vaporization.
- The droplet of 3-OH FAME C4, C6, C8, C10 and C12 and their blends followed the d^2-law throughout their entire lifetime except for 10 % blend of C8-OME. Moreover, in some cases the d^2-law does not hold when the droplet is nearing its depletion where the evolution of d^2 departs from a linear variation because of accumulation of the heaviest components of the fuel.
- The accumulation of the heaviest components decreases with increasing ambient temperature. This is because the droplet evaporation rate increases more significantly than the polymerization reaction rate with increasing ambient temperature.

- The average evaporation rate of 1,3-DMO and 1,3-DMD droplet increased with ambient temperature. As a results, droplet lifetime decreases with increasing ambient temperature for both fuels.
- Moreover, the evaporation rate of 1,3-DMO and 1,3-DMD are much higher than that of biodiesel fuel and only slightly lower than that of decane, gasoline or ethanol.
- The evaporation rate of 1,3-DMO and 1,3-DMD decreased with increasing ambient pressure whereas increased with turbulence intensity and ambient temperatures which is in agreement with the trend of established fuels.
- The 10% blends of these biofuels with biodiesel led to only a slight reduction in the blended fuel's heat of combustion. For instance, the maximum and minimum decrease in LHV occurs for 10% blends of C4-OME and 1,3-DMD, respectively.
- The results of heat of combustion showed that 1,3-DMO and 1,3-DMD have a lower heating value almost equal to that of pure biodiesel. Moreover, 1,3-DMO and 1,3-DMD showed higher heat of combustion compared to alcohol type fuels. For example, the lower heating value of 1,3-DMO is approximately 50% and 29% greater than that of methanol and ethanol, respectively. Similarly, 1,3-DMD shows 50% and 33% higher lower heating value than methanol and ethanol, respectively.
- The fuel properties tests done externally showed also improvement of some of the blended biodiesel properties such as cloud point, flash point and kinematic viscosity. The only fuel property that was negatively affected when bleeding biodiesel was the oxidation stability. However, blending biodiesel with improved version of 3-hydroxyl fatty acid methyl and ethyl ethers (e.g., 1,3-DMO, 1,3-DMD) resulted in a better oxidative stability and volatility.

5.2. Recommendations for Future Work

Recommendations for future research:

- Further investigation of droplet evaporation and combustion of 1,3-DMO and 1,3-DMD fuels and the effect of their blends on biodiesel. This can be accomplished using different blends with biodiesel (e.g., B0, B20, B50 and B100).
- The properties of pure 1,3-DMO and 1,3-DMD fuels should also be performed in order to assess their effect when blending with biodiesel.
- Consideration of different methods of droplet suspension should be explored in order to eliminate the effect of fiber on droplet vaporization and combustion rate. The cross fiber technique, which is available in the lab, should be used.

REFERENCES

[1] Fattah, I. R., Masjuki, H. H., Liaquat, A. M., Ramli, R., Kalam, M. A., & Riazuddin, V. N. (2013). Impact of various biodiesel fuels obtained from edible and non-edible oils on engine exhaust gas and noise emissions. Renewable and Sustainable Energy Reviews, 18, 552-567.

[2] Körbitz, W. (1999). Biodiesel production in Europe and North America, an encouraging prospect. Renewable Energy, 16(1), 1078-1083.

[3] Demirbas, A. (2009). Progress and recent trends in biodiesel fuels. Energy conversion and management, 50(1), 14-34.

[4] Liu, G., Yan, B., & Chen, G. (2013). Technical review on jet fuel production. Renewable and Sustainable Energy Reviews, 25, 59-70.

[5] Birol, F. (2008). World energy outlook. Paris: International Energy Agency.

[6] Şensöz, S., Angın, D., & Yorgun, S. (2000). Influence of particle size on the pyrolysis of rapeseed (Brassica napus L.): fuel properties of bio-oil. Biomass and Bioenergy, 19(4), 271-279.

[7] Sheehan, J., Camobreco, V., Duffield, J., Graboski, M., & Shapouri, H. (1998). An overview of biodiesel and petroleum diesel life cycles. National Renewable Energy Laboratory. US Department of Agriculture and US Department of Energy, Prepared under Task No. BF886002.

[8] Martinot, E., Dienst, C., Weiliang, L., & Qimin, C. (2007). Renewable energy futures: Targets, scenarios, and pathways. Annu. Rev. Environ. Resour., 32, 205-239.

[9] Azad, A. K., Khan, M. M. K., Ahasan, T., & Ahmed, S. F. (2014). Energy scenario: production, consumption and prospect of renewable energy in Australia. Journal of Power and Energy Engineering, 2(04), 19.

[10] Lund, H. (2007). Renewable energy strategies for sustainable development. Energy, 32(6), 912-919.

[11] Misra, R. D., & Murthy, M. S. (2010). Straight vegetable oils usage in a compression ignition engine—A review. Renewable and Sustainable Energy Reviews, 14(9), 3005-3013.

[12] Azad, A. K., Rasul, M. G., Khan, M. M. K., Sharma, S. C., & Hazrat, M. A. (2015). Prospect of biofuels as an alternative transport fuel in Australia. Renewable and Sustainable Energy Reviews, 43, 331-351.

[13] Janaun, J., & Ellis, N. (2010). Perspectives on biodiesel as a sustainable fuel. Renewable and Sustainable Energy Reviews, 14(4), 1312-1320.

[14] Sarin, A., Arora, R., Singh, N. P., Sarin, R., Malhotra, R. K., & Sarin, S. (2010). Blends of biodiesels synthesized from non-edible and edible oils: effects on the cold filter plugging point. Energy & Fuels, 24(3), 1996-2001.

[15] Kondili, E. M., & Kaldellis, J. K. (2007). Biofuel implementation in East Europe: Current status and future prospects. Renewable and Sustainable Energy Reviews, 11(9), 2137-2151.

[16] Barnwal, B. K., & Sharma, M. P. (2005). Prospects of biodiesel production from vegetable oils in India. Renewable and sustainable energy reviews, 9(4), 363-378.

[17] Graboski, M. S., & McCormick, R. L. (1998). Combustion of fat and vegetable oil derived fuels in diesel engines. Progress in energy and combustion science, 24(2), 125-164.

[18] Ramadhas, A. S., Jayaraj, S., & Muraleedharan, C. (2004). Use of vegetable oils as IC engine fuels—a review. Renewable energy, 29(5), 727-742.

[19] Meher, L. C., Sagar, D. V., & Naik, S. N. (2006). Technical aspects of biodiesel production by transesterification—a review. Renewable and sustainable energy reviews, 10(3), 248-268.

[20] Smith, P. C., Ngothai, Y., Nguyen, Q. D., & O'Neill, B. K. (2010). Improving the low-temperature properties of biodiesel: Methods and consequences. Renewable Energy, 35(6), 1145-1151.

[21] De Torres, M., Jiménez-Osés, G., Mayoral, J. A., & Pires, E. (2011). Fatty acid derivatives and their use as CFPP additives in biodiesel. Bioresource technology, 102(3), 2590-2594.

[22] Smith, P. C., Ngothai, Y., Nguyen, Q. D., & O'Neill, B. K. (2010). The addition of alkoxy side-chains to biodiesel and the impact on flow properties. Fuel, 89(11), 3517-3522.

[23] Misra, R. D., & Murthy, M. S. (2011). Blending of additives with biodiesels to improve the cold flow properties, combustion and emission performance in a compression ignition engine—A review. Renewable and Sustainable Energy Reviews, 15(5), 2413-2422.

[24] Demirbas, A. H., & Demirbas, I. (2007). Importance of rural bioenergy for developing countries. Energy Conversion and Management, 48(8), 2386-2398.

[25] Daho, T., Vaitilingom, G., Sanogo, O., Ouiminga, S. K., Segda, B. G., Valette, J., ... & Koulidiati, J. (2012). Study of droplet vaporization of various vegetable oils and blends of

domestic fuel oil–cottonseed oil under different ambient temperature conditions. biomass and bioenergy, 46, 653-663.

[26] Sarin, R., Sharma, M., Sinharay, S., & Malhotra, R. K. (2007). Jatropha–palm biodiesel blends: an optimum mix for Asia. Fuel, 86(10), 1365-1371.

[27] Demirbas, A. Biodiesel: a realistic fuel alternative for diesel engines, 2008.

[28] Chiu, C. W., Schumacher, L. G., & Suppes, G. J. (2004). Impact of cold flow improvers on soybean biodiesel blend. Biomass and Bioenergy, 27(5), 485-491.

[29] Jain, S., & Sharma, M. P. (2010). Stability of biodiesel and its blends: a review. Renewable and Sustainable Energy Reviews, 14(2), 667-678.

[30] Daho, T., Vaitilingom, G., Sanogo, O., Ouiminga, S. K., Zongo, A. S., Piriou, B., & Koulidiati, J. (2014). Combustion of vegetable oils under optimized conditions of atomization and granulometry in a modified fuel oil burner. Fuel, 118, 329-334.

[31] Daho, T., Vaitilingom, G., & Sanogo, O. (2009). Optimization of the combustion of blends of domestic fuel oil and cottonseed oil in a non-modified domestic boiler. Fuel, 88(7), 1261-1268.

[32] Ramadhas, A. S., Jayaraj, S., & Muraleedharan, C. (2005). Characterization and effect of using rubber seed oil as fuel in the compression ignition engines. Renewable energy, 30(5), 795-803.

[33] Kalam, M. A., & Masjuki, H. H. (2004). Emissions and deposit characteristics of a small diesel engine when operated on preheated crude palm oil. Biomass and Bioenergy, 27(3), 289-297.

[34] Demirbas, A. (2008). New liquid biofuels from vegetable oils via catalytic pyrolysis. Energy education science and technology, 21(1-2), 1-59.

[35] Srivastava, A., & Prasad, R. (2000). Triglycerides-based diesel fuels. Renewable and sustainable energy reviews, 4(2), 111-133.

[36] Knothe, G. (2008). "Designer" Biodiesel: Optimizing Fatty Ester Composition to Improve Fuel Properties†. Energy & Fuels, 22(2), 1358-1364.

[37] Burton, R., Fan, X., & Austic, G. (2010). Evaluation of two-step reaction and enzyme catalysis approaches for biodiesel production from spent coffee grounds. International Journal of Green Energy, 7(5), 530-536.

[38] Kafuku, G., & Mbarawa, M. (2010). Effects of biodiesel blending with fossil fuel on flow properties of biodiesel produced from non-edible oils. International Journal of Green Energy, 7(4), 434-444.

[39] Tao, J., Dai, C. C., Yang, Q. Y., Guan, X. Y., & Shao, W. L. (2010). Production of biodiesel with acid hydrolysate of populus euramevicana cv leaves by Rhodotorula glutinis. International Journal of Green Energy, 7(4), 387-396.

[40] Demirbas, A. (2007). Recent developments in biodiesel fuels. International Journal of Green Energy, 4(1), 15-26.

[41] Rakopoulos, C. D., Antonopoulos, K. A., Rakopoulos, D. C., Hountalas, D. T., & Giakoumis, E. G. (2006). Comparative performance and emissions study of a direct injection diesel engine using blends of diesel fuel with vegetable oils or bio-diesels of various origins. Energy conversion and management, 47(18), 3272-3287.

[42] Sahoo, P. K., Das, L. M., Babu, M. K. G., & Naik, S. N. (2007). Biodiesel development from high acid value polanga seed oil and performance evaluation in a CI engine. Fuel, 86(3), 448-454.

[43] Sinha, S., Agarwal, A. K., & Garg, S. (2008). Biodiesel development from rice bran oil: Transesterification process optimization and fuel characterization. Energy conversion and management, 49(5), 1248-1257.

[44] Murugesan, A., Umarani, C., Subramanian, R., & Nedunchezhian, N. (2009). Bio-diesel as an alternative fuel for diesel engines—a review. Renewable and Sustainable Energy Reviews, 13(3), 653-662.

[45] Junming, X., Jianchun, J., Yanju, L., & Jie, C. (2009). Liquid hydrocarbon fuels obtained by the pyrolysis of soybean oils. Bioresource technology, 100(20), 4867-4870.

[46] Maher, K. D., & Bressler, D. C. (2007). Pyrolysis of triglyceride materials for the production of renewable fuels and chemicals. Bioresource technology, 98(12), 2351-2368.

[47] Kubičková, I., Snåre, M., Eränen, K., Mäki-Arvela, P., & Murzin, D. Y. (2005). Hydrocarbons for diesel fuel via decarboxylation of vegetable oils. Catalysis Today, 106(1), 197-200.

[48] Hazar, H., & Aydin, H. (2010). Performance and emission evaluation of a CI engine fueled with preheated raw rapeseed oil (RRO)–diesel blends. Applied Energy, 87(3), 786-790.

[49] Yilmaz, N., & Morton, B. (2011). Effects of preheating vegetable oils on performance and emission characteristics of two diesel engines. biomass and bioenergy, 35(5), 2028-2033.

[50] Agarwal, D., & Agarwal, A. K. (2007). Performance and emissions characteristics of Jatropha oil (preheated and blends) in a direct injection compression ignition engine. Applied thermal engineering, 27(13), 2314-2323.

[51] Azoumah, Y., Blin, J., & Daho, T. (2009). Exergy efficiency applied for the performance optimization of a direct injection compression ignition (CI) engine using biofuels. Renewable Energy, 34(6), 1494-1500.

[52] Wang, Y. D., Al-Shemmeri, T., Eames, P., McMullan, J., Hewitt, N., Huang, Y., & Rezvani, S. (2006). An experimental investigation of the performance and gaseous exhaust emissions of a diesel engine using blends of a vegetable oil. Applied Thermal Engineering, 26(14), 1684-1691.

[53] Moser, B. R. (2008). Influence of blending canola, palm, soybean, and sunflower oil methyl esters on fuel properties of biodiesel†. Energy & Fuels, 22(6), 4301-4306.

[54] Echim, C., Maes, J., & De Greyt, W. (2012). Improvement of cold filter plugging point of biodiesel from alternative feedstocks. Fuel, 93, 642-648.

[55] Dunn, R. O., & Bagby, M. O. (1995). Low-temperature properties of triglyceride-based diesel fuels: transesterified methyl esters and petroleum middle distillate/ester blends. Journal of the American Oil Chemists' Society, 72(8), 895-904.

[56] Foglia, T. A., Nelson, L. A., Dunn, R. O., & Marmer, W. N. (1997). Low-temperature properties of alkyl esters of tallow and grease. Journal of the American Oil Chemists' Society, 74(8), 951-955.

[57] Park, J. Y., Kim, D. K., Lee, J. P., Park, S. C., Kim, Y. J., & Lee, J. S. (2008). Blending effects of biodiesels on oxidation stability and low temperature flow properties. Bioresource technology, 99(5), 1196-1203.

[58] Kazancev, K., Makareviciene, V., Paulauskas, V., & Janulis, P. (2006). Cold flow properties of fuel mixtures containing biodiesel derived from animal fatty waste. European Journal of Lipid Science and Technology, 108(9), 753-758.

[59] Udomsap, P., Sahapatsombat, U., Puttasawat, B., Krasae, P., Chollacoop, N., & Topaiboul, S. (2008). Preliminary investigation of cold flow improvers for palm-derived biodiesel blends. Journal of Metals, Materials and Minerals, 18(2), 99-102.

[60] Dunn, R. O., Shockley, M. W., & Bagby, M. O. (1996). Improving the low-temperature properties of alternative diesel fuels: vegetable oil-derived methyl esters. Journal of the American Oil Chemists' Society, 73(12), 1719-1728.

[61] Gómez, M. G., Howard-Hildige, R., Leahy, J. J., & Rice, B. (2002). Winterisation of waste cooking oil methyl ester to improve cold temperature fuel properties. Fuel, 81(1), 33-39.

[62] Kerschbaum, S., Rinke, G., & Schubert, K. (2008). Winterization of biodiesel by micro process engineering. Fuel, 87(12), 2590-2597.

[63] Bouaid, A., Hahati, K., Martinez, M., & Aracil, J. (2014). Biodiesel production from biobutanol. Improvement of cold flow properties. Chemical Engineering Journal, 238, 234-241.

[64] Lee, I., Johnson, L. A., & Hammond, E. G. (1995). Use of branched-chain esters to reduce the crystallization temperature of biodiesel. Journal of the American Oil Chemists' Society, 72(10), 1155-1160.

[65] Wang, S., Shen, J., & Reaney, M. J. (2012). Lubricity-enhancing low-temperature diesel fuel additives. Journal of the American Oil Chemists' Society, 89(3), 513-522.

[66] Wadumesthrige, K., Salley, S. O., & Ng, K. S. (2009). Effects of partial hydrogenation, epoxidation, and hydroxylation on the fuel properties of fatty acid methyl esters. Fuel Processing Technology, 90(10), 1292-1299.

[67] Kongyai, C., Chalermsinsuwan, B., & Hunsom, M. (2013). Epoxidation of waste used-oil biodiesel: Effect of reaction factors and its impact on the oxidative stability. Korean Journal of Chemical Engineering, 30(2), 327-336.

[68] Mushtaq, M., Tan, I. M., Nadeem, M., Devi, C., Lee, S. Y., & Sagir, M. (2014). A convenient route for the alkoxylation of biodiesel and its influence on cold flow properties. International Journal of Green Energy, 11(3), 267-279.

[69] Serrano, M., Oliveros, R., Sánchez, M., Moraschini, A., Martínez, M., & Aracil, J. (2014). Influence of blending vegetable oil methyl esters on biodiesel fuel properties: oxidative stability and cold flow properties. Energy, 65, 109-115.

[70] Tang, H., Salley, S. O., & Ng, K. S. (2008). Fuel properties and precipitate formation at low temperature in soy-, cottonseed-, and poultry fat-based biodiesel blends. Fuel, 87(13), 3006-3017.

[71] Dunn, R. O., & Bagby, M. O. (2000). Low-temperature phase behavior of vegetable oil/co-solvent blends as alternative diesel fuel. Journal of the American Oil Chemists' Society, 77(12), 1315-1323.

[72] Cao, L., Wang, J., Liu, K., & Han, S. (2014). Ethyl acetoacetate: A potential bio-based diluent for improving the cold flow properties of biodiesel from waste cooking oil. Applied Energy, 114, 18-21.

[73] Smith, P. C., Ngothai, Y., Nguyen, Q. D., & O'Neill, B. K. (2009). Alkoxylation of biodiesel and its impact on low-temperature properties. Fuel, 88(4), 605-612.

[74] Kleinová, A., Paligová, J., Vrbova, M., Mikulec, J., & Cvengroš, J. (2007). Cold flow properties of fatty esters. Process Safety and Environmental Protection, 85(5), 390-395.

[75] Usta, N., Aydoğan, B., Çon, A. H., Uğuzdoğan, E., & Özkal, S. G. (2011). Properties and quality verification of biodiesel produced from tobacco seed oil. Energy conversion and Management, 52(5), 2031-2039.

[76] Xu, G., & Wu, G. Y. (2003). The investigation of blending properties of biodiesel and No. 0 diesel fuel. JOURNAL-JIANGSU POLYTECHNIC UNIVERSITY, 15(2), 16-18.

[77] Kim, J. K., Yim, E. S., Jeon, C. H., Jung, C. S., & Han, B. H. (2012). Cold performance of various biodiesel fuel blends at low temperature. International journal of automotive technology, 13(2), 293-300.

[78] Wu, W. H., Foglia, T. A., Marmer, W. N., Dunn, R. O., Goering, C. E., & Briggs, T. E. (1998). Low-temperature property and engine performance evaluation of ethyl and isopropyl esters of tallow and grease. Journal of the American Oil Chemists' Society, 75(12), 1173-1178.

[79] Lown, A. L., Peereboom, L., Mueller, S. A., Anderson, J. E., Miller, D. J., & Lira, C. T. (2014). Cold flow properties for blends of biofuels with diesel and jet fuels. Fuel, 117, 544-551.

[80] Zuleta, E. C., Rios, L. A., & Benjumea, P. N. (2012). Oxidative stability and cold flow behavior of palm, sacha-inchi, jatropha and castor oil biodiesel blends. Fuel Processing Technology, 102, 96-101.

[81] Chastek, T. Q. (2011). Improving cold flow properties of canola-based biodiesel. biomass and bioenergy, 35(1), 600-607.

[82] Wang, Y., Ma, S., Zhao, M., Kuang, L., Nie, J., & Riley, W. W. (2011). Improving the cold flow properties of biodiesel from waste cooking oil by surfactants and detergent fractionation. Fuel, 90(3), 1036-1040.

[83] Lv, P., Cheng, Y., Yang, L., Yuan, Z., Li, H., & Luo, W. (2013). Improving the low temperature flow properties of palm oil biodiesel: addition of cold flow improver. Fuel Processing Technology, 110, 61-64.

[84] Giraldo, S. Y., Rios, L. A., & Suárez, N. (2013). Comparison of glycerol ketals, glycerol acetates and branched alcohol-derived fatty esters as cold-flow improvers for palm biodiesel. Fuel, 108, 709-714.

[85] Wang, J., Cao, L., & Han, S. (2014). Effect of polymeric cold flow improvers on flow properties of biodiesel from waste cooking oil. Fuel, 117, 876-881.

[86] Boshui, C., Yuqiu, S., Jianhua, F., Jiu, W., & Jiang, W. (2010). Effect of cold flow improvers on flow properties of soybean biodiesel. Biomass and bioenergy, 34(9), 1309-1313.

[87] Bhale, P. V., Deshpande, N. V., & Thombre, S. B. (2009). Improving the low temperature properties of biodiesel fuel. Renewable Energy, 34(3), 794-800.

[88] Sern, C. H., May, C. Y., Zakaria, Z., Daik, R., & Foon, C. S. (2007). The effect of polymers and surfactants on the pour point of palm oil methyl esters. European journal of lipid science and technology, 109(4), 440-444.

[89] Ming, T. C., Ramli, N., Lye, O. T., Said, M., & Kasim, Z. (2005). Strategies for decreasing the pour point and cloud point of palm oil products. European journal of lipid science and technology, 107(7-8), 505-512.

[90] Boshui, C., Yuqiu, S., Jianhua, F., Jiu, W., & Jiang, W. (2010). Effect of cold flow improvers on flow properties of soybean biodiesel. Biomass and bioenergy, 34(9), 1309-1313.

[91] Shrestha, D. S., Van Gerpen, J., & Thompson, J. (2008). Effectiveness of cold flow additives on various biodiesels, diesel, and their blends. Transactions of the ASABE, 51(4), 1365-1370.

[92] Noshadi, I., Amin, N. A. S., & Parnas, R. S. (2012). Continuous production of biodiesel from waste cooking oil in a reactive distillation column catalyzed by solid heteropolyacid: optimization using response surface methodology (RSM). Fuel, 94, 156-164.

[93] Joshi, H., Moser, B. R., Toler, J., Smith, W. F., & Walker, T. (2011). Ethyl levulinate: A potential bio-based diluent for biodiesel which improves cold flow properties. Biomass and bioenergy, 35(7), 3262-3266.

[94] Mohamad, S. A., Ahmed, N. S., Hassanein, S. M., & Rashad, A. M. (2012). Investigation of polyacrylates copolymers as lube oil viscosity index improvers. Journal of Petroleum Science and Engineering, 100, 173-177.

[95] Zhu, L., Cheung, C. S., Zhang, W. G., & Huang, Z. (2010). Emissions characteristics of a diesel engine operating on biodiesel and biodiesel blended with ethanol and methanol. Science of the Total Environment, 408(4), 914-921.

[96] Shi, X., Pang, X., Mu, Y., He, H., Shuai, S., Wang, J., ... & Li, R. (2006). Emission reduction potential of using ethanol–biodiesel–diesel fuel blend on a heavy-duty diesel engine. Atmospheric Environment, 40(14), 2567-2574.

[97] Kwanchareon, P., Luengnaruemitchai, A., & Jai-In, S. (2007). Solubility of a diesel–biodiesel–ethanol blend, its fuel properties, and its emission characteristics from diesel engine. Fuel, 86(7), 1053-1061.

[98] Lü, Y., Ouyang, F., Wang, S., & Weng, H. (2006). Carbon distribution of n-paraffins in diesel and the effects on the sensitivity of flow improvers. Petroleum science and technology, 24(10), 1205-1214.

[99] Song, Y., Ren, T., Fu, X., & Xu, X. (2005). Synthesis and evaluation of some C14MC-MCNR2 copolymers and C14MC-MA-MCNR2 terpolymers as cold flow improvers in the diesel fuels. Petroleum science and technology, 23(5-6), 669-679.

[100] Ming, T. C., Ramli, N., Lye, O. T., Said, M., & Kasim, Z. (2005). Strategies for decreasing the pour point and cloud point of palm oil products. European journal of lipid science and technology, 107(7-8), 505-512.

[101] Doğan, T. H., & Temur, H. (2013). Effect of fractional winterization of beef tallow biodiesel on the cold flow properties and viscosity. Fuel, 108, 793-796.

[102] Monkenbusch, M., Schneiders, D., Richter, D., Willner, L., Leube, W., Fetters, L. J., ... & Lin, M. (2000). Aggregation behaviour of pe–pep copolymers and the winterization of diesel fuel. Physica B: Condensed Matter, 276, 941-943.

[103] Knothe, G., Matheaus, A. C., & Ryan, T. W. (2003). Cetane numbers of branched and straight-chain fatty esters determined in an ignition quality tester☆. Fuel, 82(8), 971-975.

[104] Rajam, L., Kumar, D. S., Sundaresan, A., & Arumughan, C. (2005). A novel process for physically refining rice bran oil through simultaneous degumming and dewaxing. Journal of the American Oil Chemists' Society, 82(3), 213-220.

[105] Seames, W., Luo, Y., Ahmed, I., Aulich, T., Kubátová, A., Šťávová, J., & Kozliak, E. (2010). The thermal cracking of canola and soybean methyl esters: improvement of cold flow properties. biomass and bioenergy, 34(7), 939-946.

[106] Bi, Y., Ding, D., & Wang, D. (2010). Low-melting-point biodiesel derived from corn oil via urea complexation. Bioresource technology, 101(4), 1220-1226.

[107] Goodrum, J. W., & Geller, D. P. (2005). Influence of fatty acid methyl esters from hydroxylated vegetable oils on diesel fuel lubricity. Bioresource Technology, 96(7), 851-855.

[108] Reaume, S. J., & Ellis, N. (2013). Use of isomerization and hydroisomerization reactions to improve the cold flow properties of vegetable oil based biodiesel. Energies, 6(2), 619-633.

[109] Soriano, N. U., Migo, V. P., & Matsumura, M. (2006). Ozonized vegetable oil as pour point depressant for neat biodiesel. Fuel, 85(1), 25-31.

[110] S El Rafie, S., & Attia, N. (2008). Improvement of neat biodiesel characteristics by mixing with ozonated vegetable oil. Desalination, 228(1), 168-174.

[111] Hashimoto, N., Nomura, H., Suzuki, M., Matsumoto, T., Nishida, H., & Ozawa, Y. (2015). Evaporation characteristics of a palm methyl ester droplet at high ambient temperatures. Fuel, 143, 202-210.

[112] Manjunath, M., Raghavan, V., & Mehta, P. S. (2015). Vaporization characteristics of suspended droplets of biodiesel fuels of Indian origin and their diesel blends–An experimental study. International Journal of Heat and Mass Transfer, 88, 28-41.

[113] Birouk, M., & Toth, S. L. (2015). Vaporization and Combustion of a Soybean Biodiesel Droplet in Turbulent Environment at Elevated Ambient Pressure. Combustion Science and Technology, 187(6), 937-952.

[114] Morin, C., Chauveau, C., & Gökalp, I. (2000). Droplet vaporisation characteristics of vegetable oil derived biofuels at high temperatures. Experimental Thermal and Fluid Science, 21(1), 41-50.

[115] MORIN∗, C. É. L. I. N. E., Chauveau, C., Dagaut, P., Goekalp, I., & Cathonnet, M. (2004). Vaporization and oxidation of liquid fuel droplets at high temperature and high pressure: application to n-alkanes and vegetable oil methyl esters. Combustion science and technology, 176(4), 499-529.

[116] Daho, T., Vaitilingom, G., Sanogo, O., Ouiminga, S. K., Segda, B. G., Valette, J., ... & Koulidiati, J. (2012). Model for predicting evaporation characteristics of vegetable oils droplets based on their fatty acid composition. International journal of heat and mass transfer, 55(11), 2864-2871.

[117] Ma, Y. P., Li, X. R., Wang, X. Y., & Liu, F. S. (2012, February). An Experimental Study on Diesel Fuel Droplets Coupling Evaporation. In Advanced Materials Research (Vol. 383, pp. 3068-3076).

[118] Promvongsa, J., Vallikul, P., Fungtammasan, B., & Grehan, G. (2010). On Evaporation Constants of Biodiesel-Diesel Blends: The Effects of Blending Ratios. Journal of Metals, Materials and Minerals, 20(3), 43-45.

[119] Zhang, L., & Kong, S. C. (2010). Vaporization modeling of petroleum–biofuel drops using a hybrid multi-component approach. Combustion and Flame, 157(11), 2165-2174.

[120] Zhang, L., & Kong, S. C. (2011). High-pressure vaporization modeling of multi-component petroleum–biofuel mixtures under engine conditions. Combustion and Flame, 158(9), 1705-1717.

[121] Hallett, W. L. H., & Legault, N. V. (2011). Modelling biodiesel droplet evaporation using continuous thermodynamics. Fuel, 90(3), 1221-1228.

[122] Dirbude, S., Eswaran, V., & Kushari, A. (2012). Droplet vaporization modeling of rapeseed and sunflower methyl esters. Fuel, 92(1), 171-179.

[123] Saha, A., Kumar, R., & Basu, S. (2010). Infrared thermography and numerical study of vaporization characteristics of pure and blended bio-fuel droplets. International Journal of Heat and Mass Transfer, 53(19), 3862-3873.

[124] Barata, J. (2008). Modelling of biofuel droplets dispersion and evaporation. Renewable energy, 33(4), 769-779.

[125] Gu, X., Basu, S., & Kumar, R. (2012). Dispersion and vaporization of biofuels and conventional fuels in a crossflow pre-mixer. International Journal of Heat and Mass Transfer, 55(1), 336-346.

[126] Founti, M., Kolaitis, D., Zannis, G., Kastner, O., & Trimis, D. (2002). Experimental determination of fuel evaporation rates using IR-thermography. In Proceedings of the 6 th Int. Conference on Quantitative Infrared Thermography.

[127] Zhang, Y., & Van Gerpen, J. H. (1996). Combustion analysis of esters of soybean oil in a diesel engine (No. 960765). SAE Technical Paper.

[128] McDonald, J. F., Purcell, D. L., McClure, B. T., & Kittelson, D. B. (1995). Emissions characteristics of soy methyl ester fuels in an IDI compression ignition engine (No. 950400). SAE Technical Paper.

[129] Radwan, M. S., Dandoush, S. K., Selim, M. Y. E., & Kader, A. M. A. (1997). Ignition delay period of jojoba diesel engine fuel (No. 972975). SAE Technical Paper.

[130] Kumar, M. S., Ramesh, A., & Nagalingam, B. (2003). An experimental comparison of methods to use methanol and Jatropha oil in a compression ignition engine. biomass and bioenergy, 25(3), 309-318.

[131] Usta, N., Öztürk, E., Can, Ö., Conkur, E. S., Nas, S., Con, A. H., ... & Topcu, M. (2005). Combustion of biodiesel fuel produced from hazelnut soapstock/waste sunflower oil mixture in a diesel engine. Energy Conversion and Management, 46(5), 741-755.

[132] Dorado, M. P., Ballesteros, E., Arnal, J. M., Gomez, J., & Lopez, F. J. (2003). Exhaust emissions from a Diesel engine fueled with transesterified waste olive oil☆. Fuel, 82(11), 1311-1315.

[133] Ali, Y., & Hanna, M. A. (1997). In-cylinder pressure characteristics of a DI heavy duty diesel engine on biodiesel fuel (No. 971683). SAE Technical Paper.

[134] Senatore, A., Cardone, M., Rocco, V., & Prati, M. V. (2000). A comparative analysis of combustion process in DI diesel engine fueled with biodiesel and diesel fuel (No. 2000-01-0691). SAE Technical Paper.

[135] Selim, M. Y. E., Radwan, M. S., & Elfeky, S. M. (2003). Combustion of jojoba methyl ester in an indirect injection diesel engine. Renewable energy, 28(9), 1401-1420.

[136] Tashtoush, G., Al-Widyan, M. I., & Al-Shyoukh, A. O. (2003). Combustion performance and emissions of ethyl ester of a waste vegetable oil in a water-cooled furnace. Applied Thermal Engineering, 23(3), 285-293.

[137] Anand, K., Sharma, R. P., & Mehta, P. S. (2011). Experimental investigations on combustion, performance and emissions characteristics of neat karanji biodiesel and its methanol blend in a diesel engine. Biomass and bioenergy, 35(1), 533-541.

[138] Gumus, M. (2010). A comprehensive experimental investigation of combustion and heat release characteristics of a biodiesel (hazelnut kernel oil methyl ester) fueled direct injection compression ignition engine. Fuel, 89(10), 2802-2814.

[139] Kumar, M. S., Ramesh, A., & Nagalingam, B. (2010). A comparison of the different methods of using Jatropha oil as fuel in a compression ignition engine. Journal of Engineering for Gas Turbines and Power, 132(3), 032801.

[140] Buyukkaya, E. (2010). Effects of biodiesel on a DI diesel engine performance, emission and combustion characteristics. Fuel, 89(10), 3099-3105.

[141] Özener, O., Yüksek, L., Ergenç, A. T., & Özkan, M. (2014). Effects of soybean biodiesel on a DI diesel engine performance, emission and combustion characteristics. Fuel, 115, 875-883.

[142] Dhar, A., Kevin, R., & Agarwal, A. K. (2012). Production of biodiesel from high-FFA neem oil and its performance, emission and combustion characterization in a single cylinder DICI engine. Fuel Processing Technology, 97, 118-129.

[143] Vallinayagam, R., Vedharaj, S., Yang, W. M., Lee, P. S., Chua, K. J. E., & Chou, S. K. (2013). Combustion performance and emission characteristics study of pine oil in a diesel engine. Energy, 57, 344-351.

[144] Sudhir, C. V., Sharma, N. Y., & Mohanan, P. (2007). Potential of waste cooking oils as biodiesel feedstock. Emirates journal for engineering research, 12(3), 69-75.

[145] Yu, C. W., Bari, S., & Ameen, A. (2002). A comparison of combustion characteristics of waste cooking oil with diesel as fuel in a direct injection diesel engine. Proceedings of the Institution of Mechanical Engineers, Part D: Journal of Automobile Engineering, 216(3), 237-243.

[146] Lapuerta, M., Herreros, J. M., Lyons, L. L., García-Contreras, R., & Briceño, Y. (2008). Effect of the alcohol type used in the production of waste cooking oil biodiesel on diesel performance and emissions. Fuel, 87(15), 3161-3169.

[147] Özkan, M., Ergenç, A. T., & Deniz, O. (2005). Experimental performance analysis of biodiesel, traditional diesel and biodiesel with glycerine. Turkish Journal of Engineering & Environmental Sciences, 29(2), 89-94.

[148] Rao, G. L. N., Sampath, S., & Rajagopal, K. (2008). Experimental studies on the combustion and emission characteristics of a diesel engine fuelled with used cooking oil methyl ester and its diesel blends. International Journal Engineering and Applied Sciences, 4, 64-70.

[149] Kannan, G. R., Karvembu, R., & Anand, R. (2011). Effect of metal based additive on performance emission and combustion characteristics of diesel engine fuelled with biodiesel. Applied Energy, 88(11), 3694-3703.

[150] Ozsezen, A. N., Canakci, M., Turkcan, A., & Sayin, C. (2009). Performance and combustion characteristics of a DI diesel engine fueled with waste palm oil and canola oil methyl esters. Fuel, 88(4), 629-636.

[151] Tsolakis, A., Megaritis, A., Wyszynski, M. L., & Theinnoi, K. (2007). Engine performance and emissions of a diesel engine operating on diesel-RME (rapeseed methyl ester) blends with EGR (exhaust gas recirculation). Energy, 32(11), 2072-2080.

[152] Yoon, S. H., & Lee, C. S. (2011). Experimental investigation on the combustion and exhaust emission characteristics of biogas–biodiesel dual-fuel combustion in a CI engine. Fuel processing technology, 92(5), 992-1000.

[153] Radu, R., Petru, C., Edward, R., & Gheorghe, M. (2009). Fueling an DI agricultural diesel engine with waste oil biodiesel: effects over injection, combustion and engine characteristics. Energy Conversion and Management, 50(9), 2158-2166.

[154] Sahoo, P. K., & Das, L. M. (2009). Combustion analysis of Jatropha, Karanja and Polanga based biodiesel as fuel in a diesel engine. Fuel, 88(6), 994-999.

[155] Purushothaman, K., & Nagarajan, G. (2009). Effect of injection pressure on heat release rate and emissions in CI engine using orange skin powder diesel solution. Energy Conversion and Management, 50(4), 962-969.

[156] Qi, D. H., Geng, L. M., Chen, H., Bian, Y. Z., Liu, J., & Ren, X. C. (2009). Combustion and performance evaluation of a diesel engine fueled with biodiesel produced from soybean crude oil. Renewable Energy, 34(12), 2706-2713.

[157] Ozsezen, A. N., Canakci, M., & Sayin, C. (2008). Effects of biodiesel from used frying palm oil on the performance, injection, and combustion characteristics of an indirect injection diesel engine. Energy & Fuels, 22(2), 1297-1305.

[158] Canakci, M., Ozsezen, A. N., & Turkcan, A. (2009). Combustion analysis of preheated crude sunflower oil in an IDI diesel engine. Biomass and bioenergy, 33(5), 760-767.

[159] Canakci, M. (2007). Combustion characteristics of a turbocharged DI compression ignition engine fueled with petroleum diesel fuels and biodiesel. Bioresource technology, 98(6), 1167-1175.

[160] Lif, A., & Holmberg, K. (2006). Water-in-diesel emulsions and related systems. Advances in colloid and interface science, 123, 231-239.

[161] Sinha, S., & Agarwal, A. K. (2006, January). Combustion characteristics of rice bran oil derived biodiesel in a transportation diesel engine. In ASME 2006 Internal Combustion Engine Division Spring Technical Conference (pp. 333-340). American Society of Mechanical Engineers.

[162] Qi, D. H., Chen, H., Geng, L. M., & Bian, Y. Z. (2011). Effect of diethyl ether and ethanol additives on the combustion and emission characteristics of biodiesel-diesel blended fuel engine. Renewable Energy, 36(4), 1252-1258.

[163] Chen, H., Shi-Jin, S., & Jian-Xin, W. (2007). Study on combustion characteristics and PM emission of diesel engines using ester–ethanol–diesel blended fuels. Proceedings of the Combustion institute, 31(2), 2981-2989.

[164] Lu, X., Ma, J., Ji, L., & Huang, Z. (2008). Simultaneous reduction of NOx emission and smoke opacity of biodiesel-fueled engines by port injection of ethanol. Fuel, 87(7), 1289-1296.

[165] Dagaut, P., Gaı, S., & Sahasrabudhe, M. (2007). Rapeseed oil methyl ester oxidation over extended ranges of pressure, temperature, and equivalence ratio: Experimental and modeling kinetic study. Proceedings of the Combustion Institute, 31(2), 2955-2961.

[166] Suryanarayanan, S., Janakiraman, V. M., Sekar, J., Lakshmi, G., & Rao, N. (2007). Prediction of cetane number of a biodiesel based on physical properties and a study of their influence on cetane number (No. 2007-01-0077). SAE Technical Paper.

[167] Szybist, J. P., Song, J., Alam, M., & Boehman, A. L. (2007). Biodiesel combustion, emissions and emission control. Fuel Processing Technology, 88(7), 679-691.

[168] Marchese, A. J., Vaughn, T. L., Kroenlein, K., & Dryer, F. L. (2011). Ignition delay of fatty acid methyl ester fuel droplets: Microgravity experiments and detailed numerical modeling. Proceedings of the Combustion Institute, 33(2), 2021-2030.

[169] Zhu, M., Ma, Y., & Zhang, D. (2013). Effect of a homogeneous combustion catalyst on combustion characteristics of single droplets of diesel and biodiesel. Proceedings of the Combustion Institute, 34(1), 1537-1544.

[170] Pan, K. L., & Chiu, M. C. (2013). Droplet combustion of blended fuels with alcohol and biodiesel/diesel in microgravity condition. Fuel, 113, 757-765.

[171] Li, T. X., Zhu, D. L., Akafuah, N. K., Saito, K., & Law, C. K. (2011). Synthesis, droplet combustion, and sooting characteristics of biodiesel produced from waste vegetable oils. Proceedings of the Combustion Institute, 33(2), 2039-2046.

[172] Botero, M. L., Huang, Y., Zhu, D. L., Molina, A., & Law, C. K. (2012). Synergistic combustion of droplets of ethanol, diesel and biodiesel mixtures. Fuel, 94, 342-347.

[173] Raghavan, V., Rajesh, S., Parag, S., & Avinash, V. (2009). Investigation of combustion characteristics of biodiesel and its blends. Combustion Science and Technology, 181(6), 877-891.

[174] Rajesh, S., Raghavan, V., Shet, U. S. P., & Sundararajan, T. (2008). Analysis of quasi-steady combustion of Jatropha bio-diesel. International Communications in Heat and Mass Transfer, 35(9), 1079-1083.

[175] Prakash, P., Raghavan, V., & Mehta, P. S. (2013). Analysis of Multimode Burning Characteristics of Isolated Droplets of Biodiesel–Diesel Blends. Journal of Energy Resources Technology, 135(2), 024501.

[176] Raslavičius, L., & Bazaras, Ž. (2010). Variations in oxygenated blend composition to meet energy and combustion characteristics very similar to the diesel fuel. Fuel Processing Technology, 91(9), 1049-1054.

[177] Raslavičius, L., & Bazaras, Ž. (2010). Prediction of multi-component effects on ignition delay of oxygenated diesel fuel blends. Indian Journal of Engineering and Materials Sciences, 17(4), 243-250.

[178] Pan, K. L., Li, J. W., Chen, C. P., & Wang, C. H. (2009). On droplet combustion of biodiesel fuel mixed with diesel/alkanes in microgravity condition. Combustion and Flame, 156(10), 1926-1936.

[179] Lakshmi Narayana Rao, G., Durga Prasad, B., Sampath, S., & Rajagopal, K. (2007). Combustion analysis of diesel engine fueled with jatropha oil methyl ester-diesel blends. International Journal of Green Energy, 4(6), 645-658.

[180] Hazar, H. (2009). Effects of biodiesel on a low heat loss diesel engine. Renewable Energy, 34(6), 1533-1537.

[181] Murillo, S., Miguez, J. L., Porteiro, J., Granada, E., & Moran, J. C. (2007). Performance and exhaust emissions in the use of biodiesel in outboard diesel engines. Fuel, 86(12), 1765-1771.

[182] Hansen, A. C., Gratton, M. R., & Yuan, W. (2006). Diesel engine performance and NOX emissions from oxygenated biofuels and blends with diesel fuel. Transactions of the ASABE, 49(3), 589-595.

[183] Song, J. T., & Zhang, C. H. (2008). An experimental study on the performance and exhaust emissions of a diesel engine fuelled with soybean oil methyl ester. Proceedings of the Institution of Mechanical Engineers, Part D: Journal of Automobile Engineering, 222(12), 2487-2496.

[184] Kim, H., & Choi, B. (2010). The effect of biodiesel and bioethanol blended diesel fuel on nanoparticles and exhaust emissions from CRDI diesel engine. Renewable energy, 35(1), 157-163.

[185] Usta, N. (2005). Use of tobacco seed oil methyl ester in a turbocharged indirect injection diesel engine. Biomass and bioenergy, 28(1), 77-86.

[186] Gumus, M., & Kasifoglu, S. (2010). Performance and emission evaluation of a compression ignition engine using a biodiesel (apricot seed kernel oil methyl ester) and its blends with diesel fuel. Biomass and bioenergy, 34(1), 134-139.

[187] Zhu, L., Zhang, W., Liu, W., & Huang, Z. (2010). Experimental study on particulate and NO x emissions of a diesel engine fueled with ultra low sulfur diesel, RME-diesel blends and PME-diesel blends. Science of the Total Environment, 408(5), 1050-1058.

[188] Godiganur, S., Murthy, C. S., & Reddy, R. P. (2010). Performance and emission characteristics of a Kirloskar HA394 diesel engine operated on fish oil methyl esters. Renewable Energy, 35(2), 355-359.

[189] Godiganur, S., Murthy, C. S., & Reddy, R. P. (2009). 6BTA 5.9 G2-1 Cummins engine performance and emission tests using methyl ester mahua (Madhuca indica) oil/diesel blends. Renewable Energy, 34(10), 2172-2177.

[190] Lujan, J. M., Bermúdez, V., Tormos, B., & Pla, B. (2009). Comparative analysis of a DI diesel engine fuelled with biodiesel blends during the European MVEG-A cycle: Performance and emissions (II). biomass and bioenergy, 33(6), 948-956.

[191] Sahoo, P. K., Das, L. M., Babu, M. K. G., Arora, P., Singh, V. P., Kumar, N. R., & Varyani, T. S. (2009). Comparative evaluation of performance and emission characteristics of jatropha, karanja and polanga based biodiesel as fuel in a tractor engine. Fuel, 88(9), 1698-1707.

[192] Fontaras, G., Karavalakis, G., Kousoulidou, M., Tzamkiozis, T., Ntziachristos, L., Bakeas, E., ... & Samaras, Z. (2009). Effects of biodiesel on passenger car fuel consumption, regulated and non-regulated pollutant emissions over legislated and real-world driving cycles. Fuel, 88(9), 1608-1617.

[193] Korres, D. M., Karonis, D., Lois, E., Linck, M. B., & Gupta, A. K. (2008). Aviation fuel JP-5 and biodiesel on a diesel engine. Fuel, 87(1), 70-78.

[194] Raheman, H., & Ghadge, S. V. (2007). Performance of compression ignition engine with mahua (Madhuca indica) biodiesel. Fuel, 86(16), 2568-2573.

[195] Canakci, M. (2005). Performance and emissions characteristics of biodiesel from soybean oil. Proceedings of the Institution of Mechanical Engineers, Part D: Journal of Automobile Engineering, 219(7), 915-922.

[196] Nabi, M. N., Hoque, S. N., & Akhter, M. S. (2009). Karanja (Pongamia Pinnata) biodiesel production in Bangladesh, characterization of karanja biodiesel and its effect on diesel emissions. Fuel Processing Technology, 90(9), 1080-1086.

[197] Lertsathapornsuk, V., Pairintra, R., Aryusuk, K., & Krisnangkura, K. (2008). Microwave assisted in continuous biodiesel production from waste frying palm oil and its performance in a 100 kW diesel generator. Fuel Processing Technology, 89(12), 1330-1336.

[198] Lin, B. F., Huang, J. H., & Huang, D. Y. (2009). Experimental study of the effects of vegetable oil methyl ester on DI diesel engine performance characteristics and pollutant emissions. Fuel, 88(9), 1779-1785.

[199] NURUN NABI, M., Najmul Hoque, S. M., & SHAMIM AKHTER, M. (2009). Karanja (Pongamia Pinnata) biodiesel production in Bangladesh, characterization of karanja biodiesel and its effect on diesel emissions. Fuel processing technology, 90(9), 1080-1086.

[200] P. K. Devan and N. V. Mahalakshmi, "A study of the performance, emission and combustion characteristics of a compression ignition engine using methyl ester of paradise oil–eucalyptus oil blends," *Appl. Energy*, vol. 86, no. 5, pp. 675–680, May 2009.

[201] Zheng, M., Mulenga, M. C., Reader, G. T., Wang, M., Ting, D. S., & Tjong, J. (2008). Biodiesel engine performance and emissions in low temperature combustion. Fuel, 87(6), 714-722.

[202] Karra, P. K., Veltman, M. K., & Kong, S. C. (2008). Characteristics of engine emissions using biodiesel blends in low-temperature combustion regimes. Energy & Fuels, 22(6), 3763-3770.

[203] Nabi, M. N., Akhter, M. S., & Shahadat, M. M. Z. (2006). Improvement of engine emissions with conventional diesel fuel and diesel–biodiesel blends. Bioresource Technology, 97(3), 372-378.

[204] Aydin, H., & Bayindir, H. (2010). Performance and emission analysis of cottonseed oil methyl ester in a diesel engine. Renewable Energy, 35(3), 588-592.

[205] Raheman, H., & Phadatare, A. G. (2004). Diesel engine emissions and performance from blends of karanja methyl ester and diesel. Biomass and Bioenergy, 27(4), 393-397.

[206] Utlu, Z., & Koçak, M. S. (2008). The effect of biodiesel fuel obtained from waste frying oil on direct injection diesel engine performance and exhaust emissions. Renewable Energy, 33(8), 1936-1941.

[207] Sharma, D., Soni, S. L., & Mathur, J. (2009). Emission reduction in a direct injection diesel engine fueled by neem-diesel blend. Energy Sources, Part A, 31(6), 500-508.

[208] Armas, O., Yehliu, K., & Boehman, A. L. (2010). Effect of alternative fuels on exhaust emissions during diesel engine operation with matched combustion phasing. Fuel, 89(2), 438-456.

[209] Cheung, C. S., Zhu, L., & Huang, Z. (2009). Regulated and unregulated emissions from a diesel engine fueled with biodiesel and biodiesel blended with methanol. Atmospheric Environment, 43(32), 4865-4872.

[210] Nascimento, M. A., Lora, E. S., Corrêa, P. S., Andrade, R. V., Rendon, M. A., Venturini, O. J., & Ramirez, G. A. (2008). Biodiesel fuel in diesel micro-turbine engines: Modelling and experimental evaluation. Energy, 33(2), 233-240.

[211] Puhan, S., Vedaraman, N., Ram, B. V., Sankarnarayanan, G., & Jeychandran, K. (2005). Mahua oil (Madhuca Indica seed oil) methyl ester as biodiesel-preparation and emission characterstics. Biomass and Bioenergy, 28(1), 87-93.

[212] Baiju, B., Naik, M. K., & Das, L. M. (2009). A comparative evaluation of compression ignition engine characteristics using methyl and ethyl esters of Karanja oil. Renewable energy, 34(6), 1616-1621.

[213] Puhan, S., Vedaraman, N., Sankaranarayanan, G., & Ram, B. V. B. (2005). Performance and emission study of Mahua oil (Madhuca indica oil) ethyl ester in a 4-stroke natural aspirated direct injection diesel engine. Renewable Energy, 30(8), 1269-1278.

[214] Kalligeros, S., Zannikos, F., Stournas, S., Lois, E., Anastopoulos, G., Teas, C., & Sakellaropoulos, F. (2003). An investigation of using biodiesel/marine diesel blends on the performance of a stationary diesel engine. Biomass and Bioenergy, 24(2), 141-149.

[215] Lapuerta, M., Armas, O., Ballesteros, R., & Fernández, J. (2005). Diesel emissions from biofuels derived from Spanish potential vegetable oils. Fuel, 84(6), 773-780.

[216] Banapurmath, N. R., Tewari, P. G., & Hosmath, R. S. (2008). Performance and emission characteristics of a DI compression ignition engine operated on Honge, Jatropha and sesame oil methyl esters. Renewable energy, 33(9), 1982-1988.

[217] Wang, W. G., Lyons, D. W., Clark, N. N., Gautam, M., & Norton, P. M. (2000). Emissions from nine heavy trucks fueled by diesel and biodiesel blend without engine modification. Environmental Science & Technology, 34(6), 933-939.

[218] Durbin, T. D., & Norbeck, J. M. (2002). Effects of biodiesel blends and Arco EC-diesel on emissions from light heavy-duty diesel vehicles. Environmental science & technology, 36(8), 1686-1691.

[219] Keskin, A., Gürü, M., & Altıparmak, D. (2008). Influence of tall oil biodiesel with Mg and Mo based fuel additives on diesel engine performance and emission. Bioresource technology, 99(14), 6434-6438.

[220] Gürü, M., Koca, A., Can, Ö., Çınar, C., & Şahin, F. (2010). Biodiesel production from waste chicken fat based sources and evaluation with Mg based additive in a diesel engine. Renewable Energy, 35(3), 637-643.

[221] Kalam, M. A., & Masjuki, H. H. (2008). Testing palm biodiesel and NPAA additives to control NOx and CO while improving efficiency in diesel engines. Biomass and Bioenergy, 32(12), 1116-1122.

[222] Ryu, K. (2010). The characteristics of performance and exhaust emissions of a diesel engine using a biodiesel with antioxidants. Bioresource technology, 101(1), S78-S82.

[223] Pang, X., Shi, X., Mu, Y., He, H., Shuai, S., Chen, H., & Li, R. (2006). Characteristics of carbonyl compounds emission from a diesel-engine using biodiesel–ethanol–diesel as fuel. Atmospheric environment, 40(36), 7057-7065.

[224] Ghobadian, B., Yusaf, T., Najafi, G., & Khatamifar, M. (2009). Diesterol: An environment-friendly IC engine fuel. Renewable Energy, 34(1), 335-342.

[225] Qi, D. H., Chen, H., Matthews, R. D., & Bian, Y. Z. (2010). Combustion and emission characteristics of ethanol–biodiesel–water micro-emulsions used in a direct injection compression ignition engine. Fuel, 89(5), 958-964.

[226] Kumar, M. S., Kerihuel, A., Bellettre, J., & Tazerout, M. (2006). Ethanol animal fat emulsions as a diesel engine fuel–part 2: engine test analysis. Fuel, 85(17), 2646-2652.

[227] Di, Y., Cheung, C. S., & Huang, Z. (2009). Comparison of the effect of biodiesel-diesel and ethanol-diesel on the gaseous emission of a direct-injection diesel engine. Atmospheric Environment, 43(17), 2721-2730.

[228] Zhu, L., Cheung, C. S., Zhang, W. G., & Huang, Z. (2011). Combustion, performance and emission characteristics of a DI diesel engine fueled with ethanol–biodiesel blends. Fuel, 90(5), 1743-1750.

[229] Szybist, J. P., Boehman, A. L., Taylor, J. D., & McCormick, R. L. (2005). Evaluation of formulation strategies to eliminate the biodiesel NO x effect. Fuel Processing Technology, 86(10), 1109-1126.

[230] Lin, C. Y., & Lin, H. A. (2007). Engine performance and emission characteristics of a three-phase emulsion of biodiesel produced by peroxidation. Fuel Processing Technology, 88(1), 35-41.

[231] Keskin, A., Gürü, M., & Altıparmak, D. (2007). Biodiesel production from tall oil with synthesized Mn and Ni based additives: effects of the additives on fuel consumption and emissions. Fuel, 86(7), 1139-1143.

[232] Xiaoyan, S. H. I., Yunbo, Y. U., Hong, H. E., Shuai, S., Hongyi, D. O. N. G., & Rulong, L. I. (2008). Combination of biodiesel-ethanol-diesel fuel blend and SCR catalyst assembly to reduce emissions from a heavy-duty diesel engine. Journal of Environmental Sciences, 20(2), 177-182.

[233] Labeckas, G., & Slavinskas, S. (2005). Influence of fuel additives on performance of direct-injection Diesel engine and exhaust emissions when operating on shale oil. Energy conversion and management, 46(11), 1731-1744.

[234] Kass, M. D., Lewis, S. A., Swartz, M. M., Huff, S. P., Lee, D. W., Wagner, R. M., & Storey, J. M. E. (2009). Utilizing water emulsification to reduce NOx and particulate emissions associated with biodiesel. Transactions of the ASABE, 52(1), 5-13.

[235] Balaji, G., & Cheralathan, M. (2014). Experimental investigation to reduce emissions of CI (compression ignition) engine fuelled with methyl ester of cottonseed oil using antioxidant. International Journal of Ambient Energy, 35(1), 13-19.

[236] Sajith, V., Sobhan, C. B., & Peterson, G. P. (2010). Experimental investigations on the effects of cerium oxide nanoparticle fuel additives on biodiesel. Advances in Mechanical Engineering, 2, 581407.

[237] Venkatesan, S. P., & Kadiresh, P. N. (2014). Influence of an aqueous cerium oxide nanofluid fuel additive on performance and emission characteristics of a compression ignition engine. International Journal of Ambient Energy, (ahead-of-print), 1-4.

[238] Lin, C. Y., & Lin, H. A. (2006). Diesel engine performance and emission characteristics of biodiesel produced by the peroxidation process. Fuel, 85(3), 298-305.

[239] Fangsuwannarak. K and Triratanasirichai. K (2013). Effect of metalloid compound and bio-solution additives on biodiesel engine performance and exhaust emissions. *Am. J. Appl. Sci.*, vol. 10, no. 10, pp. 1201–1213.

[240] Cheng, C. H., Cheung, C. S., Chan, T. L., Lee, S. C., Yao, C. D., & Tsang, K. S. (2008). Comparison of emissions of a direct injection diesel engine operating on biodiesel with emulsified and fumigated methanol. Fuel, 87(10), 1870-1879.

[241] Ulusoy, Y., Tekin, Y., Cetinkaya, M., & Karaosmanoglu, F. (2004). The engine tests of biodiesel from used frying oil. Energy Sources, 26(10), 927-932.

[242] Ramadhas, A. S., Muraleedharan, C., & Jayaraj, S. (2005). Performance and emission evaluation of a diesel engine fueled with methyl esters of rubber seed oil. Renewable energy, 30(12), 1789-1800.

[243] Labeckas, G., & Slavinskas, S. (2006). The effect of rapeseed oil methyl ester on direct injection diesel engine performance and exhaust emissions. Energy Conversion and Management, 47(13), 1954-1967.

[244] Chauhan, B. S., Kumar, N., & Cho, H. M. (2012). A study on the performance and emission of a diesel engine fueled with Jatropha biodiesel oil and its blends. Energy, 37(1), 616-622.

[245] Carraretto, C., Macor, A., Mirandola, A., Stoppato, A., & Tonon, S. (2004). Biodiesel as alternative fuel: experimental analysis and energetic evaluations. Energy, 29(12), 2195-2211.

[246] Wu, F., Wang, J., Chen, W., & Shuai, S. (2009). A study on emission performance of a diesel engine fueled with five typical methyl ester biodiesels. Atmospheric Environment, 43(7), 1481-1485.

[247] Krahl, J., Munack, A., Schröder, O., Stein, H., & Bünger, J. (2003). Influence of biodiesel and different designed diesel fuels on the exhaust gas emissions and health effects (No. 2003-01-3199). SAE Technical Paper.

[248] Ng, H. K., & Gan, S. (2010). Combustion performance and exhaust emissions from the non-pressurised combustion of palm oil biodiesel blends. Applied Thermal Engineering, 30(16), 2476-2484.

[249] Mofijur, M., Masjuki, H. H., Kalam, M. A., & Shahabuddin, M. (2012). Experimental study of additive added palm biodiesel in a compression ignition engine. Energy Educ Sci Technol Part A: Energy Sci Res, 30, 737e48.

[250] Swaminathan, C., & Sarangan, J. (2012). Performance and exhaust emission characteristics of a CI engine fueled with biodiesel (fish oil) with DEE as additive. biomass and bioenergy, 39, 168-174.

[251] Labeckas, G., & Slavinskas, S. (2009, May). Performance and emission characteristics of off-road diesel engine operating on rapeseed oil and petrol blends. In Proceedings of the8th International Scientific Conference 'Engineering for Rural Development'. Latvia, University of Agriculture, Jelgava (pp. 135-140).

[252] Ghobadian, B., Rahimi, H., Nikbakht, A. M., Najafi, G., & Yusaf, T. F. (2009). Diesel engine performance and exhaust emission analysis using waste cooking biodiesel fuel with an artificial neural network. Renewable Energy, 34(4), 976-982.

[253] Fattah, I. R., Masjuki, H. H., Kalam, M. A., Wakil, M. A., Ashraful, A. M., & Shahir, S. A. (2014). Experimental investigation of performance and regulated emissions of a diesel engine with Calophyllum inophyllum biodiesel blends accompanied by oxidation inhibitors. Energy Conversion and Management, 83, 232-240.

[254] Canakci, M., Sayin, C., & Gumus, M. (2008). Exhaust emissions and combustion characteristics of a direct injection (DI) diesel engine fueled with methanol− diesel fuel blends at different injection timings. Energy & Fuels, 22(6), 3709-3723.

[255] Haas, M. J., Scott, K. M., Alleman, T. L., & McCormick, R. L. (2001). Engine Performance of Biodiesel Fuel Prepared from Soybean Soapstock: A High Quality Renewable Fuel Produced from a Waste Feedstock||. Energy & Fuels, 15(5), 1207-1212.

[256] Lapuerta, M., Armas, O., Ballesteros, R., & Carmona, M. (2000). Fuel formulation effects on passenger car diesel engine particulate emissions and composition (No. 2000-01-1850). SAE Technical Paper.

[257] Chen, K. S., Lin, Y. C., Hsieh, L. T., Lin, L. F., & Wu, C. C. (2010). Saving energy and reducing pollution by use of emulsified palm-biodiesel blends with bio-solution additive. Energy, 35(5), 2043-2048.

[258] Xiaoyan, S. H. I., Yunbo, Y. U., Hong, H. E., Shuai, S., Hongyi, D. O. N. G., & Rulong, L. I. (2008). Combination of biodiesel-ethanol-diesel fuel blend and SCR catalyst assembly to reduce emissions from a heavy-duty diesel engine. Journal of Environmental Sciences, 20(2), 177-182.

[259] Subbaiah, G. V., Gopal, K. R., Hussain, S. A., Prasad, B. D., & Reddy, K. T. (2010). Rice bran oil biodiesel as an additive in diesel-ethanol blends for diesel engines.

[260] Keskin, A., Gürü, M., & Altiparmak, D. (2010). The investigation of performance and emissions characteristics of tall oil biodiesel with a co-based additive. Energy Sources, Part A: Recovery, Utilization, and Environmental Effects, 32(20), 1899-1907.

[261] Shahir, S. A., Masjuki, H. H., Kalam, M. A., Imran, A., & Ashraful, A. M. (2015). Performance and emission assessment of diesel–biodiesel–ethanol/bioethanol blend as a fuel in diesel engines: A review. Renewable and Sustainable Energy Reviews, 48, 62-78.

[262] Fabbro, S. (2012). An experimental test facility for studying the effects of turbulence on the evaporation of fuel droplets at elevated pressure and temperature conditions.

[263] Birouk, M., & Fabbro, S. C. (2013). Droplet evaporation in a turbulent atmosphere at elevated pressure–Experimental data. Proceedings of the Combustion Institute, 34(1), 1577-1584.

[264] Toth, S. L. (2014). Experimental study of droplet vaporization and combustion of diesel, biodiesel and their blends in a turbulent environment at elevated pressure and temperature conditions.

[265] Nomura, H., Ujiie, Y., Rath, H. J., Sato, J. I., & Kono, M. (1996, December). Experimental study on high-pressure droplet evaporation using microgravity conditions. In Symposium (International) on Combustion (Vol. 26, No. 1, pp. 1267-1273). Elsevier.

[266] Spalding, D. B. (1953, December). The combustion of liquid fuels. In Symposium (international) on combustion (Vol. 4, No. 1, pp. 847-864). Elsevier.

[267] Godsave, G. A. E. (1953, December). Studies of the combustion of drops in a fuel spray—the burning of single drops of fuel. In Symposium (International) on Combustion (Vol. 4, No. 1, pp. 818-830). Elsevier.

[268] Birouk, M. (2014). A hydrocarbon droplet evaporating in turbulent environment at elevated ambient pressure and temperature. Combustion Science and Technology, 186(10-11), 1295-1308.

[269] Kobayasi, K. (1954). A Study on the Evaporation Velocity of a Single Liquid Droplet. Technol. Rep. Tohoko Univ.

[270] Gan, Y., & Qiao, L. (2011). Evaporation characteristics of fuel droplets with the addition of nanoparticles under natural and forced convections. International Journal of Heat and Mass Transfer, 54(23), 4913-4922.

[271] Birouk, M., & Fabbro, S. C. (2013). Droplet evaporation in a turbulent atmosphere at elevated pressure–Experimental data. Proceedings of the Combustion Institute, 34(1), 1577-1584.

[272] Birouk, M., & Toth, S. L. (2015). Vaporization and Combustion of a Soybean Biodiesel Droplet in Turbulent Environment at Elevated Ambient Pressure. Combustion Science and Technology, 187(6), 937-952.

[273] Qi, D. H., Chen, H., Geng, L. M., Bian, Y. Z., & Ren, X. C. (2010). Performance and combustion characteristics of biodiesel–diesel–methanol blend fuelled engine. Applied Energy, 87(5), 1679-1686.

[274] Rakopoulos, D. C., Rakopoulos, C. D., Papagiannakis, R. G., & Kyritsis, D. C. (2011). Combustion heat release analysis of ethanol or n-butanol diesel fuel blends in heavy-duty DI diesel engine. Fuel, 90(5), 1855-1867.

[275] Sagadeev, E. V., Kafiatullin, R. A., Sagadeev, V. V., & Sagadeev, V. I. (2003). Applying an additive scheme to the calculation of the heat of combustion of saturated hydrocarbons. Theoretical Foundations of Chemical Engineering, 37(1), 92-95.

[276] Kitano, T., Nishio, J., Kurose, R., & Komori, S. (2014). Evaporation and combustion of multicomponent fuel droplets. Fuel, 136, 219-225.

[277] Monyem, A., & Van Gerpen, J. H. (2001). The effect of biodiesel oxidation on engine performance and emissions. Biomass and Bioenergy, 20(4), 317-325.

[278] Lin, C. Y., & Chiu, C. C. (2009). Effects of oxidation during long-term storage on the fuel properties of palm oil-based biodiesel. Energy & Fuels, 23(6), 3285-3289.

Appendix A. INSTRUMENTATION

A list of instruments that have been used for the experiment is provided in the subsequent paragraphs.

Temperature Measurement Devices:

- K type thermocouples from Omega Engineering Inc.
    - Model No. KQXL-18G-[**], where [**] refers to the length of the thermocouple probe. Lengths of 6 and 12 inches were used.
    - Accuracy of ±2.20C or 0.75% of the rated temperature range.

Pressure Measurement Devices:

- Digital pressure gauge from Cecomp Electronics (USA)
    - Model No.: DPG1000B500PSIG-ON-CC
    - Accuracy: ± 0.25% of full scale ± least significant digit
- Mechanical Pressure release valve from Swagelok
    - Model No.: SS-4CA-150
    - Adjustable cracking pressure range: 150-350 psi

Fan Speed Measurement Devices:

- Stroboscope from Shimpo Instruments (by ELECTROMATIC Equip't Co., Inc.)
    - Model No.: DT-315A
    - Flash Speed Range: 100-30,000 flashes per minute
    - Accuracy: +0.01% of reading

Lower heating value (LHV) measurement Devices:

- IKA bomb calorimeter
    - Model No: IKA C200 S1
    - Maximum measuring range: 40000 J
    - Temperature measurement resolution: 0.0001 K

Appendix B. CHAMBER SEALS

B.1. Introduction

The details regarding the various seals (e.g., gaskets, o-rings and the fan shaft seals) of the spherical chamber are presented in this section.

B.2. Gasket Seals

Gasket seals are used to create a seal against the surface of a quartz window; there are two sizes of windows corresponding to chamber port openings with diameters of 4 and 5 inches.

Table 5.1: Gasket size specifications

Gasket Location	Inside Diameter [in]	Outside Diameter [in]	Thickness [in]
4 inch View Port	4	4 15/16	3/16, 3/32
5 inch View Port	5	5 15/16	3/16, 3/32

The current gasket material in service is called Extreme-Temperature Silicone Rubber Gaskets, however previous experimentation was done using gaskets made of the following materials; NA-60, graphite and Teflon. The material properties for all of the gasket materials are listed below.

Table 5.2: Gasket material properties

Property	Silicone Rubber Gaskets	NA-60 [web]	Graphite	PTFE (Teflon)
Max Pressure Rating (psi).	650	1000	2000	300
Max Temp. Limit (°F)	500	700	850	500

Max Contin. Temp. Limit (°F)	N/A	400	N/A	N/A
Max P x T (psi x F)	N/A	350,000	N/A	150,000
Colour	Orange to Red	Green	Silver-gray	White

B.3. O-ring Seals:

Sealing the rest of the flange ports was done with static o-ring seals as well as two dynamic o-ring seals for the droplet injection system. The various o-rings sizes are listed below for each respective seal in Table B.3, while the o-ring materials are listed in Table B.4. It should be noted that Viton Fluoroelastomer is a registered trademark of DuPont.

Table 5.3: O-ring size specifications

O-ring Locations	Inside Diameter [in]	Outside Diameter [in]	Thickness [in]	AS568A Dash No.
5 inch View Port	5 3/8	5 5/8	1/8	253
4 inch View Port	4 3/8	4 5/8	1/8	245
Fan Hub Assembly	4 1/4	4 1/2	1/8	244
Fan Shaft Seal	3/4	7/8	1/16	018
Accessory Ports incl. Top Center and Bottom	7/8	11/16	3/32	118
Sensor ports	7/8	11/16	3/32	118
Injector Adapter and	1	1 3/16	3/32	120

Piston				
Injector Fuel Piston #1	1/2	11/16	3/32	112
Injector Fuel Piston #2	3/8	5/8	1/8	204
Injector Teflon Insert	3/8	9/16	3/32	110

Table 5.4: O-ring material properties

O-ring material	Temperature Rating [^{o}C]	Durometer Hardness	Colour
High-Temperature Silicone	-51 to 204	A70	Red
Buna-Nitrile	-37 to 121	A70	Black
Viton Fluoroelastomer	-9 to 204	A75	Brown or Black
Silcone	-53 to 218	A70	Red-orange
Teflon	-73 to 260	D55	White

B.4. Fan Shaft Seals

The properties and supplier of poly-amide filled Teflon are presented in this section as well as a dimensioned drawing of the fan shaft seal.

Table 5.5: Material properties of poly-amide filled Teflon.

Property	Test Method	Value
Operating Temperature	N/A	-350 ^{o}F to 500^{o}F
Tensile Strength	ASTM D-4745	2200 psi

Tensile Elongation	ASTM D-4745	175%
Specific Gravity	ASTM D-4745	1.83
Filler Content	N_2 Burn Out	N/A
Deformation	RT, 2000 psi, 24 hrs. 212^{o}F, 2000 psi, 24 hrs.	3.5 - 4.0% 7.4%
Thermal Expansion	120 – 300^{o}F	5.6

Supplier: Laird Plastics

8 Plymount Street

Winnipeg, MB R2X 2V7

Phone: (204) 632-1136

Appendix C. MATLAB CODE

C.1. Introduction

An in-house developed Matlab code was used to determine the projected surface area of the droplet by analyzing image contrast of still images. The original Matlab code was developed by Toth [264]. Only few modifications have been made for the experimental purpose. This code uses a method of edge detection in combination with closure conditions to determine the upper and lower edges of the droplet by using a threshold to separate dark pixels (such as the droplet and suspension fiber) from the white background as well as the noise caused by a gradual build-up of particles on the viewing window. Once the droplet starting point has been found, the code examines the length of the each successive row using the detected left and right edges where the area of the droplet is determined by using trapezoidal integration between adjacent rows. After tabulating the area, the code corrects the area by using calibration sizes for the height and width of the image to determine the actual size of droplet. The droplet area is approximated as a circle where the area is divided by 4π to give the squared diameter of the droplet before finally printing the image number as well as the squared diameter to a text file.

C.2. Matlab Code

```
clear all;

clc;
close all;
dplot= false; % Troubleshooting use true with limited number of images

firstpic=0;
picstep=1;
lastpic=1200;
mst='ImgA000000'; % Use with MotionPro
% mst = 'ImgA0000'; % Use with PIV trigger
tdco=220;%Threshold for detecting start of drop, default 160
fiber_approx_start = 1; %Default setting is 1
```

```
fiber_approx_finish = 30; %Depends on image
dstartmin=fiber_approx_finish+10;
pixeldif = 6; %original value of 4; usually 6 works
contrastcontin = 4; %original value of 8
Fiber_avg_correction = 0;
Threshold = 200; % Global image threshold
Image_Examine = false;
Calibration_length = 3.67647; % Units are in mm, this assumes a square image.
tic;
for fco= 3: 4  % Number of experiments to process

   FileLocation=['Z:\Iqbal MSc Projects\new 10\New c10,100C,2000Rpm,1Bar\New
c10,100C,2000Rpm,1Bar_00',int2str(fco)];
%    dir(FileLocation)
%    return
   cd(FileLocation);
   hf = fopen('test.dat','wt');
   tic;
   icount=0;
   D2=zeros(length(firstpic:picstep:lastpic),1);
   Du=zeros(length(firstpic:picstep:lastpic),1);
   Dl=zeros(length(firstpic:picstep:lastpic),1);
   dstartt=zeros(length(firstpic:picstep:lastpic),1);
   for mco=firstpic:picstep:lastpic
      fprintf('mco = %d\tfco = %d\n',mco,fco);
      sno=num2str(mco);
      strng = [mst,sno];
            strng(5:(length(strng)-10+5-1))=''; % Use with MotionPro
%        strng(5:(length(strng)-8+5-1)) = ''; % Use with PIV trigger
      strng=[strng,'.tif'];
      %        strng = ['Fiber.tif'];
      if (exist(strng,'file')==0)
         disp(['No File']);
         continue;
      end
      [Img, map]= imread(strng);
      image = Img;
%        Threshold = graythresh(Img)*255;
      icount=icount+1;
%       % Removes needle from picture

      if(Image_Examine)
         size(ima2)
         figure,imshow(image);
         figure,imshow(Img);
```

```
    return
end
pos = find(Img<Threshold);
ima = zeros(size(Img));
ima(:,:) = 255;
ima(pos) = Img(pos);
Img = ima;

if dplot
    figure,imshow(image);
    figure
    imshow(Img);
    hold on
end
le=zeros(size(Img,1),1);
re=zeros(size(Img,1),1);
[row column] = size(Img);
for i=1:1:size(Img,1)
    der=diff(double(Img(i,:)));
    if ~isempty(find(abs(der)>0,1))
        le(i)= find(abs(der)>0,1)+2; %Defines left edge in each row, Which was 2 pixels out.
        re(i)= find(abs(der)>0,1,'last')-1; %Defines right edge in each row, out by 1 pixel.
    end
end
names =zeros(row,column);
maxrow = zeros(row,1);
count = 1;
for j=1:1:row
    dark=find(Img(j,:)<Threshold);
    count = 1;
    for k=1:1:length(dark)-1
        change = dark(k+1)-dark(k);
        if(change == 1)
            names(j,dark(k))= count;
        elseif(change > 1)
            count = count+1;
            names(j,dark(k+1)) = count;
        end
    end
    maxrow(j) = max(names(j,:));
end
pmax = zeros(row,1);
Area = zeros(row,column);
possizematrix = zeros(row,1);
index = zeros(row,1);
```

```
r = 381;
for m= 1:1:row
    for n=1:1:maxrow(m)
        pos = find(names(m,:)== n);
        possize(n) = length(pos);
    end

    possizematrix(m) = max(max(possize));
    pcheck = find(possize==max(possize));
    if(length(pcheck) > 1)
        pmax(m) = round(mean(pcheck));
        %                   disp(['Assuming an average value']);
    elseif(length(pcheck)==1)
        pmax(m) = pcheck;
    elseif(isempty(pcheck))
        pmax(m) =1;
        disp(['Fail Safe']);
    end
    posarea = find(names(m,:) == pmax(m));
    if(isempty(posarea))
        %                   disp(['Dropping row number ',int2str(m)]);
        continue;
    end
    for q=posarea(1):1:posarea(end)
        Area(m,q) = 1;
    end
end
toc
i=1;
while i<=length(le)
    if le(i)==0&&re(i)==0
        le(i)=[];
        re(i)=[];
    else
        i=i+1;
    end
end
if dplot
    for i=1:1:length(le)
        plot(le(i),i,'.k');
    end

    for i=1:1:length(re)
        plot(re(i),i,'.k');
    end
```

```
end
ic=1;
in=1;
ld=[];
while ic+in<=length(le)
    if abs(le(ic+in)-le(ic))<20
        if dplot
            line([le(ic) le(ic+in)],[ic (ic+in)]);
        end
        ic=ic+in;
        in=1;
    else
        %                   disp(['Dropping left edge point number ' int2str(ic+in)]);
        ld=[ld;ic+in];
        in=in+1;
    end
end
ic=1;
in=1;
rd=[];
while ic+in<=length(re)
    if abs(re(ic+in)-re(ic))<20
        if dplot
            line([re(ic) re(ic+in)],[ic (ic+in)]);
        end
        ic=ic+in;
        in=1;
    else
        %                   disp(['Dropping right edge point number ' int2str(ic+in)]);
        rd=[rd;ic+in];
        in=in+1;
    end
end
if dplot
    line([le(end) re(end)],[length(le) length(re)]);
end
fl=length(fiber_approx_start:fiber_approx_finish);
fibre = zeros(fl,1);

%% Centerline for determining droplet start point
centermatrix = zeros(size(fibre));
for k=fiber_approx_start:1:fiber_approx_finish
    fibre(k) = re(k)-le(k)+1;
    centermatrix(k) = round(mean([re(k),le(k)]));
end
```

```
centerline = round(mean(centermatrix));
fibreavg = mean(fibre)+Fiber_avg_correction;

i=dstartmin;
notfound=true;
dstart=0;
Trip_hazard = false;
while i<min([length(le) length(re)])&&notfound
   w = re(i)-le(i)+1;
   oldw = re(i-1)-le(i-1)+1;
   if(i+contrastcontin>length(le))||(i+contrastcontin>length(re))
      Trip_hazard = true;
      break;
   end
   if (Img(i,round(mean([le(i) re(i)])))<=tdco)&&((re(i)-le(i)+1)>(fibreavg+pixeldif))&&(w>oldw)&&(Img(i+contrastcontin,round(mean([le(i+contrastcontin) re(i+contrastcontin)])))<tdco)%&&(grey_check)
      dstart=i;
      dstartt(icount)=dstart;
      notfound=false;
   else
      i=i+1;
   end
end
if(Trip_hazard)
   disp(['Possibly overly bright image']);
   continue;
end
if notfound
   disp('Warning drop start not found...');
   continue;
else
   if dplot
      line([le(dstart) re(dstart)],[dstart dstart]);
   end

   mvl=round(mean([le(i) re(i)]));

   if dplot
      line([mvl mvl],[dstart max([length(le) length(re)])]);
   end
   ic=dstart;
   in=1;
   lpc=0;
   llb=0;
```

```
lub=0;
while ic+in<=length(le)
   if abs(le(ic+in)-le(ic))<20
      lpc=lpc+0.5*(2*mvl-le(ic+in)-le(ic))*in;
      llb=llb+0.5*(2*mvl-le(ic+in)-le(ic)+2)*in;
      lub=lub+0.5*(2*mvl-le(ic+in)-le(ic)-2)*in;
      if dplot
         patch([le(ic) mvl mvl le(ic+in)],[ic ic ic+in ic+in],[1 0 0]);
      end
      ic=ic+in;
      in=1;
   else
      in=in+1;
   end
end
llb=llb-(mvl-le(1)+1);
llb=llb-(mvl-le(end)+1);
lub=lub+(mvl-le(1)-1);
lub=lub+(mvl-le(end)-1);
ic=dstart;
in=1;
rpc=0;
rlb=0;
rub=0;
while ic+in<=length(re)
   if abs(re(ic+in)-re(ic))<20
      rpc=rpc+0.5*(-2*mvl+re(ic+in)+re(ic))*in;
      rlb=rlb+0.5*(-2*mvl+re(ic+in)+re(ic)-2)*in;
      rub=rub+0.5*(-2*mvl+re(ic+in)+re(ic)+2)*in;
      if dplot
         patch([re(ic) mvl mvl re(ic+in)],[ic ic ic+in ic+in],[0 1 0]);
      end
      ic=ic+in;
      in=1;
   else
      in=in+1;
   end
end
rlb=rlb-(-mvl+re(1)-1);
rlb=rlb-(-mvl+re(end)-1);
rub=rub+(-mvl+re(1)+1);
rub=rub+(-mvl+re(end)+1);

tpc=lpc+rpc;
tlb=llb+rlb;
```

```
        tub=lub+rub;
        % Last updated pixel size January 17, 2012, For MotionPro
        %Piv values 4.9048 mm
        % PIV values updated Feb 23, 2013

        %motionpro values 5.849 mm by 4.8799 mm
        %               xscale=size(Img,2)/5.9633; %pixel per mm MotionPro
        %               yscale = size(Img,1)/7.9511; %pixel per mm MotionPro
%           xscale=size(Img,2)/3.863; %pixel per mm PIV
%           yscale = size(Img,1)/3.863; %pixel per mm PIV
        xscale = (size(image,2)/Calibration_length);
        yscale = (size(image,1)/Calibration_length);
        sf=xscale*yscale; %Scaling Factor [pixel^2/mm^2]
        Area=(tpc); %Area of the droplet pixels^2

        D2(icount)=Area*(4/pi)*(1/sf);
        Du(icount)=tub*(4/pi)*(1/sf);
        Dl(icount)=tlb*(4/pi)*(1/sf);
        Dsquared = Area*(4/pi)*(1/sf);
        adjust = 0;
%           if(mco<80)
%               Dsquared = Dsquared-adjust;
%               D2(icount)=Area*(4/pi)*(1/sf)-adjust;
%               Du(icount)=tub*(4/pi)*(1/sf)-adjust;
%               Dl(icount)=tlb*(4/pi)*(1/sf)-adjust;
%           end
        Diameter=sqrt(D2);
        oldD = Dsquared;
      end
      fprintf(hf,'%d\t%d\n',mco,Dsquared);
   end
   toc
   figure
   plot(D2)
   hold on
   plot(Du,'r')
   plot(Dl,'g')
   fclose(hf);
   %    figure
   %    plot(dstartt)
   cd ..
end
totaltime=toc
```

Appendix D. ERROR ANALYSIS

Uncertainty Measurement for Droplet Size Calculation

The uncertainty measurement for determining the droplet size from still images using Matlab based image processing is dependent on the errors associated with magnification and image resolution. The use of a telephoto lens and magnifying lenses provided a magnification of image which is approximately 2.95 mm by 2.95 mm. Since the image resolution used was 700 by 700 pixels and the pixels on the camera are square, the corresponding pixel size was 4.21 μm in both the vertical and horizontal directions. This gave a spatial resolution of 56305 pixels/mm2. The high contrast ratio between the droplet and the image background makes the edge detection a function of the threshold used in image processing. An assumption of ±2 pixels on both the left and right edges was made in Matlab to measure the maximum error for a given droplet size. Two droplet sizes were compared; one having a width of 4 pixels larger than the measured droplet size and the other having 4 pixels fewer. Additionally, the calculation of the maximum relative error is shown below.

$$\frac{\Delta r}{r} = \frac{r_{max}}{D^2} * 100\%$$

Where Δr/r is the maximum relative error (expressed as a percentage) and D^2 is the squared diameter of the droplet. Therefore, the smallest droplet produces the largest percentage error. The droplet becomes smallest when the droplet size becomes approximately the size of fiber nodule in its end of evaporation. A sample calculation using the smallest diameter possible should show the maximum relative error of the droplet size. Assuming a perfectly circular nodule with a diameter of 600 μm the following calculations can be made:

$$\mathrm{D} = 600\ \mu\mathrm{m} * \left(\frac{\mathrm{pixel}}{4.21\ \mu\mathrm{m}}\right) = 142\ \mathrm{pixels}$$

The largest and smallest diameters correspond to 142+4 and 142-4 pixels, respectively. The difference in the areas and subsequently the squared diameters can be calculated by:

$$Area = \frac{\pi}{4}(D)^2$$

$$D^2\ difference = \frac{1}{2}\left[(142+4)^2 - (142-4)^2\right] = 1136\ pixels$$

$$r_{max} = D^2\ difference = 1136\ pixels$$

$$\frac{\Delta r}{r} = \frac{1136\ pixels}{142^2} * 100\% = 5.63\ \%$$

The maximum relative error for the droplet size was found to be 816 pixel or approximately 5.63 %.

Error analysis for heat of combustion

In this case, a simple error analysis is sufficient. Estimate the error in Ccal, ΔU and ΔH by calculating the mean absolute error (MAE). The following relations should be used:

$$MAE = \frac{1}{n}\sum_{i=1}^{n}|f_i - y_i| = \frac{1}{n}\sum_{i=1}^{n}|e_i|$$

Where, N is the number of points. As the name suggests, the mean absolute error is an average of the absolute errors $|e_i| = |f_i - y_i|$, where f_i is the prediction and y_i the true value.

For example, three experiments have been done to calculate the heat of combustion of 10% C4-OET.

LHV for test 1: -37949.04655 KJ/kg

LHV for test 2: -38388.67197 KJ/kg

LHV for test 3: -38104.4611 KJ/kg

Average: -38147.39 KJ/kg

MAE is then calculated as,

$$MAE = \frac{1}{3}(|(-37949.04655 + 38147.39)| + |(-38388.67197 + 38147.39)| + |(-38104.4611 + 38147.39)|)$$

$$MAE = 160.85$$

% of error can be calculated as,

$$\%\ of\ error = \frac{MAE}{Average} = \frac{160.85}{38147.93} = 0.42\%$$